

Mirror Surface Finishing of Miniature V-grooves Using

MCF (magnetic compound fluid) Slurry

MCF (磁気混合流体) スラリーを用いた

微細 V 溝の鏡面仕上げ

Youliang Wang

September 2016

Mirror Surface Finishing of Miniature V-grooves Using

MCF (magnetic compound fluid) Slurry

MCF (磁気混合流体) スラリーを用いた

微細 V 溝の鏡面仕上げ

By

Youliang Wang

Submitted in Partial Fulfillment

of the

Requirements for the Degree

Doctor of Philosophy

Supervised by

Professor Yongbo Wu

Graduate School of

Systems Science and Technology

Akita Prefectural University

Akita, Japan

September 2016

This page intentionally left blank.

Contents

Abstract	i
Chapter I Introduction.....	1
1.1 Fresnel lens	1
1.2 Manufacture process of Fresnel lens	3
1.3 Magnetic field-assisted polishing	4
1.4 Magnetic compound fluid (MCF) slurry	7
1.5 Polishing process with MCF slurry	8
1.6 Overview of thesis	10
References	12
Chapter II Experiment apparatus and details	17
2.1 Experiment setup	17
2.2 Metrology and characterization	18
2.3 MCF slurry	21
Reference	26
Chapter III Working life of MCF and its performance in flat surface finishing	27
3.1 The working life of MCF slurry	27
3.2 Polishing of non-magnetic work-surface (oxygen-free copper).....	37
3.3 Polishing of magnetic work-surface (Ni-P plated STAVAX).....	46
3.4 Conclusions	74
Reference	76
Chapter IV Feasibility study on surface finishing of linear V-grooves ..	81
4.1 Introduction	81
4.2 Processing principle and experimental details.....	85
4.3 Fundamental research of linear V-groove	88
4.4 Surface finishing of linear V-grooves (OFC)	93

4.5 Ni-P plated surface polishing	118
4.6 Conclusions	125
References	128
Chapter V Finishing of circular V-groove using MCF slurry.....	133
5.1 Introduction	133
5.2 Surface finishing of circular V-grooves (OCF)	134
5.3 Ni-P plated circular grooves polishing	141
5.4 Conclusion	145
Chapter VI Conclusions and Future Suggestions	147
Acknowledgements.....	151
Accomplishments.....	153

Abstract

Magnetic field-assisted finishing (MAF) is a novel surface finishing technique in which a magnetic field is used to force abrasive particles acting on the work surface. The magnetic fluid (MF) or magnetorheological (MR) fluids being the finishing tools have been successfully used to precision surface polishing process. These fluids are intelligent materials which show a reversible and very fast transition from a liquid to a nearly solid state under the presence of external magnetic fields. This property makes them very good for applications in mechanical system. MAF processes have been developed for a wide variety of applications.

The work focuses on miniature V-grooves finishing using magnetic compound fluid (MCF) slurry. The MCF is produced by mixing the MF containing nanometer size magnetite particles and MR fluid containing micron size carbonyl iron powder (CIP) in the same base solvent. MCF slurry exhibits higher magnetic pressure and apparent viscosity than MFs and a more stable distribution of particles than MR fluids under a magnetic field. The uncoated-CIPs (carbonyl-iron-powders) within the conventional MCF slurry have low ability against aqueous corrosion, leading to the performance deterioration and working life shortening of the conventional MCF slurry. We proposed a new MCF slurry containing ZrO_2 -coated CIPs instead of the uncoated CIPs.

Oxygen-free copper (OFC) is a popular material used for molds/dies in injection molding of plastic lens. In this article, the construction of an experimental rig to realize the proposed method was described at first. Then the effects of process parameters including MCF slurry composition, workpiece oscillation frequency f and clearance Δ between workpiece and MCF carrier on work-surface roughness and material removal were experimentally investigated. As a result, nano-precision surface polish of OFC was successfully attained with MCF slurry. Develop a novel polishing technique for mirror surface finishing of this kind of magnetic material using magnetic compound fluid (MCF) slurry. The effects of the magnetic force and the gravitational force acting on the carbonyl-iron-particles (CIPs) and the abrasive particles (APs) within the MCF

slurry were discussed and the behaviors of CIPs and APs were predicted. Then, experiments were performed to confirm the prediction by investigating the distributions of the CIPs and APs on the working-surface of MCF slurry. Finally, four MCF slurries containing CIPs and APs with different diameters were employed to finish the Ni-P plated STAVAX steel specimen at different working gaps.

The feasibility of finishing linear V-grooves generated on an oxygen-free copper substrate using a magnetic compound fluid (MCF) slurry was experimentally investigated, and the fundamental finishing characteristics were elucidated. The polishing experiments were performed to clarify the fundamental polishing characteristics, including the effects of the polishing time on the material removal, the form accuracy (i.e. the form retention rate and symmetry error), and the surface roughness at different polishing locations/positions in the polishing zone. Thereafter, the fundamental characteristics were examined by investigating the distribution of abrasive particles in the polishing zone, the relative velocity of abrasive particles compared to the V-groove, and the impact angle of abrasive particles against the V-groove side surface. Finally, the effect of the MCF carrier rotation speed n_c on the characteristics was elucidated, and an appropriate value of n_c was proposed.

To complete the finishing of miniature V-grooves, the circular grooves polishing using MCF slurry was studied through the investigation on surface roughness and form accuracy.

According to the above results, the magnetic field-assisted polishing using MCF slurry is a promising technique for the mirror precision finishing of miniature of V-grooves.

Chapter I Introduction

1.1 Fresnel lens

With the development of the society, the demanding energy which depends on the coal, wood, fossil fuels and so on increase quickly. Therefore the environmental pollution became one of the greatest problems which is facing today, in addition, it was caused huge and irresistible destroy to our earth. To work this problem, people in the world propose timely potential “green energy” for development of the earth. And some kinds of green technologies, including wind, solar, water and so on have been realized as the effective “green energy” to relieve the environmental pollution [1]. Moreover, the solar energy among the “green energy” is considered to the most convenient and the least polluted energy [2]. There are two dissimilar types of utilization channel in solar energy: conversion of the photovoltaic and the photo-thermal. In our life, the solar cells on the roof are usually used to absorb solar energy and improve the efficiency of solar energy photovoltaic conversion. However, the cost of solar cell is very high which limit its widespread use for more families.

To decrease the cost of the usage price of the solar cell, one of the advanced methods is reducing the area of solar cell under the premise of obtaining the equal energy from the sun. The conventional convex lens was chosen to gather the sunlight to the solar cell to develop the affordable and clean solar energy technologies. This method can improve the photoelectric conversion efficiency, cost-effective use of solar energy in solar photovoltaic power generation. Nevertheless, this kind of convention lens is thicker at its center and the weight of the lens is high. In order to obtain the lens which with light-weight and inexpensive, people found that the incident light change the direction on the curved surface and the end surface. In this case, the material between the curve surface and the end surface can be removed in conventional lens

shown in Fig. 1.1, afterwards, the new lens can be made much thinner than a conventional convex lens and form a flat sheet. This kind of novel lens was named as Fresnel lens. Initially, the Fresnel lens is applied for lighthouses. The Fresnel lens is usually produced by glass or plastic which have been applied successfully in solar energy, lighthouses, projection televisions, spot lights and so on.

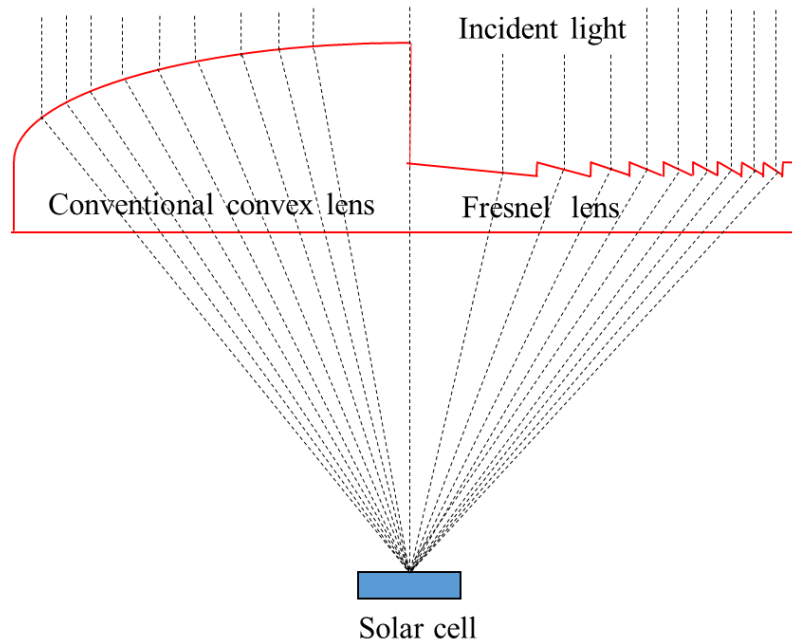


Fig.1.1 Conventional convex lens and Fresnel lens

This kind of lens is generally produced by generating parallel distributed linear V-grooves or concentrically distributed circular V-grooves on a colourless and transparent optical glass like BK7 or a plastic like a PMMA substrate. The former is called a linear Fresnel lens (Fig. 1.2 (a)), and the latter is called a circular one (Fig. 1.2 (b)). The facula of incident light crossing Fresnel lens with linear grooves is a line while a circular point will be formed when the Fresnel lens with circular grooves used. In the changeover system of the photovoltaic, the diffraction efficiency is one of the significant factors which depend on the surface quality and form accuracy of the Fresnel lens. Hence, in order to improve the surface quality and form accuracy of the lens, the manufacture process might be investigate firstly. The manufacture process of the Fresnel lens will be introduced in the next section.

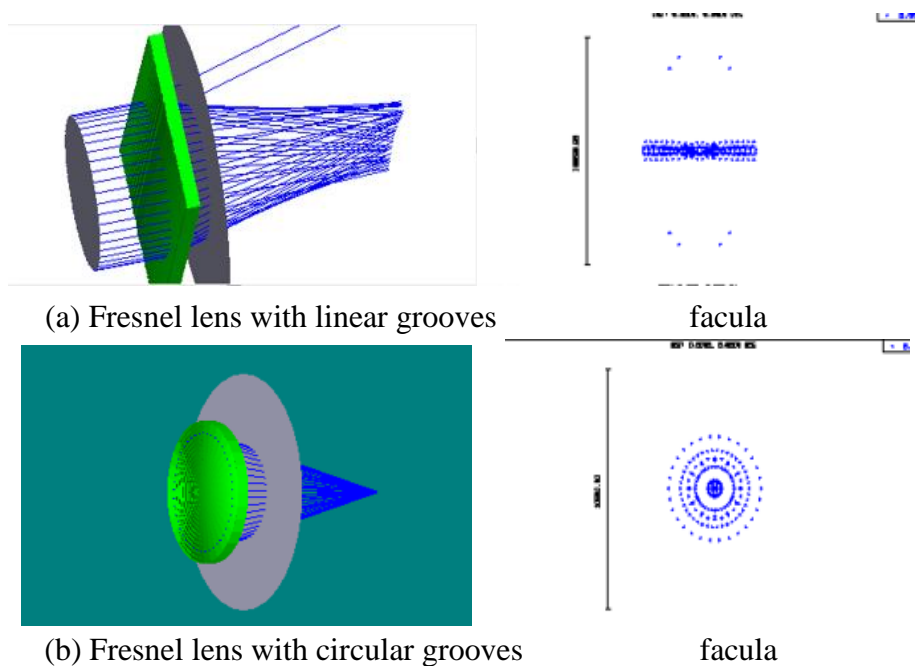


Fig. 1.2 Fresnel lens with (a) linear grooves and (b) circular grooves

1.2 Manufacture process of Fresnel lens

Their fabrication commonly relies on either diamond cutting or diamond grinding one by one, leading to a difficulty in the popularization of concentrating PV systems due to their high fabrication cost and low productivity [3]. Therefore, it is essential to provide high-quality and low-cost Fresnel lenses in order to expand the application of concentrating PV systems. For this purpose, the simplest and most cost-effective method is to utilize a polymer like PMMA as the substrate material and mass-produce them by hot pressing or injection moulding.

As a diffractive focus lens, the optical efficiency, which is defined as the ratio of the transmitted light energy to the incident light energy, is a significant assessment standard. The transmitted light energy is closely related to the form accuracy and surface roughness of the lens, with better values for these resulting in a higher amount of transmitted light energy, which contributes to a high optical efficiency. Consequently, it is very important to manufacture high-precision structured moulds for the hot pressing/injection moulding of plastic Fresnel lenses. The existing precision machining

processes like diamond machining and precision grinding are well suited for manufacturing such structured moulds. However, in some cases, a subsequent polishing operation should be performed on the structured surface to improve the surface roughness or remove the tool feed marks caused by pre-machining, which may result in light scattering effects [4].

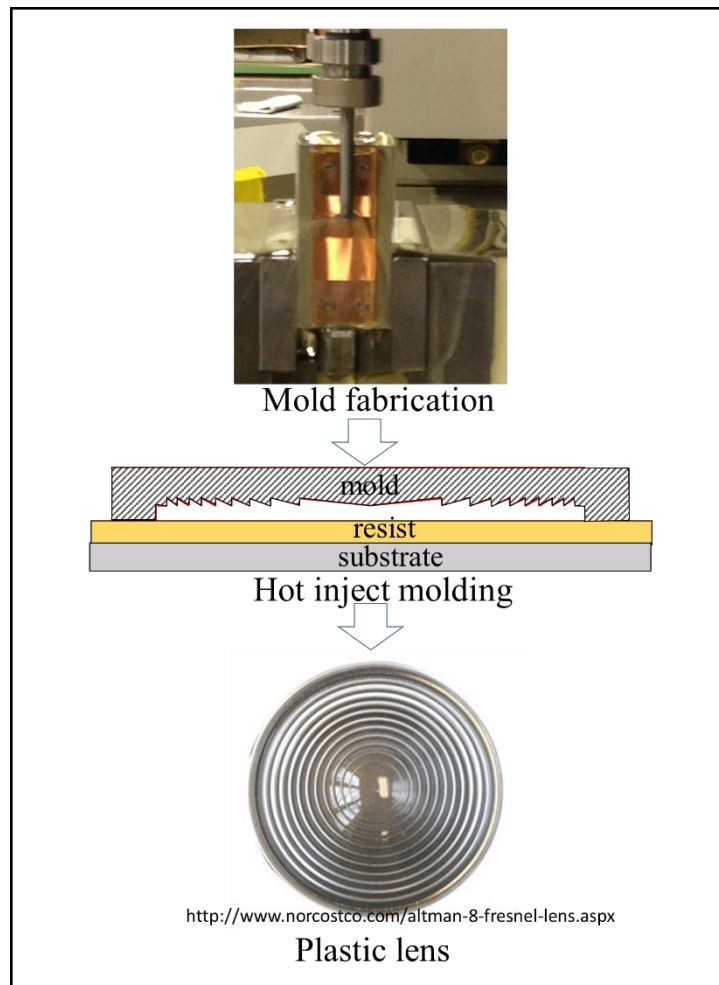


Fig. 1.3 The manufacture process of Fresnel lens

1.3 Magnetic field-assisted polishing

Some efforts have previously been made to finish such structured surfaces. Gessenharter et al. [5] proposed a new polishing process for finishing V-grooves using conical pin-type and conical wheel-type polishing tools. In their work, a polishing

slurry consisting of a polymer fluid, abrasives, and additives was impressed into the tools used, and the surface roughness and form accuracy of the structured electroless nickel-plated substrates were successfully improved, while the edges at the bottom and top of the grooves were rounded. Brinksmeier et al. [6] performed surface finishing of structured optical elements using the same method, and the surface roughness of a V-groove reached 5 nm Ra. However, on an actual Fresnel lens, the dimensions and cross-section profiles of the V-grooves are different at different locations. Thus, several tools with different dimensions and geometries should be prepared to geometrically fit the dimensions and the cross-section profiles of the V-grooves being finished, and the tools should be frequently exchanged during the polishing of a single workpiece in the case of utilizing the method by Gessenharter et al. Undoubtedly, their method leads to a high equipment investment cost and long process time. Therefore, a flexible tool capable of geometrically fitting the V-groove by itself is necessary to solve this problem.

One promising surface finishing technique is magnetic field-assisted polishing, in which a magnetic fluid (MF), magnetorheological fluid (MRF), or magnetic compound fluid (MCF) slurry is employed as the flexible abrasive tool. Once a magnetic field is applied, flexible chain-shaped magnetic clusters are immediately formed within the slurry along the magnetic lines of force, and the lengths and orientations of these clusters can be changed according to the shape of the work surface. Kim et al. [7] proposed a field-assisted finishing technique that utilizes MRF slurries for polishing three-dimensional silicon microchannel structures. They investigated the influences of the process parameters on the material removal and compared the surface topographies before and after finishing. The obtained results indicated that after polishing, the average roughness was reduced to 11.1 nm Ra on the bottom surface and 18.1 nm Ra on the side wall, but the depth of the microchannel was reduced by up to 10.4%. Lim et al. [8] presented a polishing technique for three-dimensional copper electroplating and silicon microchannel structures using MRF slurries. Their results showed that the

average surface roughness dropped by more than an order with little change in the original geometries, and the performances of both structures were improved. Natsume et al. [9] described a new type of magnetic abrasive machining for finishing a surface with a shallow groove on stainless steel. The results indicated that the surface quality of the groove bottom was improved significantly, and the finished surface roughness was $0.052 \mu\text{m Ra}$. Kawakubo et. al [10-12] proposed a magnetic field-assisted machining method to finish a die with an R-groove, in which the relative motion between the slurry and workpiece was produced by reciprocating the workpiece in the groove direction. The results demonstrated that the surface roughness was related not only to the radius of the groove but also to the diameter of the ferromagnetic particle. In addition, the form error on the edge of the grooves was higher than that at other positions. Hence, magnetic field-assisted polishing is supposed to be an excellent candidate for polishing the moulds for structure such as microchannel grooves and R-grooves. However, under a given magnetic field, the particles are less stably distributed in an MRF slurry than in an MF slurry, whereas the magnetic pressure and apparent viscosity of the former are larger than those of the latter, leading to a difficulty in stabilizing their performances in surface finishing.

To overcome the respective disadvantages and make use of the respective advantages of MF and MRF slurries, a novel magnetic slurry called MCF slurry was proposed by Shimada et al. [13, 14]. In practice, this new slurry is produced by blending micrometer-size carbonyl iron powders (CIPs), abrasive particles, and α -celluloses whenever necessary into a water-based MF containing nanometre-size magnetite particles with the respective blend ratios. Hence, under a magnetic field, the behaviour of the particles within the MCF slurry can be controlled, and the slurry exhibits a higher magnetic pressure and apparent viscosity and a more stable distribution of particles, while maintaining a fluid-like behaviour. As engineering applications, the MCF slurry has been successfully used to polish various engineering materials, including stainless

steels, polymers, optical glasses, ceramics, oxygen-free copper, and a Ni-P plating layer [15, 16-21]. For example, Goo et al. performed the polishing of a Ni-P plating layer [15] and PMMA [17] using a zirconia-coated CIP-based MCF slurry, and the results showed that the surface roughness of the workpieces was improved to the nanometre-level without causing scratches or the embedding of particles. Wang et al. polished the flat surface of an oxygen-free copper specimen using MCF slurries containing different CIPs and determined a strategy to prolong the slurry working life [18]. Furuya et al. polished a metal work-surface utilizing the MCF polishing technique and optimized the experimental parameters [21]. In particular, it should be noted that an MCF slurry is capable of finishing the structured surface of a stainless specimen with deep rectangle grooves [22], implying that the MCF slurry is potentially capable of playing an important role in V-groove surface finishing.

1.4 Magnetic compound fluid (MCF) slurry

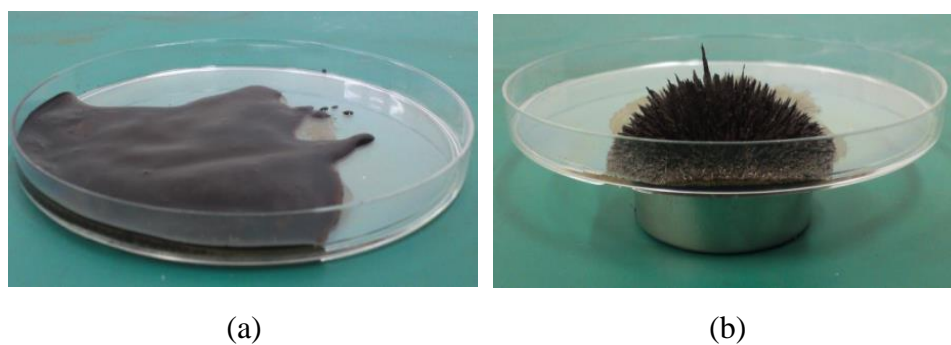


Fig. 1.4 MCF slurry (a) without magnet and (b) with magnet

Magnetic compound fluid (MCF) slurry is produced by blending carbonyl-iron-particles (CIPs), abrasive grains and α -cellulose whenever necessary in a magnetic fluid (MF). The behavior of grains within it can be controlled by a magnetic field applied, and hence it is a promising candidate for slurry used in magnetic field-assisted polishing. MCF slurry is intelligent material which show a reversible and very fast transition from a liquid (see Fig.1.4 (a)) to a nearly solid state (see Fig.1.4 (b)) under the presence of

external magnetic fields. The slurry can exhibit changes in apparent viscosity of several order of magnitude. This outstanding property makes them very good candidates for applications in precision polishing.

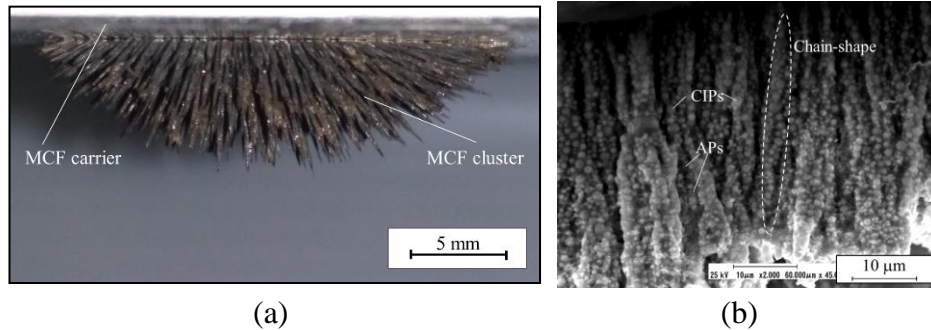


Fig.1.5 (a) Optical image and (b) SEM microscopy of the formative clusters under a magnetic field

As shown in the Fig. 1.5, chain-shaped magnetic clusters composed of nanometer-size magnetite particles and micrometer-size carbonyl-iron particles (CIPs) are immediately formed along the magnetic lines of force. Non-magnetic abrasive particles are entrapped in the clusters or distributed between the clusters, and α -cellulose fibers are interwoven with the clusters if they are employed. In addition, all of the clusters are forcibly collected by the magnetic attraction force, and they are concentrated in the area where the magnetic field is the strongest.

1.5 Polishing process with MCF slurry

Fig. 1.6 schematically illustrates the processing principle of polishing V-grooves with a MCF slurry. A disc-shaped permanent magnet is attached on the lower end face of its holder with an eccentricity of r . An MCF slurry carrier, i.e., an aluminum plate, is located below the magnet with a clearance δ . When the magnet holder is rotated at a speed of n_m , the magnet revolves around the axis of the holder at the same speed. Thereby a dynamic magnetic field is generated in which the magnetic flux density is constant but the magnetic lines of force constantly revolve around the magnet holder

axis; hereinafter this kind of dynamic magnetic field is called rotary magnetic field.

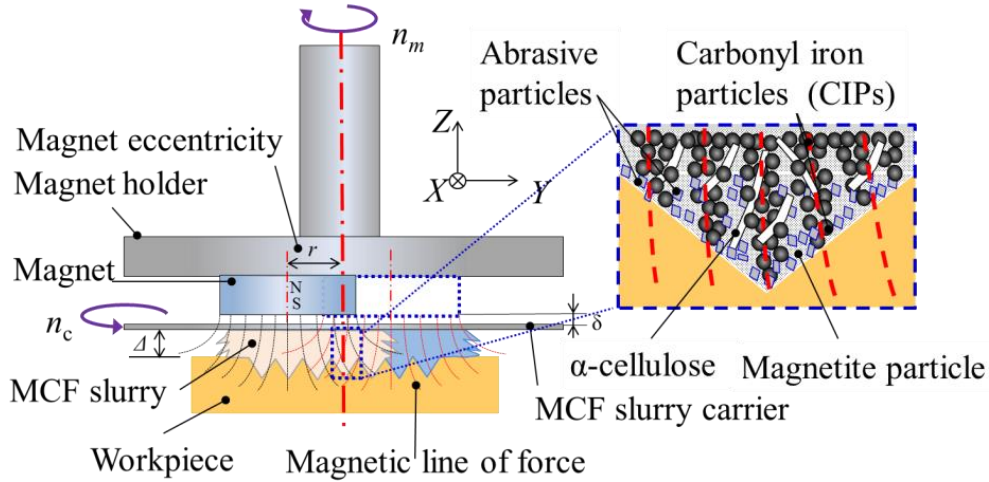


Fig. 1.6. Illustration of the processing principle of V-groove polishing with MCF slurry

Once the clearance Δ between the top of groove and the carrier has received a certain volume of MCF slurry, as shown in the right portion of Fig. 1.4, chain-shaped magnetic clusters composed of nanometer sized magnetite particles and micron sized CIPs (Carbonyl-iron-particles) are formed along the magnetic lines of force immediately; non-magnetic abrasive particles are entrapped into the clusters or distributed between clusters and α -cellulose fibers have interwoven with the clusters if the fibers are employed. It is also known that in a magnetic field non-magnetic substances suffer a so-called magnetic levitation force [7], and of course gravitational force acts on the same substances. Therefore, under the combined effect of both magnetic levitation and gravitational forces, the majority of nonmagnetic abrasive particles within the MCF slurry move downward towards the work surface. In addition, all of the clusters are collected forcibly by the magnetic attraction force and they are concentrated in the area where the magnetic field is stronger. When the MCF slurry comes into contact with the work-surface vibrating at a frequency of f and an amplitude of A_{p-p} , a normal polishing force is imposed on the workpiece and then a friction is induced between the workpiece and abrasive particles; hence the work-materials are

removed by the micro cutting actions of the abrasive particles. Besides, the MCF carrier is rotationally driven at a proper speed of n_c in order for the abrasive particles not to stay in the same polishing area during polishing.

1.6 Overview of thesis

The objectives of this thesis research work are to clarify the useful life of the MCF slurry and the distribution of the particles within slurry under a rotary magnetic field, to smooth miniature V-grooves surface finishing with MCF slurry.

Chapter I first introduces the Fresnel lens and its manufacture process and then briefly reviews magnetic field-assisted polishing processes. Popular techniques for achieving mirror surface finishing are outlined. Then the development of MCF slurry polishing process is introduced.

Chapter II details describes experimental approaches and the experimental setup used in this thesis work.

Chapter III first investigates the useful life of the MCF slurry and propose a new ZrO₂-coated CIPs instead of the conventional CIPs to prolong the MCF slurry useful life acting on the flat oxygen-free copper workpiece. Then, effects of frequency/Amplitude of the workpiece f/A , compositions of the MCF slurry and the working gap on the surface roughness and the material removal are discussed. Finally, the behaviors of particles within MCF slurry is analyzed to make clear the difference of the active abrasive particles on both the non-magnetic work-surface (oxygen-free copper) and magnetic work-surface (Ni-P plated surface).

Chapter IV reports the feasibility study on surface finishing of miniature linear V-grooves. The fundamental characteristics were determined by investigating the distribution of the abrasive particles in the polishing zone, relative velocity of the abrasive particles compared to the V-groove, and impact angle of the abrasive particles against the V-groove side surface. Finally, the effect of the MCF carrier rotation speed

n_c on the characteristics was elucidated, and an appropriate value for n_c was proposed from the viewpoint of the balance between the form accuracy and surface quality Ra.

Chapter V dedicates the mirror surface finishing on miniature circular V-grooves using MCF slurry. The surface roughness and form accuracy of the circular was evaluated with different workpiece rotational speed using MCF slurry.

Chapter VI summarizes and gives suggestions for future work on MCF slurry.

References

- [1] Solar Energy Perspectives: Executive Summary". International Energy Agency. 2011. Archived from the original on 2011-12-03.
- [2] EA Says Solar May Provide a Third of Global Energy by 2060". Bloomberg Businessweek. December 1, 2011.
- [3] Chien-Yao Huang, Chun-Chieh Chen, Hsiao-Yu Chou, Chang-Pin Chou. Fabrication of Fresnel lens by glass molding technique. *Optical Review*. 2013; 20; 202-204.
- [4] Y. Tanigawa, N. Nakamura, M. Uchino, M. Sugimoto, T. Maruo, Z. Haga, et al. Development of mold manufacturing technique using a transcription method for LED. *Die Mould Technol.* 2009; 24; 140-141. (in Japanese)
- [5] H. Ohmori, Y. Hachisu, K. Maekawa, N. Tone, Y. Uehara and Y. Takizawa. Ultra fabrication technologies of large Telescope Lenses for JEM-EUSO creating new astronomy, *JSPE* **77**, 2011, 16-20. (in Japanese)
- [6] Brinksmeier E, Riemer O. Deterministic production of complex optical elements. *Int J Prod Eng Comput. Special Issue on CAPP and Advances in Cutting Technology*. 2002; 4; 63-72.
- [7] A Gessenharter, O Riemer, E Brinksmeier. Polishing processes for structured surfaces. *Proceedings of the 18th ASPE*, 2003.
- [8] Ekkard Brinksmeier, Oltmann Riemer, Alexander Gessenharter. Finishing of structured surfaces by abrasive polishing. *Precision Engineering*. 2006; 30; 325-36.
- [9] Wook-Bae Kim, Seung-Hwan Lee and Byung-Kwon Min. Surface Finishing and

- Evaluation of Three-Dimensional Silicon Microchannel Using Magnetorheological Fluid. *J. Manuf. Sci. Eng.* 2005; 126; 772-78.
- [10] Lim, C.H.; Kim, W.B.; Lee, S.H.; Lee, J.I. Surface polishing of three dimensional micro structures. *Micro Electro Mechanical Systems. 17th IEEE International Conference on (MEMS).* 2004; 709-12.
- [11] Masayuki Natsume, Takeo Shinmura and Katsumi Sakaguchi. Study of magnetic abrasive machining by use of work vibration system (characteristics of plane finishing and application to the inside finishing of groove). *The Japan Society of Mechanical Engineers.* 1998; 64; 4447-52.
- [12] Hideki Kawakubo and Tatsuya Yomogida. Finishing Characteristics of R-Groove Using Magnetic Field Assisted Machining Method. *The Japan Society for Precision Engineering.* 2006; J07; 733-34.
- [13] Hideki Kawakubo and Masaki Sato. Polishing in Groove using Workpiece Oscillation Type Magnetic Field Assisted Machining. *The Japan Society for Precision Engineering.* 2008; E47; 375-76.
- [14] Hideki Kawakubo and Masaki Kamijima. Polishing for Ferromagnetic Materials using Workpiece Oscillation Type Magnetic Polishing Method. *The Japan Society for Precision Engineering.* 2010; B43; 139-40
- [15] Kunio Shimada, Yongbo Wu and Yat Choy Wong, Effect of magnetic cluster and magnetic field on polishing using magnetic compound fluid (MCF), *Journal of Magnetism and Magnetic Materials*, 2003;262;242-47.
- [16] Shimada, K., Akagami, Y., Kamiyama, S., Fujita, T., Miyazaki, T., Shibayama, A.

- New microscopic polishing with magnetic compound fluid (MCF). *J. Intel. Mater.Syst. Struct.* 2002; 13; 405-08.
- [17] Huiru Guo, Yongbo Wu, Dong Lu, Masakazu Fujimoto, Mitsuyoshi Nomura, Ultrafine Polishing of Electroless Nickel-Phosphorus Plating Mold with Magnetic Compound Fluid Slurry), *Materials and Manufacturing Processes.* 2014; 29; 1502-09.
- [18] H.R. Guo, Y. Wu, Y.G. Li, J.G. Cao, M. Fujimoto and S.D. Jacobs. Technical performance of zirconia-coated carbonyl-iron-particles based magnetic compound fluid slurry in ultrafine polishing of PMMA. *Key Engineering Materials.* 2012; 523-524; 161-66.
- [19] Huiru Guo, Yongbo Wu, Dong Lu, Masakazu Fujimoto, Mitsuyoshi Nomura. Effects of pressure and shear stress on material removal rate in ultra-fine polishing of optical glass with magnetic compound fluid slurry. *Journal of Materials Processing Technology.* 2014; 214; 2759-69.
- [20] Youliang Wang, Yongbo Wu, Huiru Guo, Masakazu Fujimoto, Mitsuyoshi Nomura and Kunio Shimada, A new magnetic compound fluid slurry and its performance in magnetic field-assisted polishing of oxygen-free copper, *J. Appl. Phys.* 2015;117; 17D712-1-12-4.
- [21] Yongbo Wu, Youliang Wang, Masakazu Fujimoto, Mitsuyoshi Nomura. Nano-precision polishing of CVD SiC using magnetic compound fluid slurry, *Journal of the Korean Society of Manufacturing Technology Engineers.* 2014; 23; 547-54.
- [22] Wu Y., Sato T., Lin W., Yamamoto K., Shimada K., Mirror surface finishing of

acrylic resin using MCF-based polishing liquid, Int. J. Abras. Technol. 2010; 3; 11-24.

This page intentionally left blank.

Chapter II Experiment apparatus and details

2.1 Experiment setup

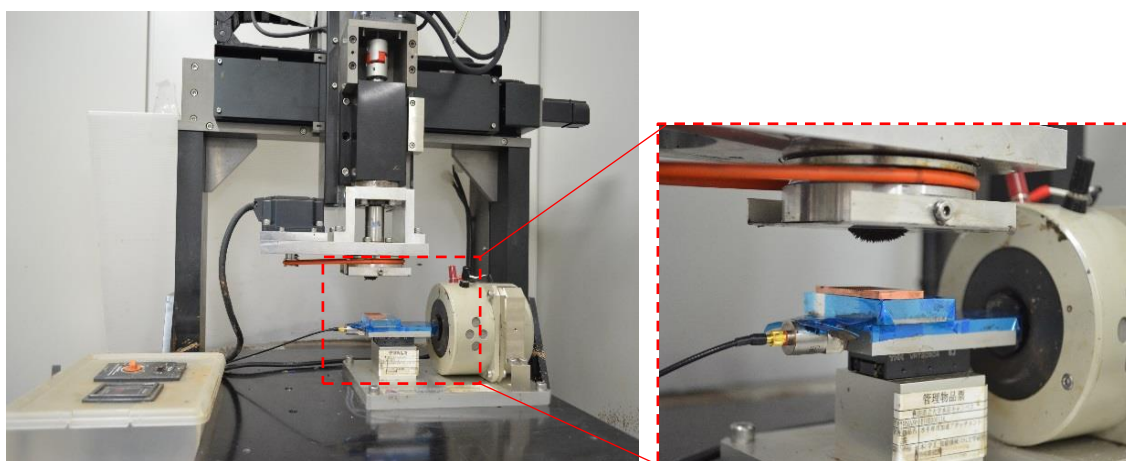


Fig. 2.1 Experimental setup for polishing the linear V-groove

An experimental apparatus was constructed in the laboratory, as shown in Fig. 2.1. A polishing unit composed of a magnet holder, an MCF carrier, and two motors, together with a belt/pulley set, was mounted on the Z-axis linear actuator of an existing polisher, allowing Z-axis motion. In addition, a commercially available wave maker (SL-0505 by Asahifactory Corp.) installed on the worktable of the same polisher to provide the workpiece with an oscillating motion in the X direction. In the MCF unit, a disc-shaped neodymium permanent magnet with a magnetic field strength of 0.45 T was set at an eccentricity of $r = 4.5$ mm. Motor 1 was connected to the magnet holder through a flexible coupling and used to give the magnet a revolutionary motion around its holder's axis. Motor 2 was connected to the MCF carrier through the belt/pulley and used to rotationally drive the carrier. The carrier (82 mm \times 82 mm \times 1 mm) was made of a non-magnetic material (aluminium in this work). Below the MCF carrier, a piece of oxygen-free copper (OFC) substrate with linear V-grooves was fixed on the work holder of the wave maker as the workpiece. This arrangement allowed the workpiece

to oscillate in the X-axis direction at frequency f and amplitude A . Thus, it allowed the relative velocity of the abrasive particles to the work surface to be in the longitudinal direction of the linear grooves. In addition, the clearance Δ could be varied by adjusting the vertical position of the MCF unit through the Z-axis linear actuator.

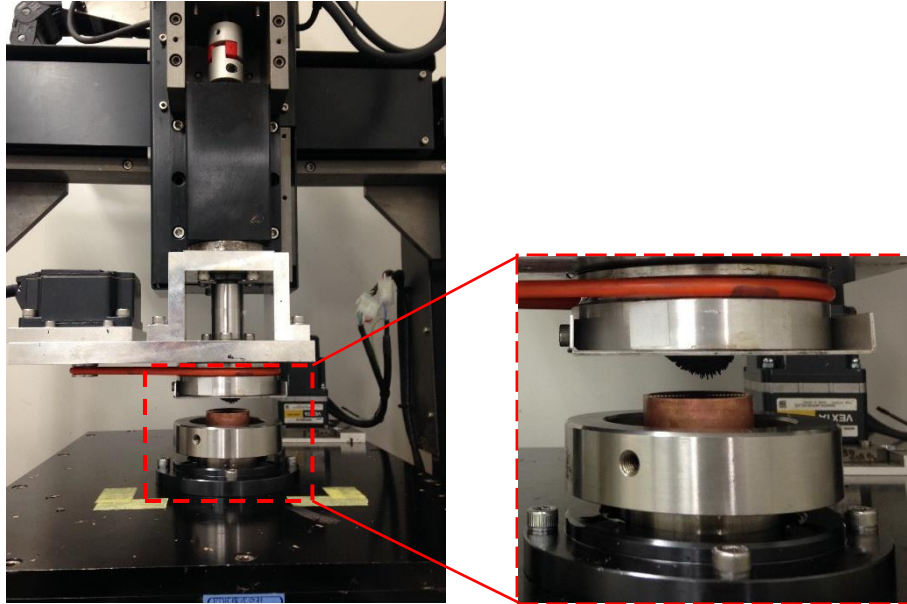


Fig. 2.2 Experimental setup for polishing the circular V-groove

Fig. 2.2 shows the experimental setup for the circular V-grooves polishing using MCF slurry. A rotational work-table instead of the wave maker was used to polish the circular V-grooves. Motor 1 and Motor 2 were the same to the Fig. 2.1. Motor 3 was connected to the work-table through the belt/pulley and used to rotationally drive the workpiece.

2.2 Metrology and characterization

2.2.3 Surface quality characterization

As shown in Fig. 2.3, a non-contact white-light 3D optical surface profiler (New View 600 by Zygo Corp.) was used to measure surface roughness. There are many different roughness parameters in use, but Ra is by far the most common. Ra is the

arithmetic average of the absolute values and the most widely used one-dimensional roughness parameter. Ra can be given by

$$R_a = \frac{1}{n} \sum_{i=1}^n |y_i| \quad (2.1)$$



Fig. 2.3 Zygo New View 600 interferometer



Fig. 2.4 EDAX ERA-8900, 3D-SEM & EDX

As the figure shows, the scanning electron microscope with four electron probes (3D-SEM ERA-8900 by Elionix Co., Ltd.) & energy dispersive x-ray spectrometer (EDX Genesis APEX by EDAX Inc.). The resolution is high not only in X and Y direction as conventional SEMs but also in Z direction, realizing the real-time 3D display of the SEM view. Elemental composition analyses were carried out using EDX to observe the distribution of the abrasive particles acting on the magnetic and

nonmagnetic work-surface. In addition, the microstructure of MCF slurry was observed to check if any embedding of abrasive particles or CIPs has occurred.

2.2.4 Form accuracy characterization



Fig. 2.5 Color 3D Laser Scanning Microscope, VK-8700

A 3D color Laser Scanning Microscope (VK-9700 by Keyence Corp.), as shown in this image, was used to observe the form accuracy of the miniature V-groove. With this instrument, the 3D topography of the polished V-grooves and cross section profiles were examined.

2.2.2 Surface cross section profile



Fig. 2.6 Taylor Hobson Form Talysurf Intra Profilometer

As this chart shows, a surface profile (Form Talysurf Intra Profilometer by Taylor Hobson Inc.) was used to measure the cross sectional profiles of a flat work-surface.

Compare to the cross sectional profiles before and after polishing to obtain the material removal under the given experimental conditions.

2.2.1 MCF slurry polishing process analysis

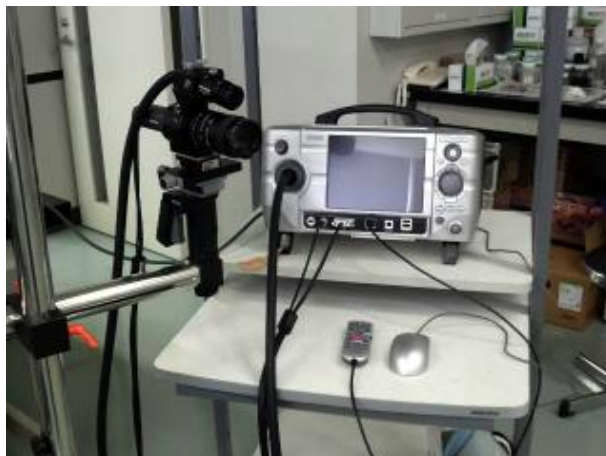


Fig. 2.7 Keyence VW6000 high speed motion analysis microscope

As displayed in the figure above, a high speed motion analysis microscope (VW6000 by KEYENCE Co., Ltd.) was used to observe the polishing process of the MCF slurry under a given magnetic field.

2.3 MCF slurry

2.3.1 Components of MCF slurry

A novel magnetic slurry named MCF slurry was proposed by Kunio Shimada et al. [1, 2]. This new slurry is in practice produced by blending micron sized carbonyl iron powders (CIPs), abrasive particles and α -celluloses whenever necessary into a water-based MF containing nanometre size magnetite particles (see Fig. 2.8) with the respective blend ratios.

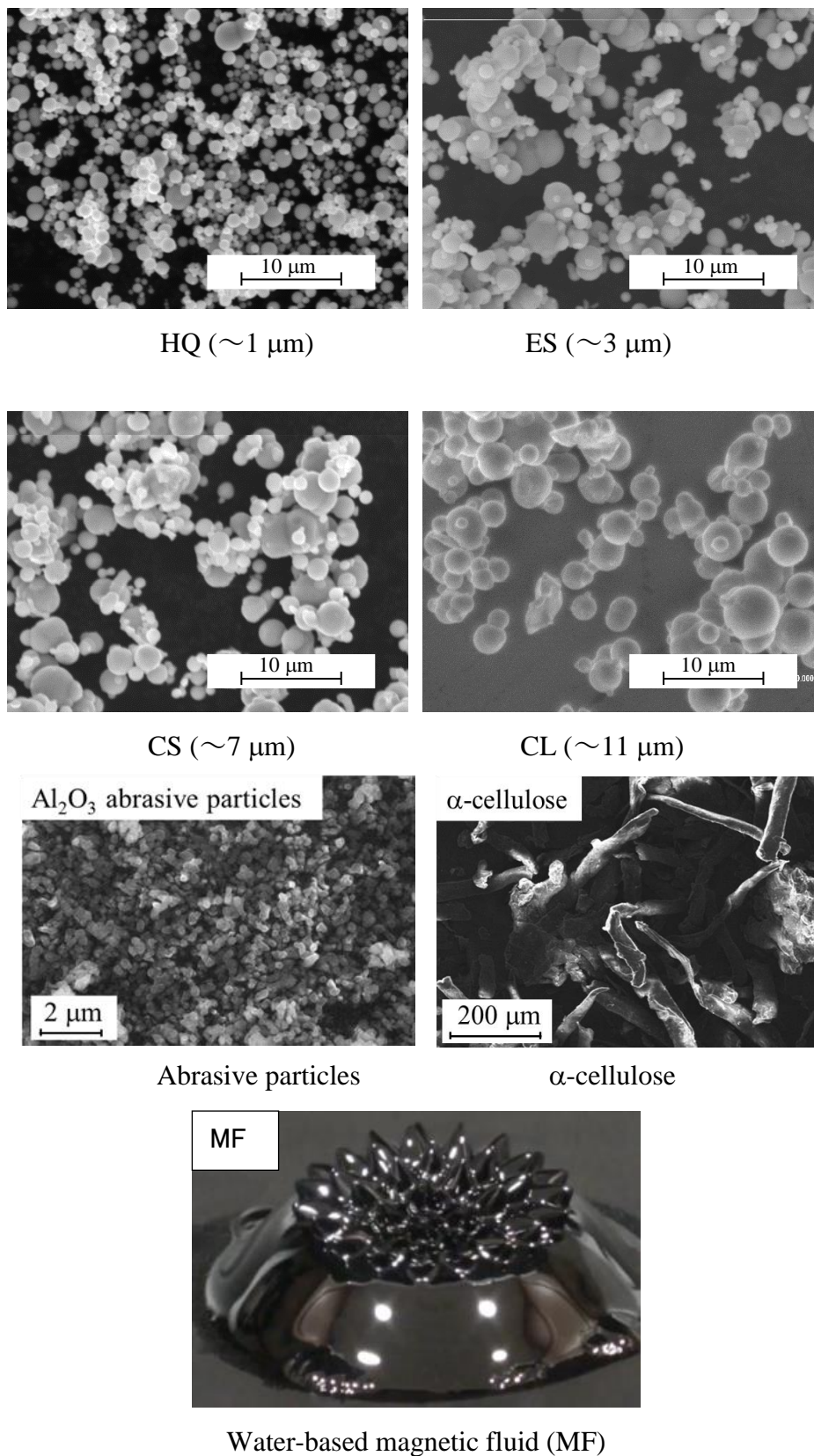


Fig. 2.8 Components of the MCF slurry used

2.3.2 The setup for the MCF slurry mixing



Fig. 2.9 Ultrasonic mixer (Handy Sonic UR-20P, TOMY)

The ultrasonic mixer with a 0.25 cm diameter active surface area enables the simple and efficient ultrasonic treatment of very small volume of MCF slurry. The maximum frequency of the ultrasonic mixer is high of 28 KHz. And the horn material is Titanium alloy. The iron particles, abrasive particles and magnetic fluid were weighed with a scale first and then mixed using this mixer. The particles within the slurry were mixed until they are well-blended. The last step is that the preparing MCF slurry was mixed using a planetary centrifugal mixer.



Fig. 2.10 Planetary Centrifugal Mixer (AR-100, THINKY)

The planetary centrifugal mixer with the dimensions of H328 × W250 × D250 was used to improve efficiency of mixing the amounts of MCF slurry. The compact and

suitable-anywhere design has enabled itself to be selected at many universities and research institutes where a large number of equipment, devices, and facilities limit their space. This setup is suitable for initial consideration in research and development where small amounts of materials are repeatedly tested. The mixer has the Memory function for simple pre-setting of mixing condition.

2.3.3 Behavior of the MCF slurry during the miniature grooves polishing

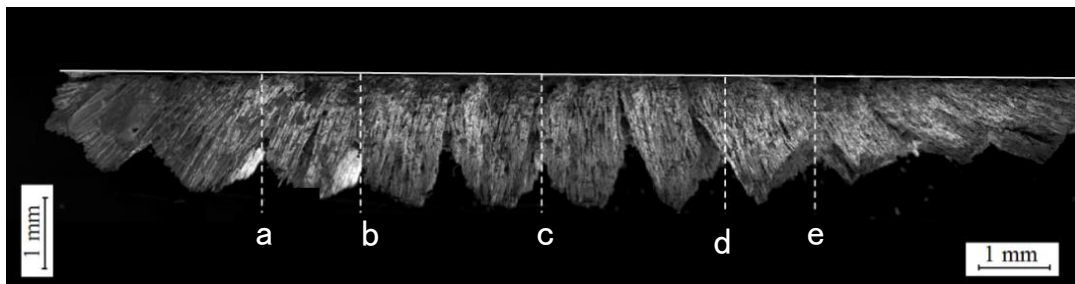


Fig. 2.11. SEM image of MCF cross-sectional profile during polishing process

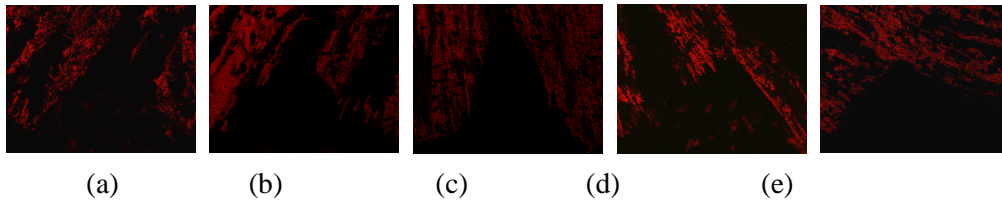


Fig. 2.12. Aluminum element distributions of MCF slurry obtained with energy dispersive X-ray

Under a magnetic field, chain-shaped magnetic clusters composed of nanometer-size magnetite particles and micrometer-size carbonyl-iron particles (CIPs) are immediately formed along the magnetic lines of force. Non-magnetic abrasive particles are entrapped in the clusters or distributed between the clusters, and α -cellulose fibers are interwoven with the clusters if they are employed. In addition, all of the clusters are forcibly collected by the magnetic attraction force, and they are concentrated in the area where the magnetic field is the strongest. The obtained SEM image of the entire cross section of the MCF slurry used investigates that the soft magnetic clusters can achieve all of the groove surfaces. Evidently, corresponding to the locations of the V-grooves on the work-surface, numerous V-shaped grooves were formed in the MCF slurry,

correspondingly due to the replication principle, and their sizes, including the depth and pitch, were approximately the same as those of the V-grooves in the workpiece (see Fig. 2.11). This indicates that the MCF slurry reached the whole surface of the V-grooves during polishing, and all the locations of the V-grooves within the polishing zone could be polished, as long as the abrasive particles were uniformly distributed in the same zone.

In order to confirm this, the aluminum element distributions were obtained, and the typical ones for the areas corresponding to locations a-e are shown in Fig. 2.12 (a)–(e), respectively. From this figure, it can be observed that the abrasive particles (Al_2O_3) were distributed evenly within the slurry. This fact excluded the possibility that the differences in the form accuracy and surface quality values at different locations/positions were caused by an uneven distribution of the abrasive particles in the polishing zone.

Therefore, under the combined effect of the magnetic levitation and gravitational forces, the majority of the nonmagnetic abrasive particles within the MCF slurry move down towards the work surface, and a normal force is thus imposed on the workpiece. When the relative motion existing between the work-surface and abrasive particles, friction is induced between the workpiece and abrasive particles. Hence, the work materials are removed by the micro-cutting actions of the abrasive particles.

Reference

- [1] Kunio Shimada, Yongbo Wu and Yat Choy Wong, Effect of magnetic cluster and magnetic field on polishing using magnetic compound fluid (MCF), Journal of Magnetism and Magnetic Materials, 262(2003) 242-247
- [2] Shimada, K., Akagami, Y., Kamiyama, S., Fujita, T., Miyazaki, T., Shibayama, A., 2002. New microscopic polishing with magnetic compound fluid (MCF). J. Intell. Mater. Syst. Struct. 13, 405–408.

Chapter III Working life of MCF and its performance in flat surface finishing

3.1 The working life of MCF slurry

In the field of solar energy, the plastic Fresnel lens is used for the purpose of gathering and concentrating sunlight onto solar cells. From the cost view of point, the lens is usually produced by injection molding using metal mold which is in general made of free-oxygen-copper. To meet the required performance, the mold should be fabricated not only with high dimensional/form accuracy but also with nm-order surface roughness. Therefore, as the final process for the manufacturing of the mold, nano-precision polishing is essentially performed.

As a promising method for the nano-precision surface finishing of the mold, the magnetic field-assisted polishing using MF (magnetic fluid) or MRF (magnetorheological fluid) slurry has been employed because the behavior of the abrasive particles within the slurry can be controlled by a magnetic field applied. The polished work-surface can achieve nano-precision with no sub-/surface damage. Dai, Y.F., et al [1] and Das, M., et al [2] polished the flat polypropylene work-surface using MF slurry and successfully improved the surface finish. A novel MRF polishing technique was proposed by Prokhorov and Golini in which a MRF slurry containing carbonyl-iron-powders (CIPs), abrasive grains, carrier fluid and stabilizers is employed [3, 4]. However, the two kinds of slurries have their respective advantages and disadvantages; under a magnetic field, the particles are more stably distributed in MF than in MRF, whereas the apparent viscosity and magnetic pressure of MF are smaller than that of MRF.

In order to overcome the disadvantages and exploit the advantages of the two conventional magnetic slurries, a novel MCF (magnetic compound fluid) slurry was developed by blending CIPs, abrasive particles and α -cellulose whenever necessary into

an MF [5]. The previous work confirmed the MCF slurry performs better than others in terms of polishing efficiency and work surface quality. The optical glass was polished using a MCF wheel and the nano-precision glass-surface was attained [6]. At the same time, the effect of the pressure and shear stress on material removal rate in ultra-fine polishing of optical glass with MCF slurry was researched [7], demonstrating that the material removal is dominantly dependent on the shear stress. The MCF slurry has been successfully used for polishing flat and curved surfaces with nano-precision and scratch-free work-surfaces [8]. In particular, the water-based MCF slurry is preferable from the viewpoint of the environmental issue and the running cost of cleaning workpiece and equipment. However, the conventional uncoated-CIPs have low ability against aqueous corrosion, leading to the performance deterioration and working life reduction of water-based MCF slurry.

As a measure against this problem, in the current work a new MCF slurry containing ZrO_2 -coated CIPs instead of the uncoated-CIPs was proposed, and the performance of the new slurry in the polishing of free-oxygen-copper was compared experimentally with that of the conventional one. This paper describes the experimental setup and procedure at first, and then experimental results on comparing the performances of the two slurries are exhibited. Finally, the difference between the performances is discussed through the investigation of property change of CIPs in the aqueous configuration.

3.1.1 Experimental setup and procedure

Fig. 3.1 shows a schematic illustration of the MCF polishing process under a rotary magnetic field. As illustrated in the left side of Fig. 3.1, a disc-shaped Nd-Fe-B permanent magnet is affixed on the end face of its holder with an eccentricity of r . The magnet holder is connected to an electric motor. Once the motor works to rotationally drive the holder, the magnet revolves around the holder axis and thus a rotary magnetic field is generated. In the rotary magnetic field, the magnetic flux density is constant, but

the magnetic lines of force constantly revolve around the magnet holder axis. Besides, a MCF slurry carrier made of non-magnetic materials, e.g., aluminum, is located below the magnet with 0.5 mm, and below the carrier a vibration table (SL-0505 by Asahi factory Corp.) is settled on which a workpiece is held with an adjustable gap of Δ between the carrier and the workpiece. When a certain volume of MCF slurry is supplied into the gap Δ , chain-shaped magnetic clusters composed of nm-sized magnetite particles and μm -sized CIPs are formed within the slurry along the magnetic lines of force immediately (the right side of Fig. 3.1). The non-magnetic abrasive particles are entrapped into the clusters or distributed between clusters and α -cellulose fibers have interwoven with the clusters if the fibers are employed [7]. Owing to the magnetic levitation force and the gravity, the abrasive particles move towards the work surface. Once the workpiece is given a vibration motion by the vibration table, a relative speed is created between the abrasive particles and the work-surface, hence the work-materials are removed by the micro cutting actions of the abrasive particles.

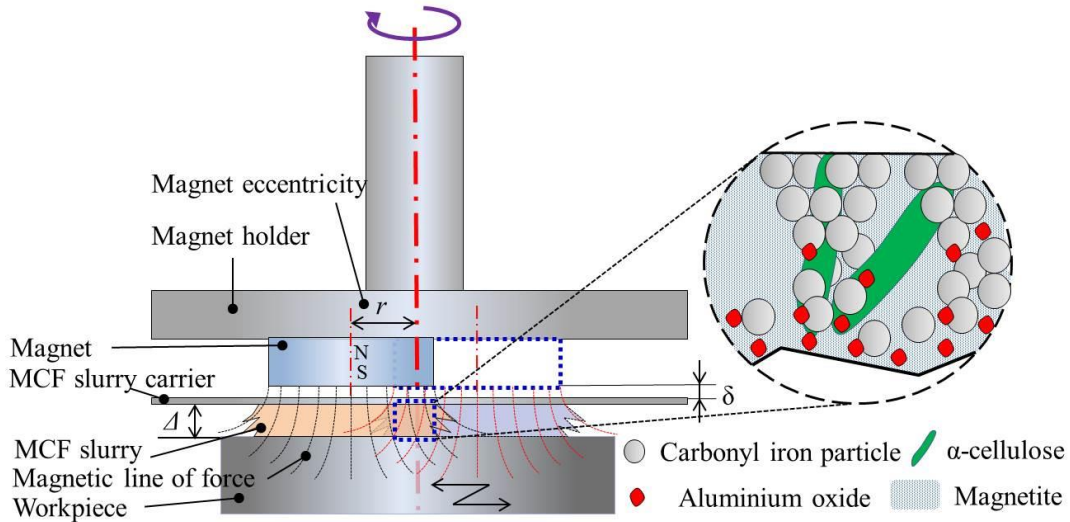


Fig. 3.1. Illustration of the MCF polishing process under a rotary magnetic field.

The purpose of this work is to validate the new MCF slurry by experimentally comparing its performance with that of the conventional one in the polishing of free-oxygen copper. Therefore, the new slurry was prepared just by replacing the uncoated-

CIPs within the conventional slurry with the ZrO₂-coated CIPs but the blend ratio was the same. That is, the conventional slurry contained the uncoated-CIPs ($\phi 7.5\mu\text{m}$) of 40wt.%, water-based MF (W11 by MGS Co., Ltd.) of 45wt.%, abrasive particle (Al₂O₃, $\phi 1\mu\text{m}$) of 12wt.% and α -cellulose of 3wt.%; whereas the new one, ZrO₂-coated CIPs ($\phi 1.4\mu\text{m}$) of 40wt.% and others were the same as those for the conventional one. The ZrO₂-coated CIPs employed for the new slurry were developed by Rochester university [9] which was produced by coating a thin, rough zirconia layer ($\sim 0\text{--}100\text{nm}$ in thickness) over the CIP ($\sim 1.1\mu\text{m}$ in diameter) surface.

Table 3.1. Experimental conditions

Workpiece	Material	Free-oxygen-copper
	Vibration	Frequency $f=30\text{ Hz}$
	Motion	Amplitude $A=4\text{ mm}_{\text{p-p}}$
Magnet		Nd-Fe-B, $\phi 18\text{mm} \times t 10\text{mm}$, 0.45T Eccentricity: $r=4.5\text{ mm}$ Revolution speed: $n=1,000\text{ rpm}$
Supply of MCF slurry		1 mL
Clearance		$\Delta=1\text{ mm}$
Polishing time		0 – 40min
Settling time		0h, 24h, 48h, 72h

In experiments, the slurry was left for a certain settling time after preparing, and then used to investigate the influence of the settling time on the work-surface finish. In order to keep the slurry fresh, the MCF slurry was kept in a rotate airtight container for a certain time. In this work, the settling time was set at different values of $t=0\text{h}$, 24h, 48h and 72h, and other process parameters were kept constant but the polishing time ranging from 0 to 40min (Table 3.1). After polishing, the work-surface finish was characterized with an optical surface profiler (Newview 600 by Zygo Corp.).

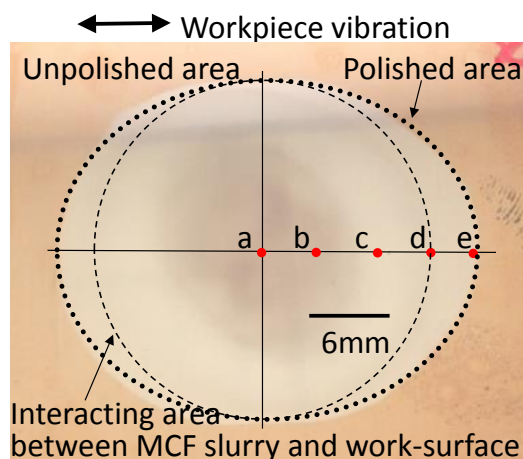


Fig. 3.2. A typical polished work-surface and the evaluated areas.

3.1.2 Results and discussion

Fig.3.2 shows a picture of a typical work-surface polished for 40min using the new MCF slurry with a settling time of 0h. Evidently, an elliptic polished area was obtained that was formed by the overlap of the circular interacting area [10] between the MCF slurry and the work-surface when the workpiece vibrated with an amplitude of 2mm. It was supposed that even the polishing conditions including the MCF slurry are the same the work-surface finish is different at different positions on the polished area, hence the surface roughness were measured at five different positions (a - e in Fig.3.2) from the center to the edge of the area along the vibration direction and the average value of them was obtained to be regarded as the surface roughness under the given conditions.

The work-surface topographies before and after polishing for 40min using different slurries with different settling times were observed by scanning white light interferometry technique as shown in Fig. 3.3. It can be seen in Fig. 3.3(a) that on the initial work-surface topography before polishing there were parallel distributed cutting marks generated in previous process of machining and the surface was rough with a roughness of $Ra25nm$. After polishing, no matter what the slurry and the settling time were, the surface finishes were greatly improved to $Ra<7nm$ except the work-surface polished using the conventional slurry with settling time of 72h (Fig.3.3(c)); there were

still cutting marks remaining, whilst on other three surfaces (Figs. 3.3(b), (d), (e)) the cutting marks were almost removed. Further, comparing Fig. 3.3(b) with Fig. 3.3(c) shows that when using the conventional slurry, the work-surface finish after polishing was affected significantly by the settling time. This phenomenon implied the property of the conventional MCF slurry has changed after being settled for a while, leading to the deterioration of its performance. By contrast, when using the new slurry containing the ZrO₂-coated CIPs, even it has been settled for 72h after preparing, the resultant work-surface finish (Fig.3.3(e)) was still in the same level as that using the fresh one with 0h settling time (Figs. 3.3(d)). This indicates that the performance of the proposed new MCF slurry can be maintained for much longer time up to several days.

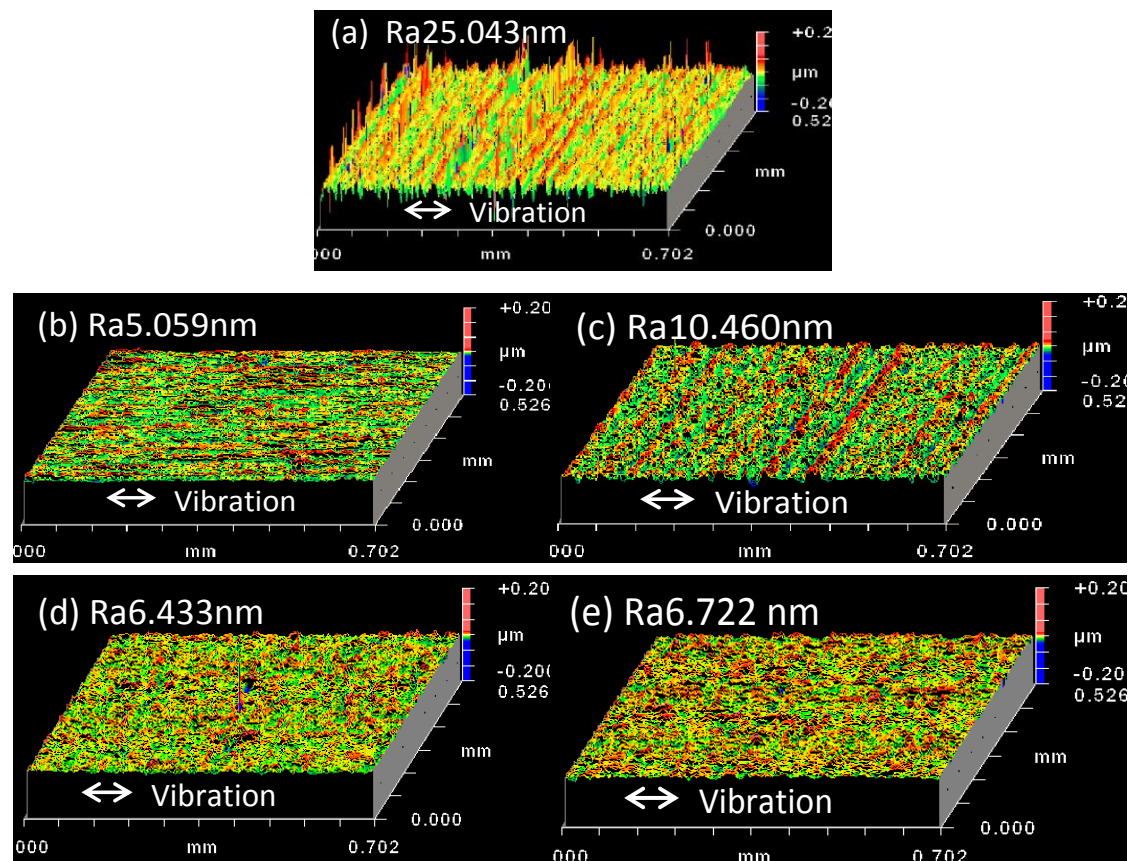


Fig. 3.3. Optical microscopic images of the work-surfaces: (a) before polishing; (b) after 40min polishing using conventional slurry with 0h settling time; (c) after 40min polishing using conventional slurry with 72h settling time; (d) after 40min polishing using new slurry with 0h settling time; (e) after 40min polishing using new slurry with 72 h settling time.

In order to systematically elucidate the fundamental polishing characteristics and the effective working life of the new MCF slurry, the variations of the work-surface roughness R_a during polishing were investigated for different settling times. For comparison, the similar investigations were also carried out with the conventional slurry. Figs. 3.4(a) and (b) show the investigation results obtained with the conventional MCF slurry and the new one, respectively. Obviously, regardless of the slurry and the settling time, the R_a decreased rapidly at beginning during polishing, and then the decrease rate became smaller gradually, eventually reached their respective stable values which depends on the settling time. In order the variation tendencies either with the conventional slurry or with the new one to be more distinct, normalized surface roughness was defined as $NR_a = R_a/R_{a0}$ where R_{a0} is the initial surface roughness before polishing, and subsequently the variations of the NR_a during polishing with different slurries for different settling times were calculated using the data in Fig. 3.4 as shown in Fig.3.5.

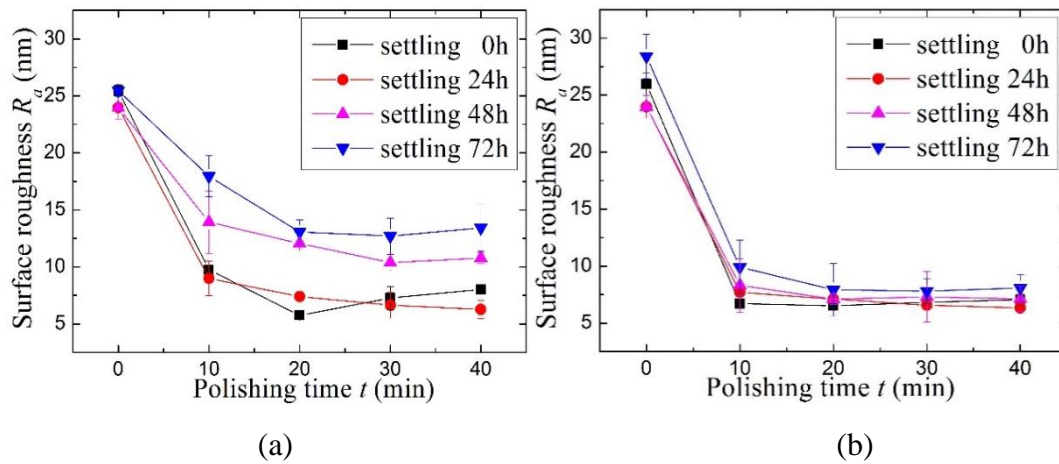


Fig. 3.4. Variations of work-surface roughness R_a during polishing for different settling times with (a) conventional MCF slurry and (b) new one.

Comparing Fig.3.5(a) with Fig.3.5(b) indicates that when the settling time was less than 24h, the variation tendency and the final value of the R_a with the new slurry was quite similar with that with the conventional one; however once the settling time was over 48h, in the case of using the conventional slurry, the settling time affected the

surface roughness considerably, showing the R_a increased significantly as the settling time increased, whereas in using the new slurry, although the R_a tended to increase with increasing settling time, the influence of the settling time on the R_a was much smaller compared with that in using the conventional slurry. In short, when either the conventional slurry or the new one is used soon after they have been prepared, i.e., a relatively short settling time (in the current work less than 24h), little performance difference can be observed between them; however after a relatively long settling time (in the current work more than 48h) the performance of the conventional slurry is deteriorated considerably whereas little deterioration can be observed on the performance of the new one. This suggests that the magnetic property of the uncoated CIPs in the conventional MCF slurry experiences a change after they have been left in an aqueous configuration for a while, whereas for the ZrO_2 -coated CIPs in the new slurry, little change occurs on their magnetic property even they have been left in the same configuration for a long while up to several days. The major reason causing the property change of the uncoated CIPs is supposed to be the rust of them in the aqueous configuration.

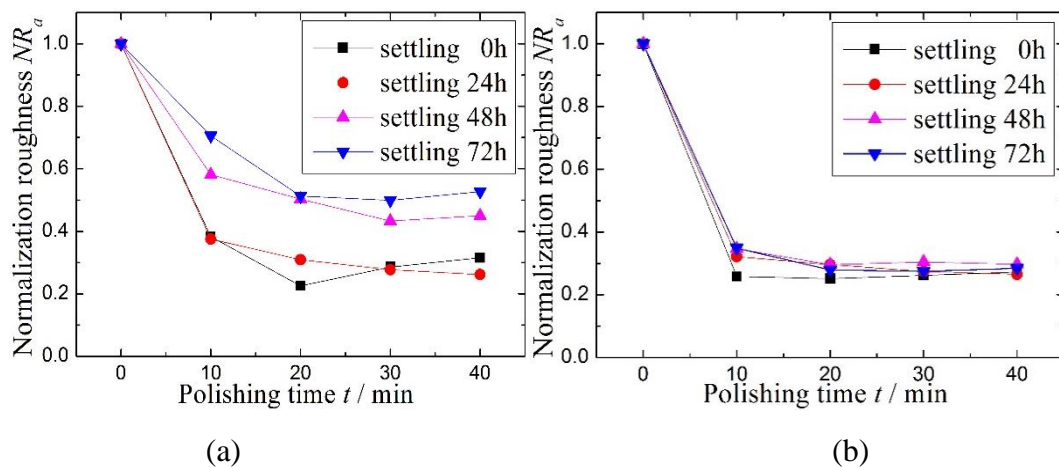


Fig. 3.5. Variations of normalized roughness NR_a during polishing for different settling times with (a) conventional MCF slurry and (b) new one.

Therefore, both the MCF slurries with the different settling times of 0h and 72h were

observed using digital camera and SEM followed by element mapping with EDS (Energy Dispersive X-ray Spectrometer) technique. Fig. 3.6 shows the optical images of the conventional (a) and new slurry (b) with settling time of 0h (left sides) and 72h (right sides). Evidently, the conventional slurry discolored to be reddish/brown after left for 72h. By contrast, the discolored area was very small on the new slurry even the settling time reached 72h. These phenomena indicate that heavy rust happen on the uncoated CIPs, leading to the deterioration of the performance of the conventional slurry. In order to further confirm this issue, the SEM images of the uncoated and ZrO_2 -coated CIPs were obtained and the element mapping for the SEM images were carried out. In the SEM observation and the element mapping, the MCF slurries were firstly dried under atmospheric configuration and then put into the chamber of SEM for observation and mapping.



(a)



(b)

Fig. 3.6. Photographs of conventional MCF slurry (a) and new one (b) with settling times of 0 h(left) and 72 h (right).

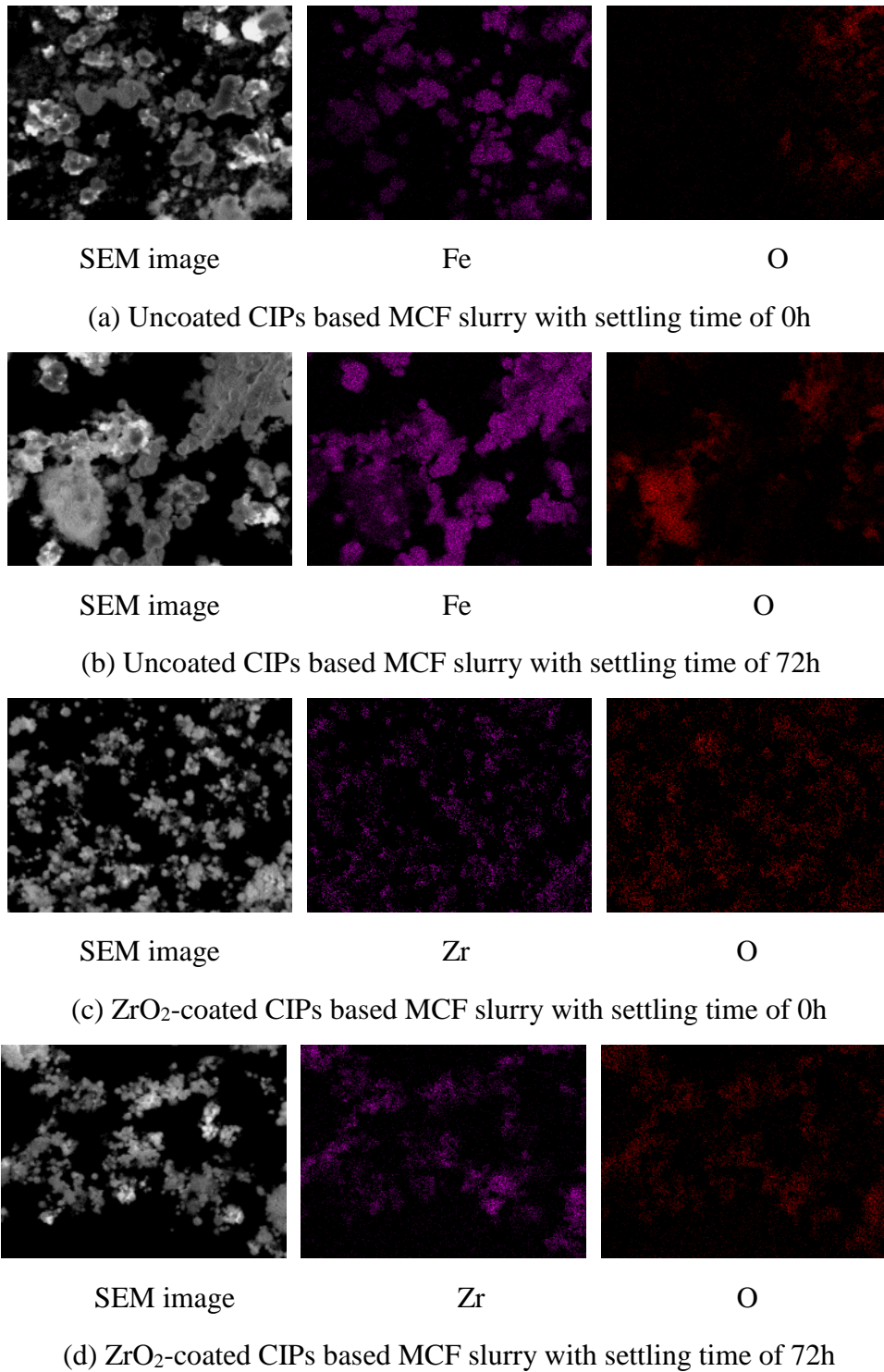


Fig. 3.7. SEM images and element mapping results

Figs. 3.7(a)-(d) show the SEM images and the element mapping results of the slurries with settling times of 0h and 72h, respectively. Comparing Fig. 3.7(a) with Fig. 3.7(b) shows that when the settling time is 0h, oxygen was detected on a small part of the CIPs,

whereas once the slurry was left for 72h, on most of the CIPs the oxygen was observed, indicating the uncoated-CIPs were heavily oxidized. However, very little difference was observed between the oxygen distributions of the ZrO₂-coated CIPs based MCF slurry with settling time of 0h (Fig.3.7(c)) and 72h (Fig.3.7(d)), confirming that little rust happen on the ZrO₂-coated CIPs and hence the performance of the new MCF slurry maintained for a long time. This means the uncoated CIPs within the conventional MCF slurry have been oxidized heavily whilst very few ZrO₂-coated CIPs within the new slurry have been oxidized because the ZrO₂ layer of several nm in thickness prevent the CIPs from being oxidized in the aqueous configuration.

A new MCF slurry was proposed by replacing the uncoated-CIPs within the conventional MCF slurry with the ZrO₂-coated CIPs, and its performance in the nano-precision polishing of oxygen-free copper was investigated experimentally. The obtained results showed that (1) The work-surface finish polished with the new slurry was in the same level as that with the conventional one when the settling time was less than 24h; (2) As the settling time increased the uncoated-CIPs within the conventional MCF slurry got rusty, leading to a deterioration in the slurry performance; (3) little rust was observed on ZrO₂-coated CIPs even the settling time reached several days, indicating the employment of ZrO₂-coated CIPs prolonged the working-life of the MCF slurry greatly.

3.2 Polishing of non-magnetic work-surface (oxygen-free copper)

Oxygen-free copper (OFC), as one of the major commercial engineering materials, is extensively used in various industries such as electronics and chemical industries, in particular, very suitable as the base material for molds/dies used in hot-press and/or injection molding of plastic lens due to its excellent electrical and thermal conductivities, high ductility, high impact strength and good creep resistance [11]. In the fabrication of molds/dies, nano-precision polishing is essential as the final process. Conventionally, OFC and its alloys are generally polished with a chemical polishing

method [12-13] to eliminate breaks, cracks and damaged layers on the work surface caused by the previous process (i.e. cutting or grinding). However, the chemical polishing technique has a shortage that the extraneous elements are usually introduced on the work surface when the chemical reaction is induced to improve the surface roughness. Hence, it is very hard to expect that the OFC-made molds/dies finished by chemical polishing process have high performance in molding of lens.

Against these problems, in the current work, a novel polishing method using magnetic compound fluid (MCF) based slurry (hereafter called MCF slurry for simplicity) is proposed. The MCF is produced by mixing the magnetic fluid (MF) containing nanometer size magnetite particles and magnetorheological fluid (MRF) containing micron size carbonyl iron powder (CIP) in the same base solvent, and exhibits higher magnetic pressure and apparent viscosity and a more stable distribution of particles under a magnetic field, while maintaining a fluid-like behavior [14]. Further mixing abrasive particles and α -cellulose into the MCF yields the MCF slurry [15-16]. The MCF slurry has been successfully used for polishing stainless steel and acrylic resin flat surfaces with nano-precision and scratch-free work-surfaces under a static and/or dynamic magnetic field [4, 17]. In particular, it was found that the MCF slurry can perform better under a rotary magnetic field [10]. It is, therefore, expected that the MCF slurry under a rotary magnetic field would be effectively employed for the nano-precision surface finishing of OFC. In this study, the effects of process parameters such as MCF slurry composition, relative motion of MCF slurry to workpiece and clearance between workpiece and MCF slurry on work-surface roughness and material removal were experimentally investigated.

3.2.1 Experimental procedure and conditions

Polishing tests were performed on the constructed experimental rig. Flat OFC plates with dimensions of L50×W50×T3 mm were used as the workpiece in

experiments. The purpose of this research was to investigate the effects of process parameters including MCF slurry composition, workpiece oscillation frequency f and clearance Δ on work-surface roughness and material removal. Therefore, four kinds of water-based MCF slurries with different compositions were prepared as shown in Table 1 to reveal how the composition of MCF slurry affects the surface roughness and material removal. Table 2 lists the experimental parameters; experiments were performed at different frequencies/corresponding amplitudes and clearances but with a constant magnet revolution speed and MCF slurry supplying amount to study the effects of the relative motion and the clearance on the polishing characteristics.

Polishing tests were performed on the constructed experimental rig. Flat OFC plates with dimensions of L50×W50×T3 mm were used as the workpiece in experiments. The purpose of this research was to investigate the effects of process parameters including MCF slurry composition, workpiece oscillation frequency f and clearance Δ on work-surface roughness and material removal. Therefore, four kinds of water-based MCF slurries with different compositions were prepared as shown in Table 3.2 to reveal how the composition of MCF slurry affects the surface roughness and material removal. Table 3.3 lists the experiment parameters; experiments were performed at different frequencies/corresponding amplitudes and clearances but with a constant magnet rotation speed and MCF slurry supply to study the effects of the relative motion and the clearance on the polishing characteristics.

Table 3.2 Compositions of MCF slurry

	MCF1	MCF2	MCF3	MCF4
Water-based Magnetic fluid (MF)	45 wt.%	43 wt.%	40 wt.%	33 wt.%
Abrasive particle (Al_2O_3 , $\phi 1\mu m$)	12 wt.%	12 wt.%	12 wt.%	12 wt.%
α -Cellulose	3 wt.%	3 wt.%	3 wt.%	3 wt.%
Carbonyl iron powder, $\phi 7\mu m$	40 wt.%	42 wt.%	45 wt.%	52 wt.%

Table 3.3 Experimental conditions

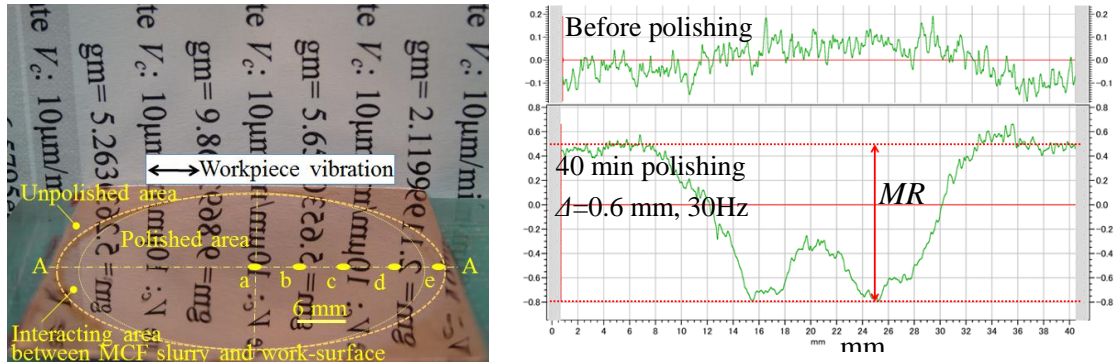
Frequency (f)/Amplitude (A_{p-p})	0Hz/0mm _{p-p} , 15Hz/5mm _{p-p} , 30Hz/4mm _{p-p} , 45Hz/2mm _{p-p}
Magnet	Nd-Fe-B: B=0.45 T Rotational speed: $n_m=1,000$ rpm
Amount of MCF slurry supplied	1 mL
Clearance (Δ)	0.6, 0.8, 1.0, 1.2 mm

Prior to the characterization of the polished work-surface with measuring instruments, the workpiece polished was washed with water followed by ultrasonic cleaning in ethyl at 25 °C for 3 min. Then the cross section profile of the polished area was measured utilizing a surface profile (Taylor Hobson, Form Talysurf Intra 2) to determine the material removal. Finally the surface roughness was measured using a white-light interferometer (Zygo Newview 600 by Zygo Corp.).

3.2.2 Results and discussion

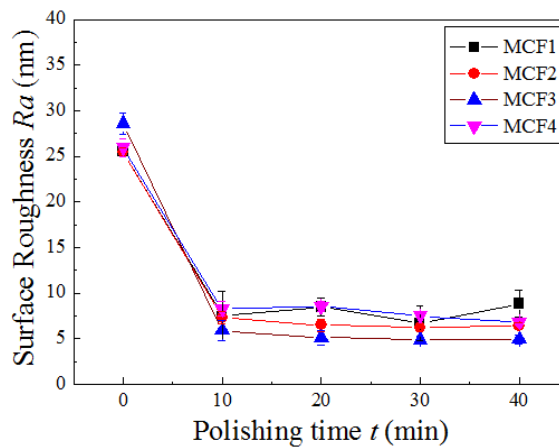
Figs. 3.8 (a) and (b) show the photo of a typical work-surface and the measured cross section profile polished with MCF3 at 30Hz/4mm_{p-p} and $\Delta=1.0$ mm. Evidently, an elliptic polished area (Fig. 3.8 (a)) was obtained that was formed by the overlap of the circular interacting area [10] between the MCF slurry and the work-surface when the workpiece oscillated with an amplitude of 2 mm. It was supposed that even the polishing conditions are the same, the work-surface finish is different at different positions on the polished area, hence the surface roughness were measured at five different positions (a -e in Fig.3.8 (a)) from the center to the edge of the area along the oscillation direction and the average value of them was obtained to be regarded as the surface roughness under the given conditions. Fig. 3.8 (b) shows A-A cross section profiles before and after 40 min polishing. The shape of work surface was like a conical mountain with a height of about 300 nm before polishing. After 40 min polishing it became a characteristic symmetrical W-shape. Around the central area of the polishing

spot, the material removal was less than the circle area with a radius of about 4.5 mm. For simplicity, the maximum depth of the polished area is hereafter regarded as the material removal MR in this research.

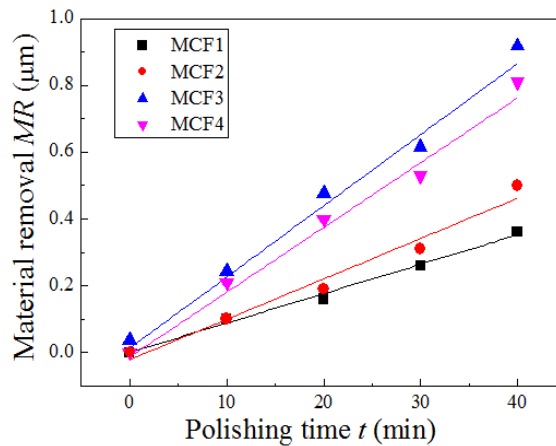


(a) Photo of a work-surface polished (b) A-A cross section profile

Fig. 3.8 A typical work-surface polished for 40 min with MCF3 at 30Hz/4 mm_{p-p}.



(a)



(b)

Fig. 3.9 Effects of compositions of slurry on (a) surface roughness and (b) material removal ($\Delta = 1.0 \text{ mm}$, $f = 30 \text{ Hz}$).

Effects of MCF slurry composition on surface roughness and material removal.

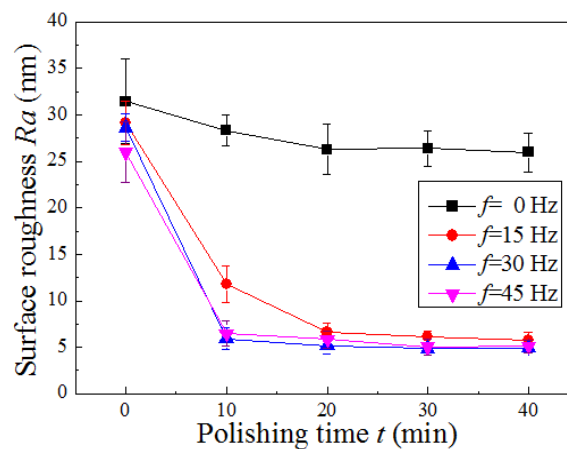
Polishing operations with different slurries were performed at $\Delta = 1.0$ mm and $f/A_{p-p} = 30\text{Hz}/4$ mm_{p-p}. Figs. 3.9 (a) and (b) show the variations of the surface roughness Ra and the material removal MR during polishing with different MCF slurries. The surface decrease rates were 65.2%, 74.9%, 82.8% and 73.8%, respectively, with MCF1 (40 wt. % of CIP), MCF2 (42 wt. % of CIP), MCF2 (45 wt. % of CIP) and MCF4 (52 wt. % of CIP). The highest roughness decrease rate was achieved by using MCF3. This indicates that in order to achieve the high decrease rate, the concentration of CIP should be determined at the optimum value. From Fig. 3.9 (b), it can be observed that the MR increased with the increase of polishing time and the relationship between the MR and polishing time t is linear under the given experimental conditions. The MR increases more quickly with MCF3 than the others. These indicate that the concentration of CIP should be determined at the optimum value, and the optimum concentration of CIP was 45 wt. % in current experiment. When the CIP concentration is low, the viscosity of the slurry under a magnetic field is not high enough to hold the abrasive particles strongly and hence the micro-cutting action of abrasive particles is weakened, resulting in the low roughness decrease rate and low material removal. By contrast, as the concentration of CIP gets high, the viscosity of slurry becomes large under the magnetic field and hence the magnetic clusters are difficult to be formed uniformly, resulting in the uneven distribution of abrasive particles, leading to the deterioration of the slurry performance. These are considered to be the reason why the MCF3 has the best polishing performance.

Effect of frequency f on surface roughness Ra and material removal MR .

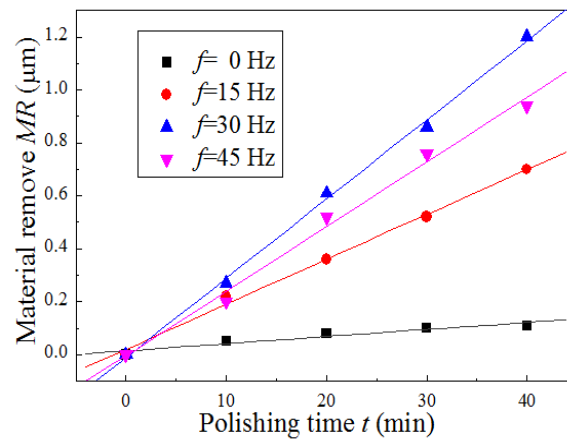
On the variations of the surface roughness and material removal with polishing time under different workpiece oscillation frequency f , the experimental results are as shown in Fig. 3.10. It can be observed from Fig. 3.10 (a) that the higher quality improvement rate and smaller final surface roughness Ra have been achieved with frequency than

without frequency. The roughness decrease rates reached 17.5%, 80.2%, 82.8% and 80.3%, respectively, at $f=0$ Hz, $f=15$ Hz, $f=30$ Hz and $f=45$ Hz. Obviously, the highest roughness decrease rate was obtain at $f=30$ Hz, meaning that in the current experimental configuration if the value of f is larger or smaller than 30 Hz, the surface finishing will be worse compared at 30 Hz.

The Ra declines rapidly at first 10 minutes and then levels off with frequency and shows a slow decline without frequency. The smoothest surface was achieved at frequency of $f=30$ Hz under the clearance $\Delta=1.0$ mm with MCF3.



(a)

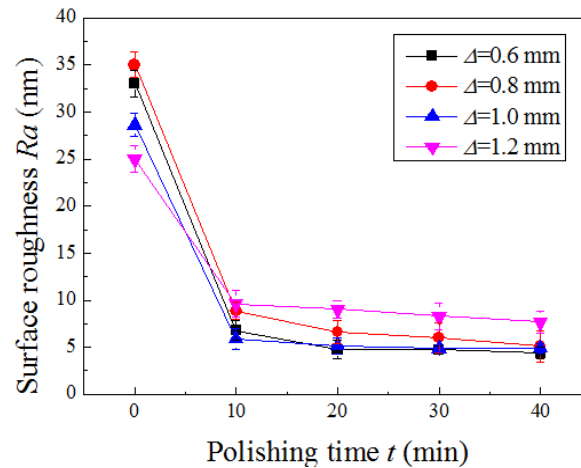


(b)

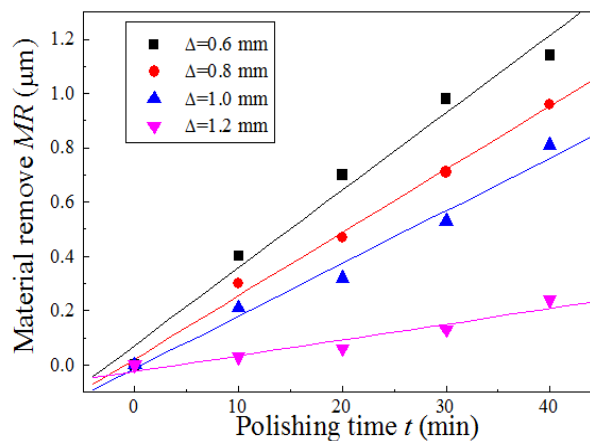
Fig. 3.10 Effects of frequency f on (a) surface roughness and (b) material removal ($\Delta=1.0$ mm, MCF3).

Fig. 3.10 (b) shows that the relationship between the MR and polishing time t is linear regardless of frequency. However the MR increases more quickly with frequency f than without frequency f . In particular, there is little material removal occurring when

the frequency $f=0$ Hz and the value of the MR is highest when the frequency $f=30$ Hz. According to the Preston hypothesis, the material removal is closely related to the pressure on the workpiece in the polishing zone and the relative velocity between the abrasive particle and the workpiece. In this part the constant MCF slurry and clearance was performed resulting in a constant pressure on the work-surface. The hypothesis revealed that the larger relative velocity was, the more MR became. The maximum relative velocity between the abrasive particle and workpiece reached 0.24 m/s, 0.38 m/s and 0.28 m/s, respectively, at $f=15$ Hz, $f=30$ Hz and $f=45$ Hz. These results indicate that the frequency f is favor of material removal and obtaining a smooth surface during the process.



(a)



(b)

Fig. 3.11 Effects of clearance Δ on (a) surface roughness Ra and (b) material removal MR ($f=30$ Hz, MCF3).

Effect of clearances Δ on surface roughness Ra and material removal MR .

The variations of the surface roughness Ra and material removal D during polishing for different clearances between MCF carrier and workpiece are as shown in Fig. 3.11. Evidently, although the Ra values had a similar decreasing tendency for all the clearances during polishing, the highest decrease rate was attained at $\Delta=0.6$ mm and reached 86.7%, whilst the decrease rates were 85.4%, 82.8% and 69.3%, respectively, at $\Delta=0.8$ mm, 1.0 mm and 1.2 mm. In particular, when the clearance was set up at a large value (e.g. $\Delta=1.2$ mm), the surface roughness was decreased slowly. From Fig. 3.11(b), it was observed that the smaller clearance resulted in the higher material removal. The research revealed that the larger the clearance was, the smaller the polishing force became [10]. This is probably the reason why the surface roughness rate decrease larger and the material removal increase more quickly as the clearance got smaller.

A novel polishing method using MCF slurry was proposed for the nano-precision surface finishing of OFC materials. A polishing unit was constructed to carry out the proposed method. Experimental investigations on the effects of process parameters on surface roughness Ra and material removal MR were performed. The obtained results can be summarized as followings.

- (1) Regardless of the process parameters, the work-surface roughness decreases monotonously with polishing time; although the final roughness depends on the polishing conditions, the roughness of the best work-surface attained in the current work was less than 5 nm Ra .
- (2) The relationship between the MR and polishing time t is linear under the given conditions. Moreover, the MR s, i.e., the polishing depths, obtained with different parameters; the highest MR s, i.e., the greatest depths, were obtained at $f=30$ Hz, $A_p=4$ mm, $\Delta=0.6$ mm with a MCF slurry (45 wt.% of CIP, 12 wt.% of abrasive particle, 3 wt.% of α -cellulose, 40 wt.% of MF). In addition, the best surface was obtained in the polished region where the polished area was the deepest.

3.3 Polishing of magnetic work-surface (Ni-P plated STAVAX)

Nickel–phosphorus (Ni–P) plating has gained popularity in various fields such as the chemical, electronic, aerospace, automobile, resin, and mold industries due to its ability to produce coatings with excellent corrosion resistance, wear properties, hardness, and abrasion resistance. Ni–P plating is particularly useful for hot embossing metal molds/dies and injection metal molds/dies because it extends the working life of the molds/dies, thus reducing production costs [18-21]. Electroless Ni–P-plated molds/dies have been practiced with single-crystal diamond turning (SCDT) [22-25]. However, unwanted turning marks that reduce the surface quality of the mold frequently occur after SCDT. Therefore, the mold has to be further polished to nano-level surface roughness in order to eliminate the SCDT-induced tool marks. Although conventional fine grinding, lapping, and polishing processes are viable ways to accomplish this, the rigid abrasive particles tend to become embedded on the work surface when pressure is applied to soft materials such as optical polymers and potassium dihydrogen phosphate used to improve the surface finish [26]. Hence, it is difficult to finish Ni–P-plated surfaces via conventional polishing processes. Consequently, to improve the surface quality, it is imperative to develop a novel polishing method that effectively eliminates the excess material while preventing tool marks.

One promising surface finishing method is magnetic field-assisted polishing, in which an abrasive slurry based on a magnetic fluid (MF) or a magnetorheological (MR) fluid or magnetic abrasives (MAs) is employed. In these techniques, flexible chain-shaped magnetic clusters are immediately formed along the magnetic lines of force once a magnetic field has been applied. Abrasive particles within the slurry are consequently entrapped between clusters, forming a kind of flexible polishing tool. So far, many researchers have worked toward developing an alternative ultra-fine polishing technique with this kind of novel polishing tool. Tani et al. proposed an MF

polishing method, and they significantly improved the surface quality of a flat polypropylene workpiece [27]. Prokhorov and Kordonski presented an MR fluid composed of carbonyl iron particles (CIPs), non-magnetic abrasive particles (APs), carrier liquids, and indispensable stabilizers [28]. Juan et al. reported that once a magnetic field is applied, the particles within an MR fluid form anisometric aggregations that span the system along the magnetic lines of force [29]. The MR fluid can exhibit changes in apparent viscosity of several orders of magnitude into a kind of Bingham fluid under a magnetic field [30]. DeGroot et al. used an MR fluid to smooth a diamond-turned polymethacrylate part, and they obtained a smooth surface with a roughness (Ra) of 0.5 nm [31]. Although most of the above-mentioned works focused on the surface finishing of non-magnetic materials, a few researchers also attempted to smooth the ferromagnetic work-surface using MR fluid slurry or MAs slurry. For example, Singh et al. proposed a ball-end MR finishing tool and applied it to finish the flat ground surface of EN31 magnetic steel and attained the final surface roughness of Ra 19.7 nm after 120 min finishing [32-35]. Kawakubo K, et al. polished the SKD11 ferromagnetic material using an MAs slurry, and the attained best surface roughness reached Rz 1 μm [36] followed by Yin S, et al. who developed a new MAs slurry for ferromagnetic surface finishing [37]. These studies have demonstrated that magnetic field-assisted polishing using an MR fluid slurry or an MAs slurry is an excellent candidate for polishing soft magnetic Ni-P-plated molds. However, the mean diameter of abrasive particles within MAs slurry are usually in the order of tens to hundreds μm and significantly bigger than those within MF or MR fluid slurry, leading the clusters to be too stiff and too thick to finish the soft work-materials with nano-precision. This indicates that the MF slurry or MR fluid slurry is more favorable for the nano-precision surface finishing of ferromagnetic work-materials compared with the MAs slurry. Nevertheless, it should be noticed that under a given magnetic field, the particles are less stably distributed in an MR fluid slurry than in an MF slurry, whereas

the magnetic pressure and apparent viscosity of the former are larger than those of the latter, leading to difficulty in stabilizing their performance in surface finishing.

To overcome the respective disadvantages and to make use of the respective advantages of MF and MR fluid slurries, a novel slurry, named a magnetic compound fluid (MCF) slurry, was proposed by Shimada et al. [16]. In practice, this new slurry is produced by blending micrometer-size CIPs, APs, and α -cellulose whenever necessary into an MF containing nanometer-size magnetite particles. Hence, the behavior of the particles within the MCF slurry can be controlled by a magnetic field; the slurry exhibits a higher magnetic pressure and apparent viscosity and a more stable distribution of particles while maintaining fluid-like behavior. The MCF slurry shows a reversible and extremely fast transition from a Newtonian fluid to a Bingham fluid in the presence of external magnetic fields [4, 35]. Under a magnetic field, the magnetic particles are magnetized and attract others along the magnetic lines of force to form clusters of 0.1-0.2 mm in diameter and over 1.0 mm in length with a certain strength. A multitude of clusters and the APs distributed within the clusters together form some stronger magnetic brushes. When relative motion is applied between the work surface and the clusters, a polishing force is imposed on the workpiece owing to the induced friction between the workpiece and the APs. The micro-cutting action of the APs removes the work material [7]. In engineering applications, the MCF slurry has been successfully employed to polish various engineering materials. As an example, Guo et al. [36] performed the polishing of a PMMA specimen using a zirconia-coated CIP-based MCF slurry, and the results demonstrated that the work-surface roughness was improved on a nanometer level without causing scratches or the embedding of particles on the work surface. Wang et al. [37, 38] polished both a flat and a quintessential structured surface of an oxygen-free copper specimen using MCF slurries containing different CIPs, and they determined a strategy to prolong the slurry working life. Wu et al. [17, 39] succeeded in polishing an acrylic resin specimen with nano-precision using an MCF

slurry. However, these engineering materials were almost non-magnetic. Subsequently, Guo et al. [26] made an attempt to polish an electroless Ni–P-plated magnetic specimen using MCF slurry, and they found that an MCF slurry containing CIPs with a mean diameter of 1–2 μm and Al_2O_3 APs with a mean diameter of 1 μm was capable of removing tool marks, but it also resulted in the occurrence of scratches and the adhesion of CIPs on the work surface. This is therefore an obstacle both to material removal and to the improvement of the surface quality in MCF polishing of magnetic materials. In order to solve this problem, the same authors prepared an alternative MCF slurry, in which ZrO_2 -coated CIPs were employed instead of naked CIPs. This new formulation was successfully used to smooth the magnetic work surface without leaving scratches or the adhesion of particles. However, ZrO_2 -coated CIPs are still in the development phase, implying that this kind of new MCF slurry cannot yet be applied in the various industrial fields. Consequently, it is essential to find an MCF slurry containing naked CIPs for the nano-precision surface finishing of electroless Ni–P-plated STAVAX steel without particle adhesion or scratching on the work surface.

3.3.1 Polishing principle

Based on the research work by Shimada K. et al. [36], the polishing principle using an MCF slurry can be considered as schematically illustrated in Fig. 1. A disc-shaped permanent magnet is attached to the lower end face of its holder with an eccentricity of r . An MCF slurry carrier, i.e., an aluminum plate, is located below the magnet with a clearance of δ . When the magnet holder is rotated at a speed of $n\text{m}$, the magnet revolves around the axis of the holder at the same speed. Thereby, a dynamic magnetic field is generated, in which the magnetic flux density is constant but the magnetic lines of force constantly revolve around the magnet holder axis. Hereinafter, this kind of dynamic magnetic field is called the rotary magnetic field. Then, once a workpiece is located below the MCF slurry carrier with a working gap of Δ , an MCF polishing setup is

established.

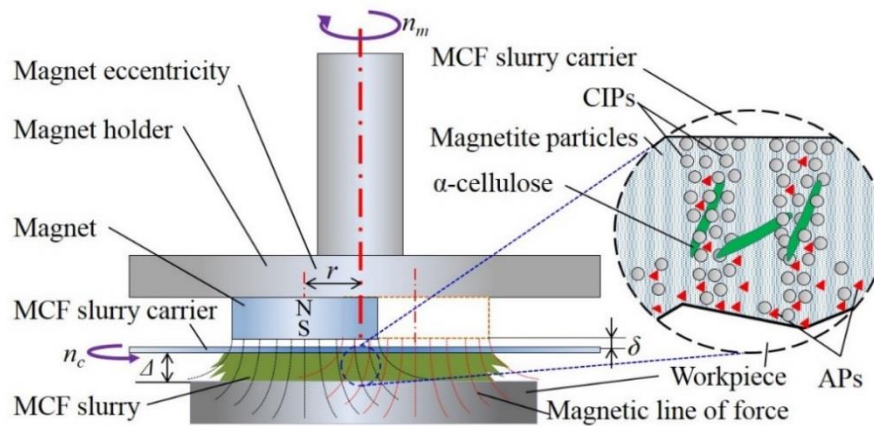


Fig. 3.12 Polishing principle of MCF polishing process

Once the working gap between the workpiece and the carrier has received a certain volume of MCF slurry, as shown in the right portion of Fig. 3.12, chain-shaped magnetic clusters composed of nanometer-size magnetite particles and micrometer-size CIPs are immediately formed along the magnetic lines of force. Non-magnetic APs are entrapped in the clusters or distributed between the clusters; α -cellulose fibers, if they are employed, are interwoven with the clusters. In addition, all of the clusters are forcibly collected by the magnetic attraction force and concentrated in the area where the magnetic field is the strongest. In the meantime, it is well known that in a magnetic field, non-magnetic substances suffer a so-called magnetic levitation force [40]; the gravitational force acts on the same substances. Therefore, under the combined effect of magnetic levitation and gravitational forces, the majority of non-magnetic APs within the MCF slurry move down towards the work surface, and a normal force is thus imposed on the workpiece. When the MCF carrier is rotationally driven at a speed of n_c , the clusters attracted to the lower surface of the carrier revolve around the carrier axis to bring rotational motion to the APs. Friction is thus induced between the workpiece and the APs, and the work material is removed by the micro-cutting action of the APs.

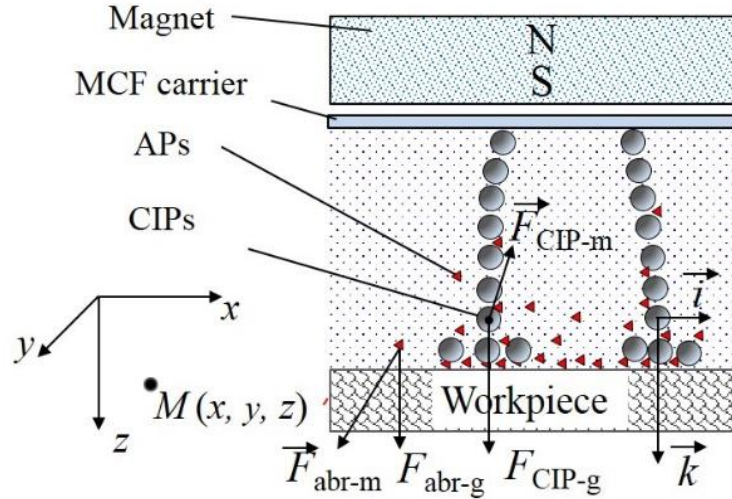


Fig. 3.13 The forces acting on a CIP and an AP under gravitational and magnetic fields.

3.3.2 Particle behavior analysis

3.3.2.1 CIP behavior

According to Li H [35], in MRF process, the CIPs within the magnetorheological fluid are subjected to the magnetic force, the gravitational force, the viscous resistance, the Van der Waals force and the buoyancy force. Among these forces, the magnetic force and the gravitational force are the primary factors to affect the behaviors of CIPs and APs during the polishing process. Based on this scenario, the resultant forces acting on the CIPs and APs and the behaviors of the two kind of particles in MCF polishing can be illustrated as in Fig. 2.

In the MCF polishing process, a magnetic field of H is applied to the MCF slurry. CIPs within the MCF slurry are consequently subjected to a magnetic force of

$$\vec{F}_{CIP-m} = \mu_0 (\vec{m} \cdot \nabla) \vec{H} \quad (3.1)$$

where μ_0 is the permeability of vacuum and \vec{m} is the magnetic dipole moment of the CIP because the CIP can be viewed as a magnetic dipole owing to its extremely small size [29].

The value of \vec{m} is further determined by the CIP volume, V_{CIP} , the CIP magnetic susceptibility, χ_m , the CIP magnetic permeability, μ , the permeability of vacuum, μ_0 ,

and the magnetic field, \vec{H} , as follows:

$$\vec{m} = V_{CIP} \chi_m \frac{3\mu_0}{(\mu + 2\mu_0)} \vec{H} \quad (3.2)$$

When a coordinate system (x, y, z) is defined as shown in Fig.3.13, the Hamiltonian operator ∇ is

$$\nabla = \frac{\partial}{\partial x} \vec{i} + \frac{\partial}{\partial y} \vec{j} + \frac{\partial}{\partial z} \vec{k} \quad (3.3)$$

where \vec{i} , \vec{j} , and \vec{k} are the unit vectors in the coordinate system, and the magnetic field vector is given by

$$\vec{H} = H_x \vec{i} + H_y \vec{j} + H_z \vec{k} \quad (3.4)$$

where H_x , H_y , and H_z are the components of the magnetic field in the x, y, and z directions, respectively. Subsequently substituting Eqs. (3.2)–(3.4) into Eq. (3.1) and re-arranging them yields the magnetic force acting on the CIP as

$$\vec{F}_{CIP-m} = F_{CIP-mx} \vec{i} + F_{CIP-my} \vec{j} + F_{CIP-mz} \vec{k} \quad (3.5)$$

$$\text{where } F_{CIP-mx} = \frac{3V_{CIP} \chi_m \mu_0^2}{\mu + 2\mu_0} \left[H_x \frac{\partial H_x}{\partial x} + H_y \frac{\partial H_x}{\partial y} + H_z \frac{\partial H_x}{\partial z} \right] \quad (3.6)$$

$$F_{CIP-my} = \frac{3V_{CIP} \chi_m \mu_0^2}{\mu + 2\mu_0} \left[H_x \frac{\partial H_y}{\partial x} + H_y \frac{\partial H_y}{\partial y} + H_z \frac{\partial H_y}{\partial z} \right] \quad (3.7)$$

$$F_{CIP-mz} = \frac{3V_{CIP} \chi_m \mu_0^2}{\mu + 2\mu_0} \left[H_x \frac{\partial H_z}{\partial x} + H_y \frac{\partial H_z}{\partial y} + H_z \frac{\partial H_z}{\partial z} \right] \quad (3.8)$$

are the components of the magnetic force in the x, y, and z directions, respectively.

In the current work, attention is paid only to the z direction because the adhesion of CIPs on the work surface is dominantly attributed to the behavior of CIPs in the vertical (i.e., z) direction. In the z direction, in addition to the vertical component of the magnetic force, F_{CIP-mz} , a CIP is subjected as well to the gravitational force given by

$$F_{CIP-g} = V_{CIP} \rho_{CIP} g \quad (3.9)$$

where ρ_{CIP} is the mass density of the CIP and g is the gravitational acceleration.

Consequently, the resultant vertical force on the CIP would be

$$F_{CIP-z} = F_{CIP-mz} + F_{CIP-g} = \frac{3V_{CIP} \chi_m \mu_0^2}{\mu + 2\mu_0} \left(H_x \frac{\partial H_z}{\partial x} + H_y \frac{\partial H_z}{\partial y} + H_z \frac{\partial H_z}{\partial z} \right) + V_{CIP} \rho_{CIP} g \quad (3.10)$$

Under the application of F_{CIP-z} , the CIP would behave vertically in one of three

patterns according to the value of FCIP-z:

1) If FCIP-z = 0, no vertical motion occurs on the CIP and the CIP remains in its original vertical position.

2) If FCIP-z > 0, the CIP moves downward toward the work surface.

3) If FCIP-z < 0, the CIP moves upward away from the work surface.

Eq. (3.8) shows that the vertical magnetic force on the CIP is affected not only by the magnetic field strength but also by the magnetic field gradient. In order to further determine FCIP-z, the strength and gradient of the magnetic field will be discussed in detail by magnetic field analysis simulation in the next section.

3.3.2.2 Abrasive particles behavior

In the MCF polishing process, the forces acting on an AP are also shown in Fig.

2. There is gravity determined by

$$F_{abr-g} = V_{abr} \rho_{abr} g \quad (3.11)$$

where V_{abr} and ρ_{abr} are the volume and the mass density of the AP, respectively.

In addition, when an AP within the MCF slurry is under a magnetic field, \vec{H} , a magnetic levitation force, F_{abr-m} , will be exerted on the AP. F_{abr-m} is proportional to the magnetic field gradient as given by [41].

$$\vec{F}_{abr-m} = -\mu_0 V_{abr} (\vec{M} \cdot \nabla) \vec{H} \quad (3.12)$$

where V_{abr} is the volume of the AP and $\vec{M} = \chi_m \vec{H}$ is the magnetization intensity of the magnetic fluid (χ_m is the MCF magnetic susceptibility). Subsequently, substituting Eq. (3.4) into Eq. (3.12) and rearranging them yields the equation for determining the vertical (z direction) component of F_{abr-m} as follows:

$$F_{abr-mz} = -\mu_0 V_{abr} \chi_m' \left[H_x \frac{\partial H_z}{\partial x} + H_y \frac{\partial H_z}{\partial y} + H_z \frac{\partial H_z}{\partial z} \right] \quad (3.13)$$

Thus, the resultant vertical force on the AP would be

$$F_{abr-z} = F_{abr-g} + F_{abr-mz} = V_{abr} \rho_{abr} g - \mu_0 V_{abr} \chi_m' \left(H_x \frac{\partial H_z}{\partial x} + H_y \frac{\partial H_z}{\partial y} + H_z \frac{\partial H_z}{\partial z} \right) \quad (3.14)$$

3.3.3 Distributions of CIPs and APs on the work surface

In the MCF polishing process, one of the most important factors affecting material removal is the amount of active APs acting on the work surface. In this section, therefore, the distribution of APs on the work surface is discussed.

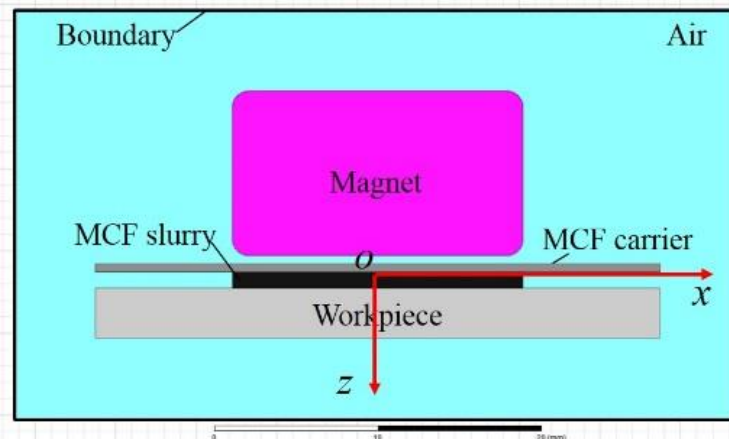


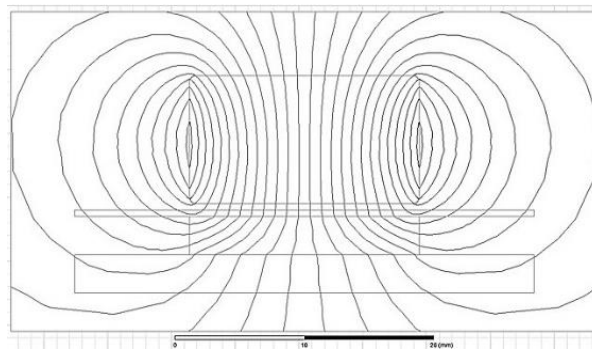
Fig. 3.14 Magnetic field analysis model.

According to Eqs. (3.10) and (3.14), in order to determine whether the resultant vertical force acts on the CIP and AP either upward or downward, all three components of the magnetic field, H_x , H_y , and H_z , and the gradients of the z component, H_z , in the x , y , and z directions, $\partial H_z / \partial x$, $\partial H_z / \partial y$, $\partial H_z / \partial z$, should already be known. For this purpose, magnetostatic finite element analysis was carried out. Fig. 3.14 shows the magnetic field analysis model in air medium developed based on the polishing principle (Fig. 3.12). Let the origin of the xyz -coordinate system O be at the point where the axis of the disc-shaped permanent magnet intersects with the lower surface of the MCF carrier and the z and x axes are along the magnet axis and the direction parallel to the magnet radial, respectively. The balloon boundary was adopted in this simulation. In this model, as tabulated in Table 3.4, the magnet was assigned as Nd–Fe, with dimensions of $\phi 16 \text{ mm} \times t 10 \text{ mm}$, a relative permeability of 1.09977, and a magnitude of -8.9×10^5 . The material of the MCF carrier was aluminum, with a relative permeability of 1. The relative permeability of the MCF slurry was assigned as 5. In regards to the work materials, nickel was used for the magnetic workpiece, with the

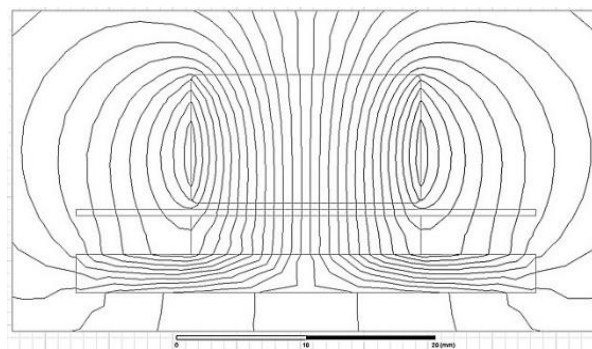
relative permeability of 600, and copper was used for the non-magnetic one, with a relative permeability of 1.

Table 3.4 Assigned parameters to magnetostatic field model.

	Material	Relative permeability	Magnitude (A/meter)
Magnet ($\phi 16 \text{ mm} \times t 10 \text{ mm}$)	Nd-Fe	1.09977	-8.9×10^5
MCF carrier	Aluminum	1	
Polishing fluid	MCF slurry	5	
Magnetic workpiece	Nickel	600	
Nonmagnetic workpiece	Copper	1	



(a) Non-magnetic workpiece, $\Delta=3 \text{ mm}$



(b) Magnetic workpiece, $\Delta=3 \text{ mm}$

Fig. 3.15 Typical finite element analysis results showing the magnetic flux distributions at a working gap of $\Delta = 3 \text{ mm}$ for a (a) non-magnetic and (b) magnetic workpiece.

Based on the developed model, the magnetostatic simulation was executed using Maxwell software to obtain the magnetic field distribution around the polishing zone at

different working gaps for the non-magnetic and magnetic workpiece. Figs. 3.15 (a) and (b) exhibit the obtained typical simulation results, showing the magnetic flux distributions with non-magnetic and magnetic workpieces, respectively, at a working gap of $\Delta = 3$ mm.

Comparing Fig. 3.15(a) to Fig. 3.15(b) reveals that the magnetic flux distribution with the non-magnetic workpiece differs from that with the magnetic workpiece. However, regardless of the work material, the distribution of the magnetic flux generated by the disc-shaped permanent magnet showed axial symmetry. In this kind of magnetic field, at an arbitrary position in any cross section that passes through the center of the magnet, e.g., the XOZ plane (Fig. 3.14), the y component of the magnetic field, H_y , would be zero, i.e., $H_y = 0$. Thus, substituting $H_y = 0$ into Eqs. (3.10) and (3.14) yields the vertical magnetic forces acting on CIPs and APs located at arbitrary positions in the XOZ plane, as expressed by Eqs. (3.15) and (3.16), respectively.

$$F_{CIP-z} = F_{CIP-mz} + F_{CIP-g} = \frac{3V_{CIP}\chi_m\mu_0}{\mu + 2\mu_0} \left(H_x \frac{\partial H_z}{\partial x} + H_z \frac{\partial H_x}{\partial z} \right) + V_{CIP}\rho_{CIP}g \quad (3.15)$$

$$F_{abr-z} = F_{abr-g} + F_{abr-mz} = V_{abr}\rho_{abr}g - \mu_0 V_{abr}\chi'_m \left(H_x \frac{\partial H_z}{\partial x} + H_z \frac{\partial H_x}{\partial z} \right) \quad (3.16)$$

Consequently, the values of H_x and H_z and the z component's gradients, $\partial H_z/\partial x$ and $\partial H_x/\partial z$, in the x and z directions, respectively, were obtained from the data of Fig. 3.15 by means of the post-processing function of the Maxwell software. The obtained typical results are shown in Fig. 3.16. Figs. 3.16(a) and (b) show the distributions of H_x and H_z on the work surface in the x direction for different workpieces with working gaps of $\Delta = 1, 2,$ and 3 mm, respectively. Beside them, the similar distribution of H_z in the z direction is also presented in Fig. 3.16(c).

It can be seen first from Fig. 3.16(a) that for non-magnetic copper, the absolute value of H_x increases at the x position closer to the magnet edge and that the value decreases as the working gap increases, whereas for magnetic nickel, the value of H_x is zero, regardless of the working gap and the x position. Fig. 3.16(b) reveals that for magnetic nickel, the absolute value of H_z decreases at the x position closer to the

magnet edge, regardless of the working gap, whereas when the workpiece material is copper, the value of H_z is slightly higher at the x position close to the magnet edge. Besides, for either the magnetic nickel or the non-magnetic copper, the larger the working gap, the smaller the value of H_z . As for the distribution of H_z along the z direction, Fig. 3.16(c) demonstrates that the absolute value of H_z tends to decrease as z increases, implying that at a position closer to the work surface, H_z decreases. However, the effect of the working gap on H_z with the magnetic nickel differs from that with the non-magnetic copper; for nickel, the value of H_z decreases as the working gap increases, a tendency similar to that of H_x and H_z in the x direction [Figs. 3.16(a) and (b), respectively], whereas for copper the tendency is reversed. In addition, it is generally worth noting that for magnetic nickel, the values of H_z in either the x or the z direction are much higher than those for the non-magnetic copper.

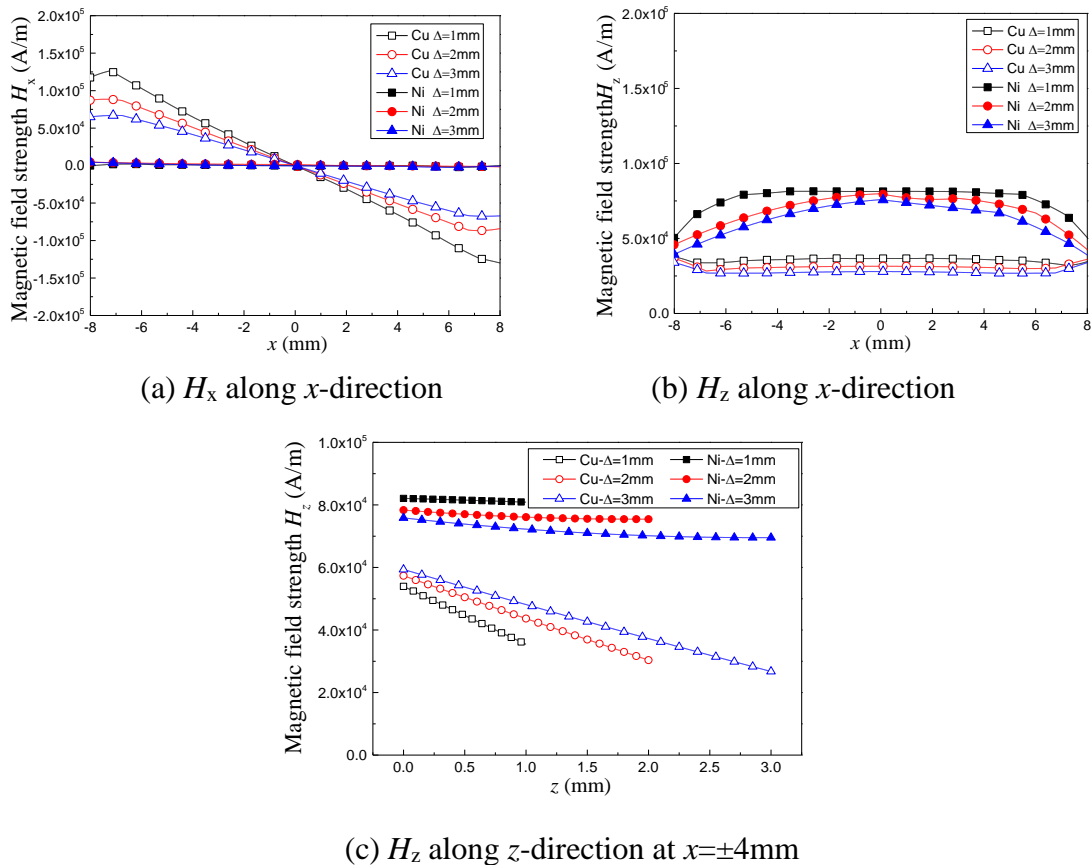


Fig. 3.16 Distribution of magnetic field strengths on the work surface along the x or z direction with different working gaps for different workpieces.

Then, using the data in Fig. 3.16, the gradients of the z component of the magnetic field H_z in the x and z directions, $\partial H_z/\partial x$ and $\partial H_z/\partial z$, at different x positions were obtained as shown in Figs. 3.17(a) and (b), respectively. Fig. 3.17(a) shows that with non-magnetic copper, the absolute gradient $\partial H_z/\partial x$ rapidly decreases from its maximum value at the magnet edge to zero at a position approximately 2 mm from the magnet edge, after which it remains zero. On the other hand, with the magnetic nickel, the absolute value of $\partial H_z/\partial x$ gradually increases from zero at the position $x = 0$ mm, i.e., at the magnet center, to its maximum value at the magnet edge. However, the working gap also has a slight effect on the distribution. $\partial H_z/\partial z$ shows a similar tendency, regardless of the work material and working gap, in that at a position close to the magnet edge, the value of $\partial H_z/\partial x$ rapidly varies, whereas in the other position, $\partial H_z/\partial x$ varies little. In addition, the working gap affects $\partial H_z/\partial x$, regardless of the work material, with non-magnetic copper having a stronger effect than magnetic nickel.

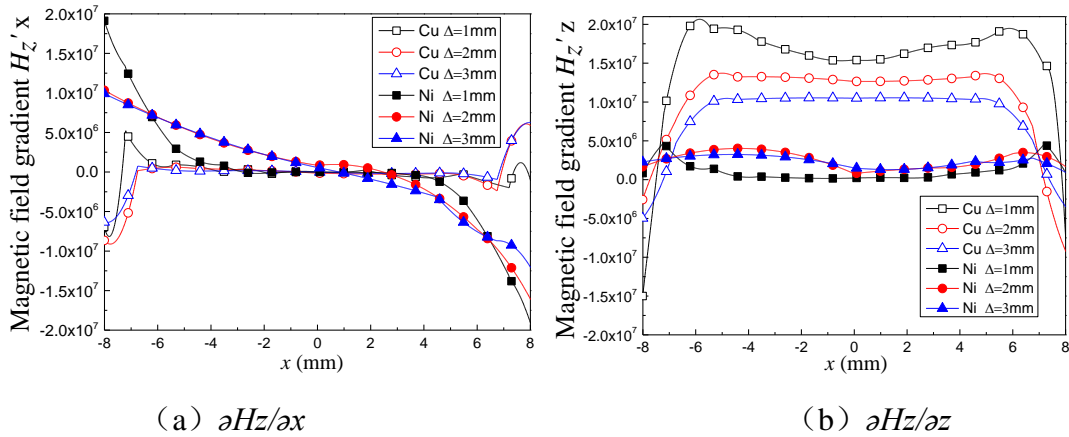
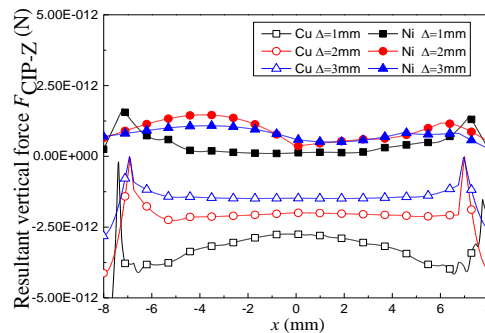


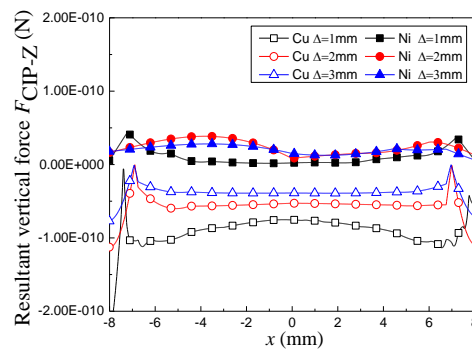
Fig. 3.17 Distributions of the magnetic field gradient along the x direction at different working gaps with different work materials.

Consequently, for example, setting the permeability of vacuum, μ_0 , the magnetic permeability of CIP, μ , and the magnetic susceptibility of CIP, χ_m , to $\mu_0 = 4\pi \times 10^{-7}$ N/A², $\mu = 5.03 \times 10^{-4}$ N/A², $\chi_m = 1 \times 10^3$, $\rho_{\text{CIP}} = 7.8 \times 10^{-3}$ kg/m³, $g = 9.8$ m/s², and the CIP diameter of dCIP (VCIP) at dCIP = 1 μm (VCIP = 5.24×10^{-1} μm^3) (Brand: HQ), 3 μm (VCIP = 1.41 μm^3) (Brand: ES), and 7 μm (VCIP = 1.8×10^2 μm^3) (Brand: CS), substituting the data in Figs. 3.5 and 3.6 into Eq. (15) yields the vertical forces on

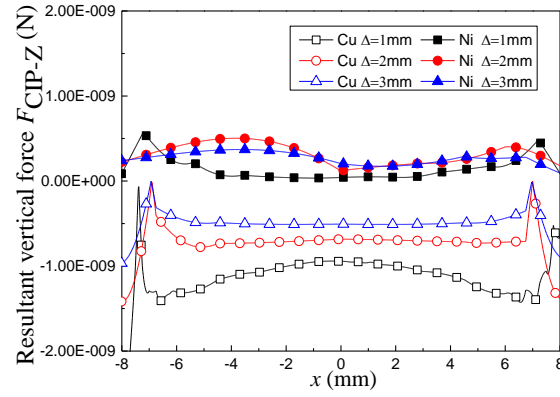
a CIP located on the work surface at different x positions, as shown in Figs. 3.18(a), (b), and (c) for HQ, ES, and CS CIPs, respectively. According to Fig. 3.18, generally speaking, the F_{CIP-z} values reached their respective peaks at positions close to the magnet edge, where $x = \pm 8$ mm, whereas at other positions, the difference between the forces at different positions is small. It is very important to notice that with the non-magnetic copper, all the values of F_{CIP-z} , including the peaks around the magnet edge, are less than zero, i.e., $F_{CIP-z} < 0$, indicating that the CIPs are moving upward away from the work surface owing to the resultant vertical force acting downward on the CIPs. By contrast, with the magnetic nickel at all the x positions, $F_{CIP-z} > 0$, indicating that the CIPs are moving downward to the work surface. In particular, a comparison of the data shown in Fig. 3.18(a) with that shown in Fig. 3.18(b) reveals that with the magnetic nickel, the resultant vertical force acting on CS CIPs with diameters of $7 \mu\text{m}$ is larger than that acting on HQ CIPs by three orders of magnitude, implying that CS CIPs would hold the abrasive particles much more strongly as compared to HQ CIPs during MCF polishing.



(a) HQ



(b) ES



(c) CS

Fig. 3.18 Forces F_{CIP-z} at different positions in the x direction with different workpieces at different working gaps.

In addition, assuming that APs are spherical with a diameter of $d_{abr} = 1 \mu\text{m}$ ($V_{abr} = 5.24 \times 10^{-1} \mu\text{m}^3$) and a mass density of $\rho_{abr} = 3.965 \times 10^{-3} \text{kg/m}^3$ and that the MF magnetic susceptibility is $\chi'_m = 0.669$, the vertical force F_{abr-z} on the APs was obtained by substituting the data in Figs. 3.16 and 3.17 into Eq. (3.16); the results are shown in Fig. 3.19. It can be seen that, regardless of the working gap, F_{abr-z} is different at different x positions for both the magnetic nickel and the non-magnetic copper. However, it should be noted that with the magnetic nickel, F_{abr-z} is less than zero at all the x positions, resulting in the upward motion of APs away from the work surface. By contrast, with the non-magnetic copper, because of $F_{abr-z} > 0$, the APs move downward toward the work surface.

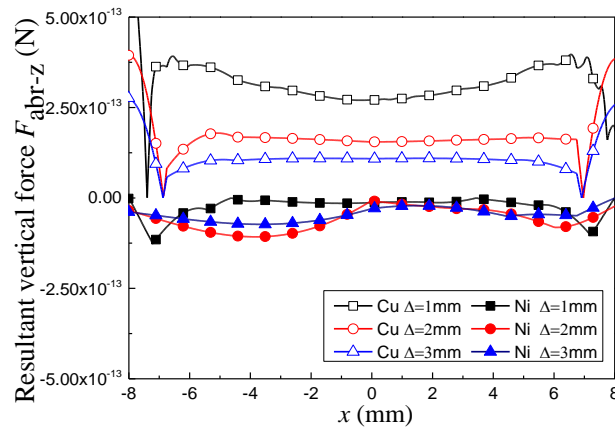


Fig. 3.19 F_{abr-z} at different positions in the x direction.

According to the aforementioned discussions on the resultant vertical forces acting on the CIPs and APs, the behavior and resultant distribution of CIPs and APs on the magnetic and non-magnetic work surfaces are illustrated in Figs. 3.20(a) and (b), respectively. With the magnetic workpiece [Fig. 3.20(a)], the resultant vertical force on the CIPs is $F_{CIP-z} > 0$ (Fig. 3.18), leading to the downward motion of CIPs to the work surface. Eventually, a mass of CIPs will collect on the work surface due to F_{CIP-z} . In the meantime, the APs are pushed away from the work surface because $F_{AP-z} < 0$ (Fig. 3.19), resulting in a decrease in the amount of active APs engaged in the material removal.

By contrast, with the non-magnetic workpiece [Fig. 3.20 (b)], the resultant vertical force on the CIPs is $F_{CIP-z} < 0$ (Fig. 3.18), leading to the upward motion of CIPs away from the work surface. At the same time, the APs are subjected to a downward vertical force, F_{AP-z} , and hence they tend to move toward the work surface, resulting in a large amount of APs participating in the material removal.

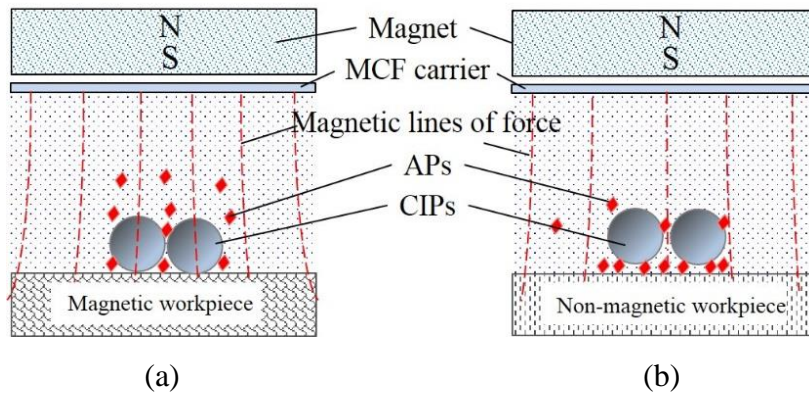


Fig. 3.20 The distribution model of CIPs and APs on magnetic/non-magnetic work surfaces.

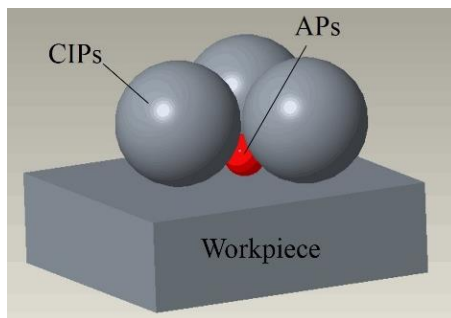
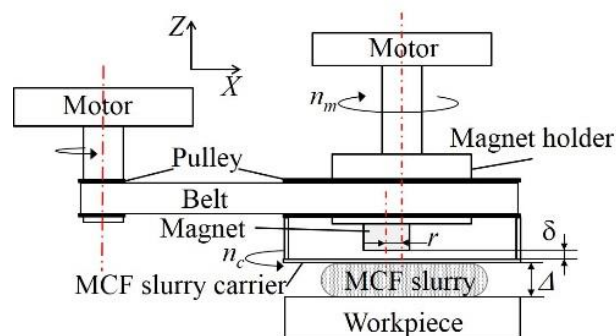


Fig. 3.21 Effective accommodation space between CIPs and the work surface.

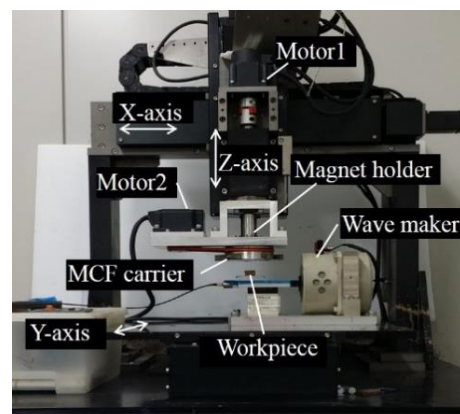
As discussed above, when the workpiece is a magnetic material, the CIPs are strongly attracted to the work surface due to the downward force of FCIP-z, and thus the spaces vacated by APs were taken over by CIPs. Consequently, as illustrated in Fig. 3.21, only the space between three adjoining CIPs and the work surface is available for accommodating the active APs. However, the size of the AP should not be larger than this space, which depends on the CIP size; otherwise, the AP cannot be accommodated within this space and thus cannot participate in material removal. From the geometrical layout of the CIPs and the workpiece, it was determined that if the CIP diameter is d_{CIP} , the AP diameter, d_{abr} , should be smaller than $d_{CIP}/3$ in order to accommodate the AP within this space; the smaller the AP is, the greater the amount of APs that can be accommodated within this space. As an example, with CIP diameters of 7, 3, and 1 μm , the maximum diameter of the containable APs is 2.35, 1, and 0.33 μm , respectively. Hence, there are numerous APs in the effective accommodation space when the CIP diameter is bigger. In other words, there is not enough space to accommodate 1 μm APs between CIPs 1 μm in diameter and the work surface.

3.3.4 Experimental

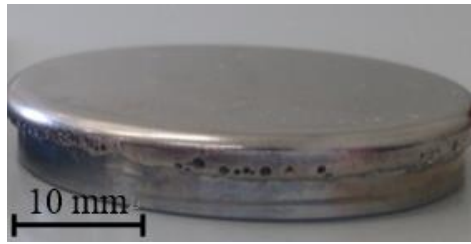
3.3.4.1 Particles distribution on the working surface of MCF slurries



(a) Illustration of experimental setup



(b) A photograph of the constructed setup



(c) A photograph of the workpiece

Fig. 3.22 Experimental setup and workpiece.

In order to confirm the predicted particle behavior discussed in section 3.3.2 (Fig. 3.20), the distributions of CIPs and APs on the working surface of the MCF slurry were investigated by scanning electron microscope (ERA-8900 by Elionix) observation and energy dispersive X-ray (EDX, Genesis APEX by EDAX) analysis. Figs. 3.22(a) and (b) show the experimental setup and a photograph of the constructed setup, respectively. A polishing unit consisting of a magnet holder, an MCF carrier, and two motors, together with a belt/pulley system [Fig. 3.22(a)], was mounted on the z-axis linear actuator [Fig. 3.22(b)] of an existing polisher, allowing z-axis motion. In the polishing unit, a disc-shaped neodymium permanent magnet with a magnetic field strength of 0.45 T was set at an eccentricity of $r = 4.5$ mm. Motor 1 was connected to the magnet holder through a flexible coupling and used to give the magnet revolutionary motion around its holder's axis. Motor 2 was connected to the MCF carrier through the belt/pulley system and used to rotationally drive the carrier. The carrier was made of a non-magnetic material (aluminum in this work). For the workpiece, disc-shaped STAVAX steel whose upper surface was coated with an electroless Ni-P-plated layer 1 mm thick was used [Fig. 3.22(c)]. The detailed investigation procedure is illustrated in Fig. 3.23 and is summarized below.

Step 1: Put a certain volume of MCF slurry onto the lower end surface of the MCF carrier using a syringe, then rotate the magnet holder to generate a rotary magnetic field for the self-shape formation and restoration of the slurry. Lower the polishing unit to set the working gap to a given value. Finally, rotate the MCF carrier to polish the work surface for 3 min under the given experimental conditions.

Step 2: Turn off the motors to stop the polishing operation and let the MCF slurry dry naturally for 12 h. After 12 h, raise the polishing unit to detach the dried MCF slurry from the work surface.

Step 3: Get the MCF carrier and the dried MCF slurry off the polishing unit and put them into the SEM for microscopic observation of the working surface and EDX mapping.

Step 4: Obtain the microscopic SEM images and the distribution of Al and Fe on the MCF slurry working surface using SEM and EDX.

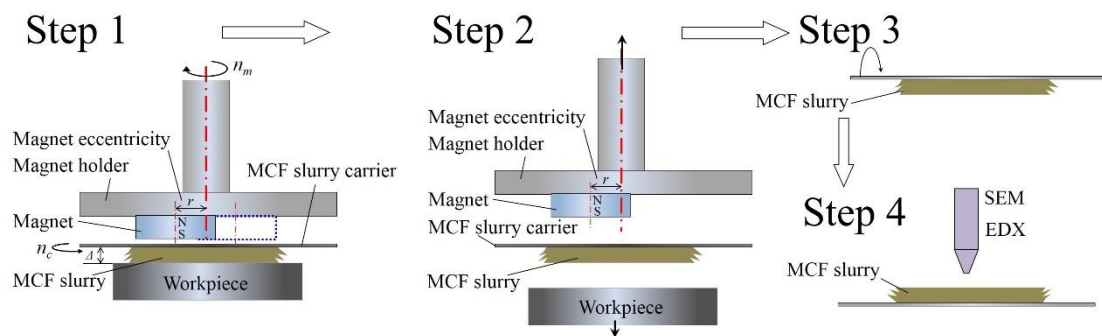


Fig. 3.23 Detailed investigation procedure of CIP distribution.

Table 3.5 Composition of MCF slurries used

	MCF1	MCF2	MCF3
CS (7 μ m)	wt.45%		
ES (3 μ m)		wt.45%	
HQ (1 μ m)			wt.45%
Abrasive particle (Al ₂ O ₃) (1 μ m)	wt.12%	wt.12%	wt.12%
Water-based magnetic fluid (MF)	wt.40%	wt.40%	wt.40%
α -cellulose	wt.3%	wt.3%	wt.3%

The compositions of the MCF slurries used are presented in Table 3.5. In order to investigate the influence of the CIP size, three kinds of MCF slurries containing CIPs with different diameters were prepared. The parameters for preparing the MCF slurry samples are tabulated in Table 3.6.

Table 3.6 Parameters in the preparation of MCF slurry samples for particle distribution investigation and polishing experiments

Workpiece	Magnetic: Ni-P plated STAVX steel Non-magnetic: Copper(only for sample preparation)
Magnet	Nd-Fe: B=0.45 T Revolution radius: $r=4.5$ mm Rotational speed: $n_m=1,000$ rpm
MCF carrier rotational speed (n_c)	600 rpm
Supply of MCF slurry (V_s)	1 mL
Polishing time	3 min (for sample preparation) 60min (for polishing experiment)
Drying temperature/time	25°C/12 h (only for sample preparation)
Working gap (Δ)	1, 2, 3 mm

The obtained SEM images and the element distributions on the working surfaces of the MCF slurries with the magnetic workpiece are exhibited in Fig. 3.24. Although the SEM images obviously demonstrate that the particle distributions are different for different MCF slurries at different working gaps, it is difficult to distinguish the respective distributions of the CIPs and the APs. Therefore, the distributions of Al and Fe representing APs and the CIPs, respectively, were obtained by EDX mapping, also shown in Fig. 3.24. It can be observed on the Al element mapping images that the Al distribution density increased as both the working gap and the CIP diameter increased. The distribution evenness of the Al was improved by increasing the CIP diameter or the working gap. On the other hand, the distribution of Fe was opposite that of Al.

Using the EDX mapping data in Fig. 3.24, the effect of the CIP diameter on the percentages of Al and Fe with different work materials at different working gaps was quantitatively obtained as shown in Fig. 3.25. It is evident from the figure that as the CIP diameter increased, the percentage of Al increased, whereas that of Fe decreased; however, the rates of increase and decrease both decreased at larger working gaps. It

should also be noted that the percentage of Al was less than 25%, regardless of the CIP diameter or working gap when the magnetic material was used as the workpiece; the percentage of Al was the highest at the largest working gap with MCF1, which contained the largest CIPs in this work.

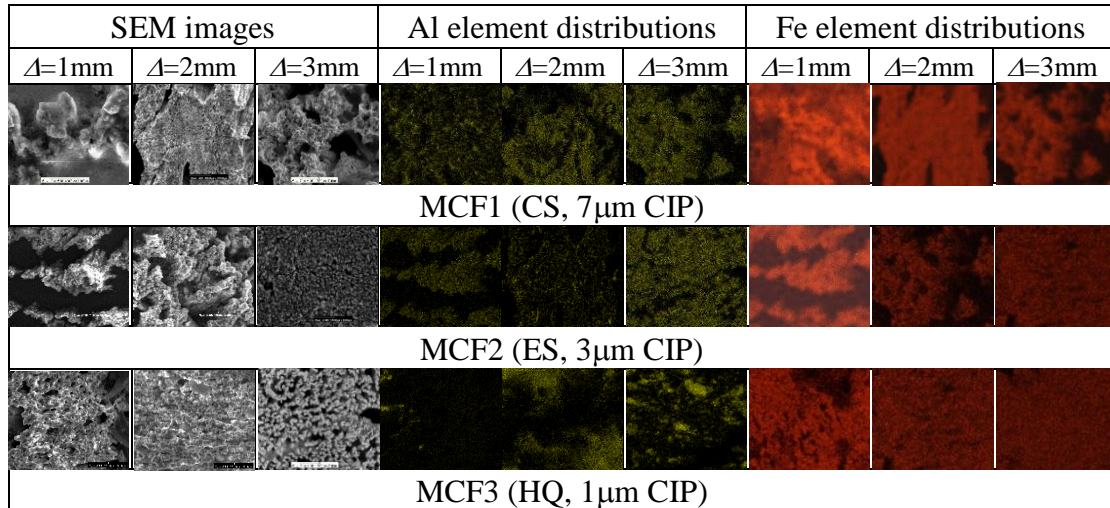


Fig. 3.24 SEM images and element distributions of MCF slurry working surface with magnetic workpiece.

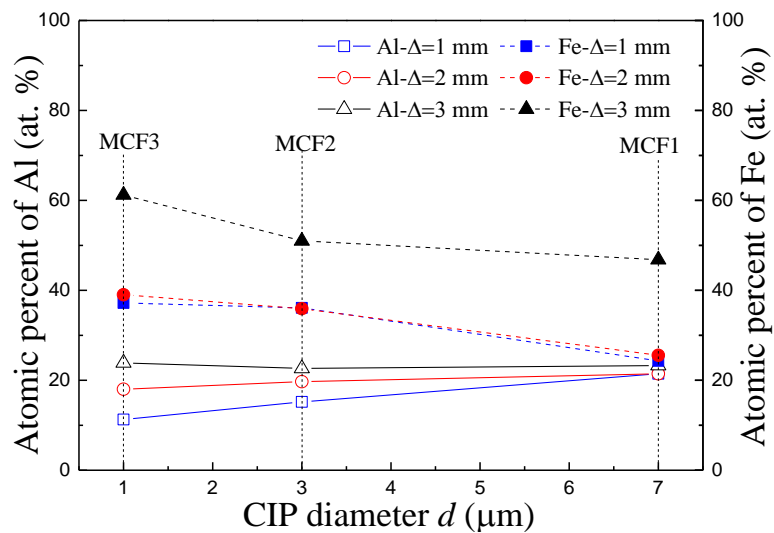


Fig. 3.25 The percentages of Al and Fe distributed on the magnetic work surface.

Generally speaking, the greater the amount of APs acting on the work surface, the higher the material removal rate and the better the work surface achieved; that is, a better surface was obtained at larger working gaps according to Fig. 3.25. However,

previous work [21] has demonstrated that increasing the working gap will decrease the polishing force, eventually reducing the material removal rate and limiting the surface quality improvement in MCF polishing of non-magnetic workpieces. This implies that the performance of an MCF slurry in the polishing of a magnetic material depends on two factors: the working gap and the amount of active APs acting on the work surface. This issue is discussed in the next section.

As for the particle distributions with the non-magnetic workpiece, Fig. 3.26 shows the SEM images and the element distributions for different MCF slurries at different working gaps. Similar to the results shown in Fig. 3.27, the Al distribution density increased with increasing working gap and CIP diameter, and its distribution evenness was improved by increasing both the working gap and the CIP diameter. The variations in the Fe distribution are also similar to those in the magnetic workpiece (Fig. 13). However, a close comparison of Fig. 3.26 to Fig. 3.24 reveals that the Al distribution density with the non-magnetic workpiece is significantly higher than that with the magnetic workpiece.

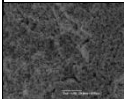
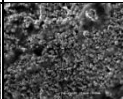
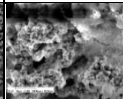
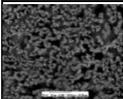
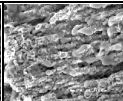
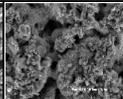
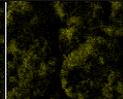
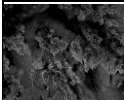
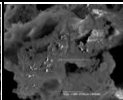
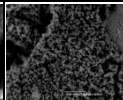
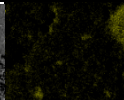
SEM images			Al element distributions			Fe element distributions		
$\Delta=1\text{mm}$	$\Delta=2\text{mm}$	$\Delta=3\text{mm}$	$\Delta=1\text{mm}$	$\Delta=2\text{mm}$	$\Delta=3\text{mm}$	$\Delta=1\text{mm}$	$\Delta=2\text{mm}$	$\Delta=3\text{mm}$
								
MCF1 (CS, 7 μm CIP)								
								
MCF2 (ES, 3 μm CIP)								
								
MCF3 (HQ, 1 μm CIP)								

Fig. 3.26 SEM images and element distributions of the MCF slurry working surface with non-magnetic workpiece.

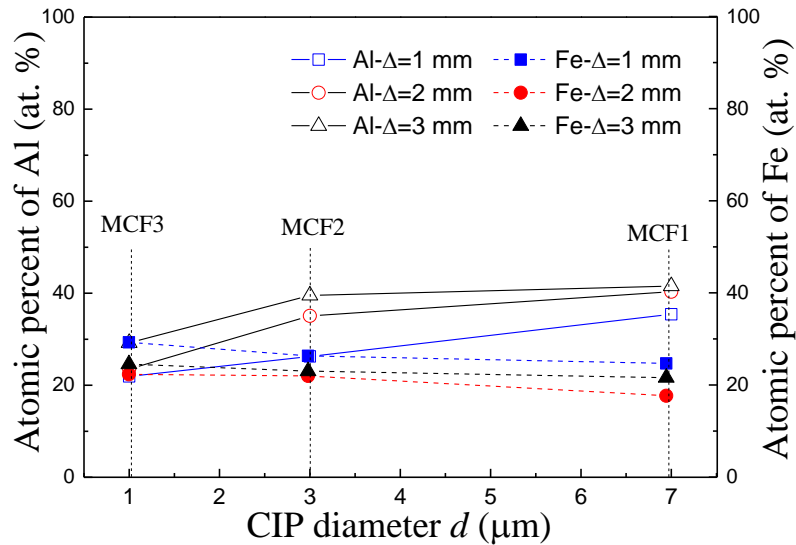


Fig. 3.27 CIP diameter vs. the Al and Fe contents on the non-magnetic work surface.

The percentages of Al and Fe distributed on the working surfaces of the MCF slurries were also obtained quantitatively by using the EDX mapping data in Fig. 3.26, and the results are shown in Fig. 3.27. Similar to the results with the magnetic workpiece (Fig. 3.25), the percentage of Al increased, whereas that of Fe decreased with increasing CIP diameter, regardless of the working gap. Investigation of the effect of the working gap on the Al percentage revealed that a larger working gap yielded a higher distribution percentage of Al. This means that more APs participate in material removal when the working gap is larger. It is further noteworthy that the percentage of Al was higher than 25% with the non-magnetic workpiece, which is considerably higher than that with the magnetic workpiece (Fig. 3.25), confirming the fact that after MCF polishing, a higher material removal rate and a better work surface are attained with the non-magnetic workpiece as compared to with the magnetic workpiece.

Comparing Fig. 3.25 and Fig. 3.27, it can be seen that with both the magnetic and non-magnetic workpieces, the larger the CIPs are, the higher the percentage of Al on the working surface, indicating that the MCF1 slurry containing the largest CIPs had the greatest amount of active APs and the best performance as compared to the MCF2 and MCF3 slurries. This phenomenon might be interpreted as a result of the

accommodation space of APs between the CIPs and the work surface discussed in section 3.3.3 (Fig. 3.21). That is, under the precondition that d_{abr} is less than $d_{CIP}/3$, the larger the CIPs are, the bigger the accommodation space, resulting in a larger amount of active APs acting on the work surface.

However, it is not yet known whether the performance of the MCF slurry is the same when the ratio of the CIP diameter to the AP diameter is the same but the diameters of the two particles are changed, e.g., ES (3 μm in diameter) CIPs to 1 μm APs and HQ (1 μm in diameter) CIPs to 0.3 μm APs. To investigate this matter, a new MCF slurry named MCF4 containing HQ CIPs and 0.3 μm APs was prepared using the same process mentioned in section 3.3.1 (Fig. 3.23). SEM observation and EDX mapping were also carried out on the prepared MCF4 slurry. Fig. 3.28 shows the SEM and EDX mapping images of the working surface of MCF4 with the magnetic and non-magnetic workpieces at different working gaps. It can be observed that regardless of the working gap, the Al distribution density with the magnetic workpiece was lower than that with the non-magnetic workpiece, whereas the Fe distribution density had the opposite tendency.

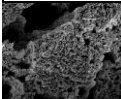
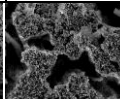
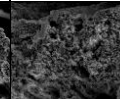
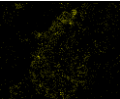
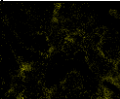
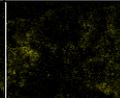
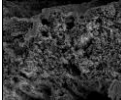
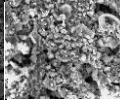
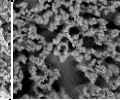
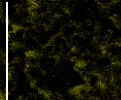
SEM images			Al element distributions			Fe element distributions		
$\Delta=1\text{mm}$	$\Delta=2\text{mm}$	$\Delta=3\text{mm}$	$\Delta=1\text{mm}$	$\Delta=2\text{mm}$	$\Delta=3\text{mm}$	$\Delta=1\text{mm}$	$\Delta=2\text{mm}$	$\Delta=3\text{mm}$
								
Magnetic workpiece								
								
Non-magnetic workpiece								

Fig. 3.28 SEM images and element distributions on the working surface of MCF4 with magnetic and non-magnetic workpieces.

The percentages of Al distributed on the working surface of MCF4 with magnetic and non-magnetic workpieces at different working gaps were compared to those of MCF2, as shown in Fig. 3.29. In all cases, the percentage of Al increased as the working

gap increased. However, it is interesting that with the non-magnetic workpiece, there was a significant difference between the percentages of Al distributed on the working surfaces of MCF2 and MCF4, whereas there was little difference with the magnetic workpiece, implying that as long as the requirement of $dabr < dCIP/3$ is met, the amount of active APs would remain at a certain level, regardless of the working gap, when the magnetic workpiece is polished using the naked CIP-based MVF slurry.

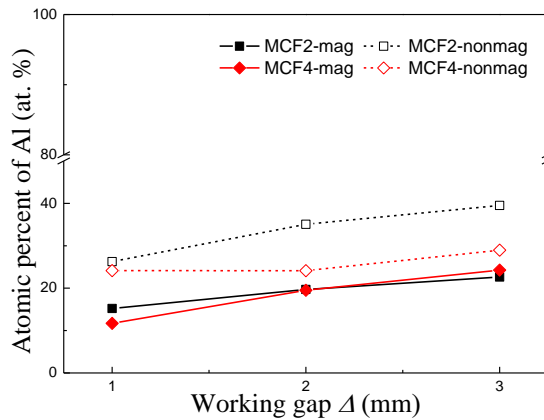


Fig. 3.29 Atomic percent of Al in MCF2 and MCF4.

3.3.4.2 Polishing experiment

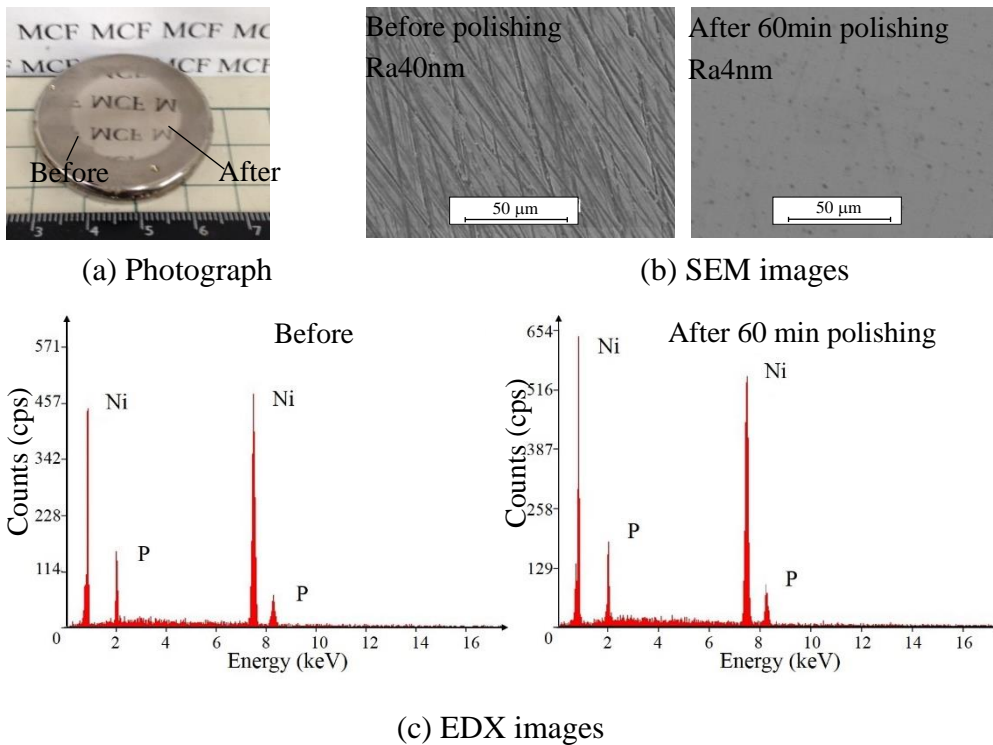


Fig. 3.30 Work surfaces before and after 60 min polishing using MCF1 at $\Delta = 1$ mm.

In order to verify the aforementioned discussions on the CIP and AP distribution, actual polishing experiments were carried out on an electroless Ni–P-plated STAVAX steel specimen using MCF1–MCF4 under the experimental conditions shown in Table 3.6. The same experimental setup and workpieces as those in the particle distribution investigation (Fig. 3.22) were used in the polishing experiments. However, it was different from the particle distribution investigation experiments that the work-surfaces of all the workpieces were treated by lapping using a roller type lapping machine (SP-As1, IMT Co., Ltd) with #1000-grit SiC sandpaper under the supplying of water before MCF polishing; their resultant roughness were around Ra40nm. As the dominant purpose of this work is to find a MCF slurry and a working gap suitable for the nano-precision surface finishing of magnetic workpieces, four kinds of MCF slurries with the same blending percentage of component which was optimally determined in previous works [37] but different ratios of the CIPs diameter to the APs diameter were employed and three different working gaps were set for polishing experiments. The others were kept constant at the values which is also optimally determined in previous works [28].

Figs. 3.30(a)–(c) exhibit an optical photograph, the SEM image, and the elemental analysis, respectively, of the work surface before and after 60 min polishing using MCF1 at a working gap $\Delta = 1$ mm. A comparison of the work surfaces before and after polishing demonstrates that the work surface quality was greatly improved and a mirror surface roughness of Ra = 4 nm without scratches was successfully achieved on the magnetic workpiece by using the MCF slurry containing naked CIPs 7 μm in diameter and APs 1 μm in diameter. In addition, the elemental analysis [Fig. 3.30 (c)] indicates that on the work surface, only the original Ni and P appeared; no Fe or Al was detected, indicating that no particles adhered on the polished work surface. These results demonstrate that MCF1 containing CS CIPs was capable of smoothing the magnetic work surface without leaving scratches or particle adhesion.

The 3D microscopic observation and the surface roughness measurement were also carried out on the initial and final work-surfaces with a white light interferometer (Zygo New view 600). Fig.3.31 shows the obtained 3D microscopic images of the initial work-surface before polishing and the final ones after polishing for 60 min at $\Delta=1$ mm with MCF1-MCF4. Obviously, the initial rough surface of $Ra=40\text{nm}$ was smoothed significantly to $Ra<22\text{nm}$ after polishing regardless of the MCF slurry type. However, the texture and roughness of the work-surface were different with different MCF slurries; the smoothest work-surface of $Ra=3.6\text{nm}$ was attained with MCF2.

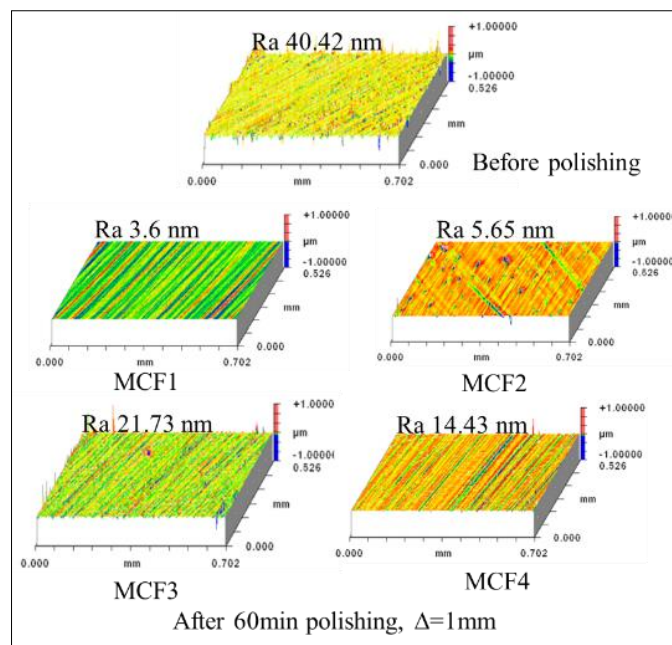


Fig. 3.31 3D microscopic images and surface roughness of workpieces before polishing and after polishing for 60 min at $\Delta=1$ mm using MCF1-MCF4.

Subsequently, the original and final work surface roughness after 60 min polishing using different MCF slurries at different working gaps are summarized in Fig. 3.32. The roughness decrease rate of $\eta = 1 - (\text{final Ra}/\text{original Ra})$ is also plotted in the figure. Overall, with any of the MCF slurries, the Ni-P-plated work surface roughness decreased after polishing; however, obviously the roughness decrease rate was different using different MCF slurries at different working gaps. Comparing the final roughness

and the decrease rates obtained using different MCF slurries at different working gaps, it was discovered that in most cases, a better final surface and a higher roughness decrease rate were obtained at smaller working gaps. Although as previously revealed in section 3.3.1 (Fig. 3.27), the amount of active APs decreased at smaller working gaps, supposedly resulting in a lower roughness decrease rate, our previous work [21] demonstrated that a smaller working gap yielded a much greater polishing force, significantly increasing the roughness decrease rate. This might be the reason why the smaller working gap resulted in the higher roughness decrease rate, in spite of the fact that the amount of active APs decreases as the working gap decreases.

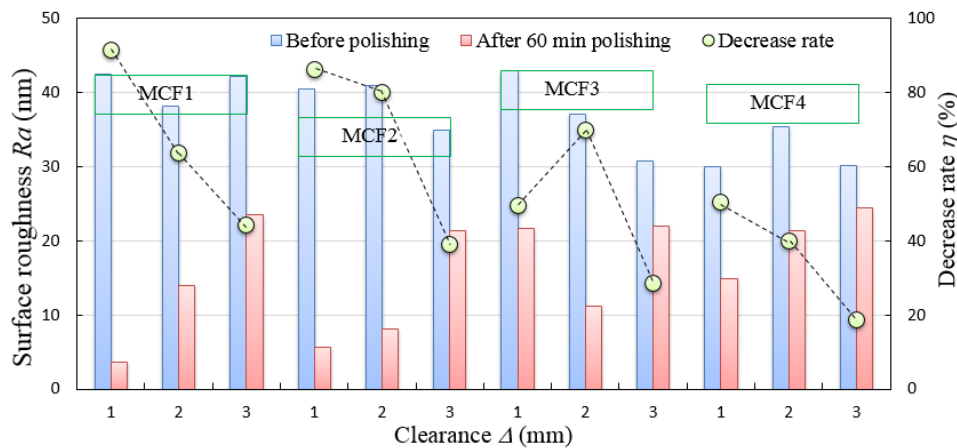


Fig. 3.32 Original and final surface roughness after 60 min polishing using different MCF slurries at different working gaps.

Regarding the effect of the MCF slurry on the roughness decrease rate, the roughness decrease rate tended to decrease in the order of MCF1 > MCF2 > MCF3 > MCF4. Considering that the ratio of CIP diameter to AP diameter decreases from 7 $\mu\text{m}/1 \mu\text{m}$ within MCF1 to 3 $\mu\text{m}/1 \mu\text{m}$ within MCF2 and further to 1 $\mu\text{m}/1 \mu\text{m}$ within MCF3, the accommodation space for the APs expands in the order of MCF1 > MCF2 > MCF3, resulting in an increase in the amount of active APs in the same order of MCF1 > MCF2 > MCF3. This is the reason why the roughness decrease rate decreased in the order of MCF1 > MCF2 > MCF3. However, it should be noted that although MCF2 and MCF4 had similar ratios of CIP diameter to AP diameter, i.e., 3 $\mu\text{m}/1 \mu\text{m}$ =

3 for MCF3 and $1\ \mu\text{m}/0.3\ \mu\text{m} = 3.3$ for MCF4 and the percentages of Al were the same (Fig. 3.29), the roughness decrease rate with MCF4 was much lower than that with MCF2. The reason might be because the magnetic force acting on the ES CIPs within MCF2 was much larger than that acting on the HQ CIPs within MCF4 (Fig. 3.18), and hence the pressure on the APs increased, thus improving the material removal ability of the MCF slurry.

Summarizing the effects of the MCF slurry and the working gap on the work surface roughness decrease rate in the MCF polishing of magnetic workpieces, it was revealed that the MCF slurry containing CS CIPs $7\ \mu\text{m}$ in diameter and APs $1\ \mu\text{m}$ in diameter should be employed and that the working gap Δ at $1\ \text{mm}$ should be set in order to perform mirror surface finishing of magnetic Ni–P-plated STAVAX steel using the naked CIP-based MCF slurry.

3.4 Conclusions

The effects of the magnetic and gravitational forces acting on naked CIPs and APs were investigated and the behaviors of the CIPs and APs in the presence of an external magnetic field were qualitatively discussed. Then, the distributions of CIPs and APs on the working surfaces of MCF slurries were experimentally investigated with both magnetic and non-magnetic work surfaces. Finally, polishing experiments were performed on the magnetic workpiece, a Ni–P-plated STAVAX steel specimen, using MCF slurries containing CIPs and APs with different diameters at different working gaps to confirm the discussion on the particle distribution. The main conclusions are summarized as follows:

(1) The resultant vertical force acting on the naked CIPs was due to the magnetic and gravitational forces, and it significantly increased with increasing CIP diameter. With the magnetic workpiece, the resultant vertical force attracted the CIPs towards the work surface, whereas APs were pushed away from the work surface. Both the CIPs

and the APs showed opposite behaviors with the non-magnetic workpiece.

(2) The percentage of active APs distributed on the working surface of an MCF slurry increased and the distributions became more even as either the diameter of the CIPs or the working gap increased. On the other hand, the distribution of CIPs was opposite that of APs. The percentage of active APs was beyond 25% with the non-magnetic workpiece, whereas it was less than 25% with the magnetic workpiece.

(3) The MCF slurry containing CS CIPs 7 μm in diameter and APs 1 μm in diameter should be employed and that the working gap Δ at 1 mm should be set in order to perform mirror surface finishing of magnetic Ni–P-plated STAVAX steel using the naked CIP-based MCF slurry. Under the experimental conditions in this work, the Ni–P-plated surface quality was significantly improved and a mirror surface roughness of $R_a = 4$ nm was successfully achieved without leaving scratches or particle adhesion with an MCF slurry containing CIPs 7 μm in diameter and APs 1 μm in diameter.

The abovementioned results demonstrated that use of an MCF slurry containing commercial naked CIPs is a realistic method for nano-precision finishing of magnetic workpieces as long as the CIPs are larger than the APs. This type of MCF slurry has great potential in industrial applications in terms of cost and performance as compared to costly slurries containing ZrO_2 -coated CIPs.

Reference

- [1] Dai, Y.F., Song, C., Peng, X.Q., and Shi, F., *Appl. Opt.* 49, 298-306(2010)
- [2] Das, M., Jain, V.K. and Ghoshdastidar, P.S., *Int. J. Mach. Tools Manuf.* 48, 415-426(2008).
- [3] Das, M., Sidpara, A., Jain, V.K. and Ghoshdastidar, P.S., *Int. J. Precis. Technol.*, 2, 51-63(2011).
- [4] Furuya, T., Wu, Y., Nomura, M., Shimada, K. and Yamamoto, K., *J. Mater. Process. Technol.* 201, 536-541(2008).
- [5] Sato, T., Wu, Y., Lin, W. and Shimada, K., *J. Jpn. Soc. Abras. Technol.* 54, 425-430(in Japanese)(2010).
- [6] L. Jiao, Y. Wu, X. Wang, H. Guo, Z. Liang. Dai, Y.F., Song, C., Peng, X.Q. and Shi, F., *Appl. Opt.* 49, 298-306(2010)
- [7] H. Guo, Y. Wu, D. Lu, M. Fujimoto and M. Nomura, *J. Mater. Process. Technol.* 214, 2759-2769(2014)
- [8] Y. Wu, T. Sato, W. Lin, et al., *Advanced Materials Research*, (76-78), 331-336(2009).
- [9] Shai N. Shafir, Henry J. Romanofsky, Michael Skarlinski, Mimi Wang, Chunlin Miao, Sivan Salzman, Taylor Chartier, Joni Mici, John C. Lambropoulos, Rui Shen, Hong Yang, and Stephen D. Jacobs. *Proc. of SPIE.* 7426. 74260B (2009)
- [10] Guo, H. and Wu, Y., *J. JSEM.* 12, 369-374, (2012)
- [11] Information on http://en.wikipedia.org/wiki/Oxygen-free_copper
- [12] C, akır, H. Temel, M. Kiyak, Chemical etching of Cu-ETP copper, *Journal of Materials Processing Technology.* 162-163 (2005) 275-279.
- [13] Kun Shan, Ping Zhou, Jiqing Cai, Renke Kang, Kang Shi, Dongming Guo, Electrogenerated chemical polishing of copper, *Precision Engineering.* 39 (2015) 161-166.

- [14] K. Shimada, T. Fujita, H. Oka, Y. Akagami, S. Kamiyama, Hydrodynamic and magnetized characteristics of MCF (magnetic compound fluid) (in Japanese), Transactions of the Japan Society of Mechanical Engineers. 67 (2001) 3034-3040.
- [15] Yongbo Wu, Youliang Wang, Masakazu Fujimoto, Mitsuyoshi Nomura. Nano-precision polishing of CVD SiC using magnetic compound fluid slurry, Journal of the Korean Society of Manufacturing Technology Engineers. 23 (2014) 547-554.
- [16] Kunio Shimada, Yoichi Akagami, Shinichi Kamiyama, Toyohisa Fujita, Toshio Miyazaki, Astushi Shibayama, New Microscopic Polishing with Magnetic Compound Fluid (MCF), Journal of Intelligent Material Systems and Structures. 13 (2002) 405-408.
- [17] Wu Y., Sato T., Lin W., Yamamoto K., Shimada K., Mirror surface finishing of acrylic resin using MCF-based polishing liquid, Int. J. Abras. Technol. 3 (2010) 11-24.
- [18] Balaraju J, Narayanan T, Seshadri S. Electroless Ni-P composite coatings. Journal of Applied Electrochemistry 2003; 33; 807-16.
- [19] Spencer L. Electroless nickel plating. Metal Finish 1974; 72; 50-54.
- [20] Metals Handbook, ninth ed. ASM. 1983; 5; 219.
- [21] Kumar P, Nair P, Studies on crystallization of electroless Ni-P deposits. Mater J. Process. Technol 1996; 56; 511-20.
- [22] Lee C. Structure, electrochemical and wear-corrosion properties of electroless nickel-phosphorus deposition on CFRP composites, Materials Chemistry and Physics 2009; 114; 125-33.
- [23] Casstevens J, Daugherty C, Diamond turning optical surfaces on electroless nickel. Precision Machining of Optics 1978; 0159; 109-13.
- [24] Pramanik A, Neo K S, Rahman M, Li X P, Sawa M, Maeda Y, Cutting performance of diamond tools during ultra-precision turning of electroless-nickel plated die materials. Journal of Materials Processing Technology 2003; 140; 308-13.

- [25] Namba Y, Shimomura T, Fushiki A, Beaucamp A, Inasaki I, Kunieda H, Ogasaka Y, Yamashita K, Ultra-precision polishing of electroless nickel molding dies for shorter wavelength applications. *CIRP Annals - Manufacturing Technology* 2008, 57, 337-40.
- [26] Guo H, Wu Y, Lu D, Fujimoto M, Nomura M. Ultrafine polishing of electroless nickel-phosphorus plating mold with magnetic compound fluid slurry, *Materials and Manufacturing Processes* 2014; 29; 1502-09.
- [27] Tani Y, Kawata K, Nakayama K. Development of high efficiency fine finishing process using magnetic fluid. *CIRP Ann.* 1984, 33 (1), 217-20.
- [28] Prokhorov I, Kordonski W. New high-precision magnetorheological instruments-based method of polishing optics. *OSA OF&T Workshop Digest* 1992, 24, 134-36.
- [29] Juan D V, Daniel J K, Roque H A. Magnetorheological fluids: a review. *Soft Matter* 2011, 7, 3701-10.
- [30] Sidpara A, Das M, Jain V K. Rheological characterization of magnetorheological finishing fluid. *Materials and Manufacturing Process* 2009, 24 (12), 1467-78.
- [31] DeGroote J E, Romanofsky H J, Kozhinova I A, Schoen J M, Jacobs S D. Polishing PMMA and other optical polymers with magnetorheological finishing. *Proceedings of SPIE* 2003, 5180, 123-34.
- [32] Singh A K, Jha S, Pandey P M. Nanofinishing of a typical 3D ferromagnetic workpiece using ball end magnetorheological finishing process. *International Journal of Machine Tools and Manufacture* 2012, 63, 21-31.
- [33] Singh A K, Jha S, Pandey P M. Magnetorheological ball end finishing process. *Materials and Manufacturing Processes* 2012, 27 (4), 389-94.
- [34] Singh A K, Jha S, Pandey P M. Nanofinishing of fused silica glass using ball-end magnetorheological finishing tool. *Materials and Manufacturing Processes* 2012, 27 (10), 1139-44.
- [35] Shimada K, Akagami Y, Kamiyama S, Fujita T, Miyazaki T, Shibayama A. New

- microscopic polishing with magnetic compound fluid. *J. Intell. Mater.Syst. Struct* 2002; 13; 405–08.
- [36]Guo H, Wu Y, Li Y, Cao J, Fujimoto M, Jacobs S. Technical performance of zirconia-coated carbonyl-iron-particles based magnetic compound fluid slurry in ultrafine polishing of PMMA. *Key Engineering Materials* 2012; 523-524; 161-66.
- [37]Wang Y, Wu Y, Guo H, Fujimoto M, Nomura M and Shimada K, A new magnetic compound fluid slurry and its performance in magnetic field-assisted polishing of oxygen-free copper, *J. Appl. Phys.* 2015;117; 17D712-14.
- [38]Wang Y, Wu Y, Nomura M. A novel magnetic field-assisted polishing method using magnetic compound slurry and its performance in mirror surface finishing of miniature V-grooves. *AIP Advances* 2016; 6; 056602-1-6.
- [39]Wu Y, Wang Y, Fujimoto M, Nomura M. Nano-precision polishing of CVD SiC using magnetic compound fluid slurry, *Journal of the Korean Society of Manufacturing Technology Engineers* 2014; 23; 547-54.
- [40]Rosenweig R E, *Ferrohydrodynamics*, New York, 1985.
- [41]Zhang Y, Qi B, *Electromagnetism*, Beijing, 1997.

This page intentionally left blank.

Chapter IV Feasibility study on surface finishing of linear V-grooves

4.1 Introduction

In recent years, as one of the most promising renewable energy technologies, solar photovoltaics (hereafter called PV) has been in rapidly increasing demand. In particular, concentrating PV, in which the sunlight is collected and concentrated onto a solar cell by means of a lens, has attracted much attention in the field of mega-solar electric power generation [1]. This is because this kind of PV system can potentially generate higher electric power with a smaller cell area, resulting in a decrease in the cost of PV [2-3]. For sunlight collection and concentration, Fresnel lenses are generally employed because they are lighter and thinner, and have less volume compared to traditional lenses, thus significantly reducing the budget spending because of the lower material consumption.

This kind of lens is generally produced by generating parallel distributed linear V-grooves or concentrically distributed circular V-grooves on a colourless and transparent optical glass like BK7 or a plastic like a PMMA substrate. The former is called a linear Fresnel lens, and the latter is called a circular one. Their fabrication commonly relies on either diamond cutting or diamond grinding one by one, leading to a difficulty in the popularization of concentrating PV systems due to their high fabrication cost and low productivity. Therefore, it is essential to provide high-quality and low-cost Fresnel lenses in order to expand the application of concentrating PV systems. For this purpose, the simplest and most cost-effective method is to utilize a polymer like PMMA as the substrate material and mass-produce them by hot pressing or injection moulding.

As a diffractive focus lens, the optical efficiency, which is defined as the ratio of the transmitted light energy to the incident light energy, is a significant assessment standard. The transmitted light energy is closely related to the form accuracy and

surface roughness of the lens, with better values for these resulting in a higher amount of transmitted light energy, which contributes to a high optical efficiency. Consequently, it is very important to manufacture high-precision structured moulds for the hot pressing/injection moulding of plastic Fresnel lenses. As the injection mould, the form retention rate (η) should be higher than 90% [4, 5]. The existing precision machining processes like diamond machining and precision grinding are well suited for manufacturing such structured moulds. However, in some cases, a subsequent polishing operation should be performed on the structured surface to improve the surface roughness or remove the tool feed marks caused by pre-machining, which may result in light scattering effects [6].

Some efforts have previously been made to finish such structured surfaces. Gessenharter et al. [7] proposed a new polishing process for finishing V-grooves using conical pin-type and conical wheel-type polishing tools. In their work, a polishing slurry consisting of a polymer fluid, abrasives, and additives was impressed into the tools used, and the surface roughness and form accuracy of the structured electroless nickel-plated substrates were successfully improved, while the edges at the bottom and top of the grooves were rounded. Brinksmeier et al. [8] performed surface finishing of structured optical elements using the same method, and the surface roughness of a V-groove reached 5 nm Ra. However, on an actual Fresnel lens, the dimensions and cross-section profiles of the V-grooves are different at different locations. Thus, several tools with different dimensions and geometries should be prepared to geometrically fit the dimensions and the cross-section profiles of the V-grooves being finished, and the tools should be frequently exchanged during the polishing of a single workpiece in the case of utilizing the method by Gessenharter et al. Undoubtedly, their method leads to a high equipment investment cost and long process time. Therefore, a flexible tool capable of geometrically fitting the V-groove by itself is necessary to solve this problem.

One promising surface finishing technique is magnetic field-assisted polishing, in

which a magnetic fluid (MF), magnetorheological fluid (MRF), or magnetic compound fluid (MCF) slurry is employed as the flexible abrasive tool. Once a magnetic field is applied, flexible chain-shaped magnetic clusters are immediately formed within the slurry along the magnetic lines of force, and the lengths and orientations of these clusters can be changed according to the shape of the work surface. Kim et al. [9] proposed a field-assisted finishing technique that utilizes MRF slurries for polishing three-dimensional silicon microchannel structures. They investigated the influences of the process parameters on the material removal and compared the surface topographies before and after finishing. The obtained results indicated that after polishing, the average roughness was reduced to 11.1 nm Ra on the bottom surface and 18.1 nm Ra on the side wall, but the depth of the microchannel was reduced by up to 10.4%. Lim et al. [10] presented a polishing technique for three-dimensional copper electroplating and silicon microchannel structures using MRF slurries. Their results showed that the average surface roughness dropped by more than an order with little change in the original geometries, and the performances of both structures were improved. Natsume et al. [11] described a new type of magnetic abrasive machining for finishing a surface with a shallow groove on stainless steel. The results indicated that the surface quality Ra of the groove bottom was improved significantly, and the finished surface roughness was 0.052 μm Ra. Kawakubo et al. [12-14] proposed a magnetic field-assisted machining method to finish a die with an R-groove, in which the relative motion between the slurry and workpiece was produced by reciprocating the workpiece in the groove direction. The results demonstrated that the surface roughness was related not only to the radius of the groove but also to the diameter of the ferromagnetic particle. In addition, the form error on the edge of the grooves was higher than that at other positions. Hence, magnetic field-assisted polishing is supposed to be an excellent candidate for polishing the moulds for structure such as microchannel grooves and R-grooves. However, under a given magnetic field, the particles are less stably distributed

in an MRF slurry than in an MF slurry, whereas the magnetic pressure and apparent viscosity of the former are larger than those of the latter, leading to a difficulty in stabilizing their performances in surface finishing.

To overcome the respective disadvantages and make use of the respective advantages of MF and MRF slurries, a novel magnetic slurry called MCF slurry was proposed by Shimada et al. [15, 16]. In practice, this new slurry is produced by blending micrometre-size carbonyl iron powders (CIPs), abrasive particles, and α -celluloses whenever necessary into a water-based MF containing nanometre-size magnetite particles with the respective blend ratios. Hence, under a magnetic field, the behaviour of the particles within the MCF slurry can be controlled, and the slurry exhibits a higher magnetic pressure and apparent viscosity and a more stable distribution of particles, while maintaining a fluid-like behaviour. As engineering applications, the MCF slurry has been successfully used to polish various engineering materials, including stainless steels, polymers, optical glasses, ceramics, oxygen-free copper, and a Ni-P plating layer [17-23]. For example, Guo et al. performed the polishing of a Ni-P plating layer [17] and PMMA [19] using a zirconia-coated CIP-based MCF slurry, and the results showed that the surface roughness of the workpieces was improved to the nanometre-level without causing scratches or the embedding of particles. Wang et al. polished the flat surface of an oxygen-free copper specimen using MCF slurries containing different CIPs and determined a strategy to prolong the slurry working life [20]. Furuya et al. polished a metal work surface utilizing the MCF polishing technique and optimized the experimental parameters [23]. In particular, it should be noted that an MCF slurry is capable of finishing the structured surface of a stainless specimen with deep rectangle grooves [24], implying that the MCF slurry is potentially capable of playing an important role in V-groove surface finishing.

In this work, in order to develop an alternative and novel polishing technique for the high-precision surface finishing of miniature V-grooves, the feasibility of finishing

V-grooves using the MCF slurry was experimentally determined, and the fundamental finishing characteristics were elucidated. This paper first describes the processing principle of the proposed polishing technique, followed by detailing the construction of an experimental setup and the experimental conditions, as well as the experimental procedure, in section 4.2. Then, in section 4.3, the experimental results are given, including the effects of the polishing time on the material removal, and the form accuracy and surface roughness values of the workpiece at different locations/positions in the polishing zone. Finally, the experimental results are discussed in detail in sections 4.4.

4.2 Processing principle and experimental details

4.2.1 Processing principle

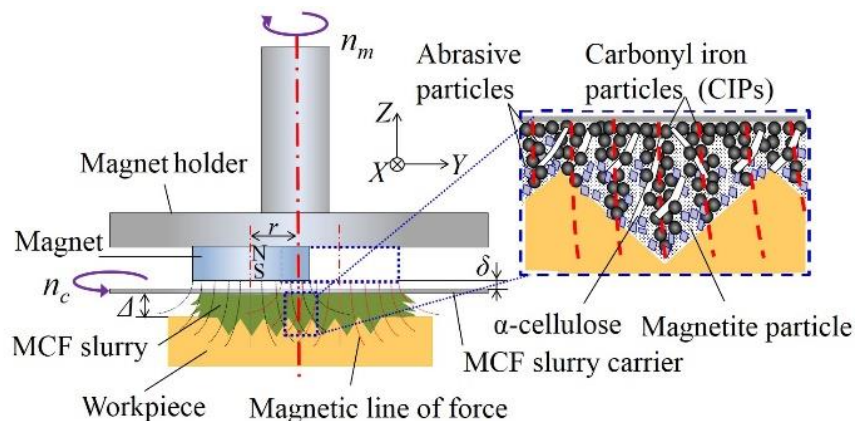


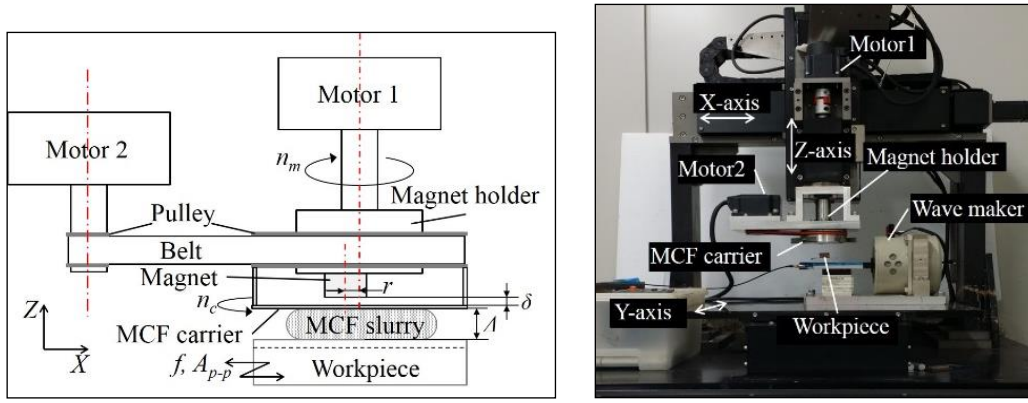
Fig. 4.1. Illustration of processing principle of V-groove polishing with MCF slurry

Fig. 4.1 schematically illustrates the processing principle of polishing V-grooves using an MCF slurry. A disc-shaped permanent magnet is attached to the lower end face of its holder with an eccentricity of r . An MCF slurry carrier, i.e. an aluminum plate, is located below the magnet with a clearance of δ . When the magnet holder is rotated at a speed of n_m , the magnet revolves around the axis of the holder at the same

speed. Thereby, a dynamic magnetic field is generated, in which the magnetic flux density is constant, but the magnetic lines of force constantly revolve around the magnet holder axis; hereinafter, this kind of dynamic magnetic field is called a rotary magnetic field. Once the clearance Δ between the top of the groove and the carrier has received a certain volume of MCF slurry, as shown in the right portion of Fig. 4.1, chain-shaped magnetic clusters composed of nanometre-size magnetite particles and micrometre-size carbonyl-iron particles (CIPs) are immediately formed along the magnetic lines of force. Non-magnetic abrasive particles are entrapped in the clusters or distributed between the clusters, and α -cellulose fibres are interwoven with the clusters if they are employed. In addition, all of the clusters are forcibly collected by the magnetic attraction force, and they are concentrated in the area where the magnetic field is the strongest. In the meantime, it is well known that in a magnetic field non-magnetic substances suffer a so-called magnetic levitation force [9], and of course the gravitational force acts on the same substances. Therefore, under the combined effect of the magnetic levitation and gravitational forces, the majority of the nonmagnetic abrasive particles within the MCF slurry move down towards the work surface, and a normal force is thus imposed on the workpiece. When the work-surface vibrates at a frequency of f and an amplitude of A in the X direction, friction is induced between the workpiece and abrasive particles. Hence, the work materials are removed by the micro-cutting actions of the abrasive particles. In addition, the MCF carrier is rotationally driven at a proper speed of n_c to prevent the abrasive particles from remaining in the same polishing area during polishing.

4.2.2 Experimental setup

To realize the polishing principle, an experimental apparatus was constructed in the laboratory, as shown in Fig. 4.2.



(a) Schematic illustration (b) External optical view of experimental apparatus

Fig. 4.2. Schematic illustration and external optical view of experimental apparatus.

A polishing unit composed of a magnet holder, an MCF carrier, and two motors, together with a belt/pulley set (Fig. 4.2(a)), was mounted on the Z-axis linear actuator (Fig. 4.2(b)) of an existing polisher, allowing Z-axis motion. In addition, a commercially available wave maker (SL-0505 by Asahifactory Corp.) was installed on the worktable of the same polisher to provide the workpiece with an oscillating motion in the X direction. In the MCF unit, a disc-shaped neodymium permanent magnet with a magnetic field strength of 0.45 T was set at an eccentricity of $r = 4.5$ mm. Motor 1 was connected to the magnet holder through a flexible coupling and used to give the magnet a revolutionary motion around its holder's axis. Motor 2 was connected to the MCF carrier through the belt/pulley and used to rotationally drive the carrier. The carrier ($82 \text{ mm} \times 82 \text{ mm} \times 1 \text{ mm}$) was made of a non-magnetic material (aluminum in this work). Below the MCF carrier, a piece of oxygen-free copper (OFC) substrate with linear V-grooves was fixed on the work holder of the wave maker as the workpiece. This arrangement allowed the workpiece to oscillate in the X-axis direction at frequency f and amplitude A . Thus, it allowed the relative velocity of the abrasive particles to the work surface to be in the longitudinal direction of the linear grooves. In addition, the clearance Δ could be varied by adjusting the vertical position of the MCF unit through the Z-axis linear actuator.

4.3 Fundamental research of linear V-groove

Table 4.1 Composition of MCF slurry used

Carbonyl iron powder (CIP)	Mean diameter	7.5 μm
	Concentration	45 wt. %
Abrasive particle (Al_2O_3)	Mean diameter	1 μm
	Concentration	12 wt. %
Water-based magnetic fluid (MF)	Mean diameter	10 nm
	Concentration	40 wt. %
α -cellulose	Concentration	3 wt. %

Table 4.2 Experimental conditions

Oscillation parameter	$f [\text{Hz}]/A_{p-p} [\text{mm}_{p-p}]$	15/5, 30/4, 45/2
Magnet type		Nd-Fe-B, B=0.45 T
Magnet revolution speed	n_m	1,000 [rpm]
MCF carrier rotational speed	n_c	0, 50 [rpm]
Amount of MCF slurry supplied	V	0.50, 0.75, 1.00 [mL]
Clearance	Δ	1.0 [mm]

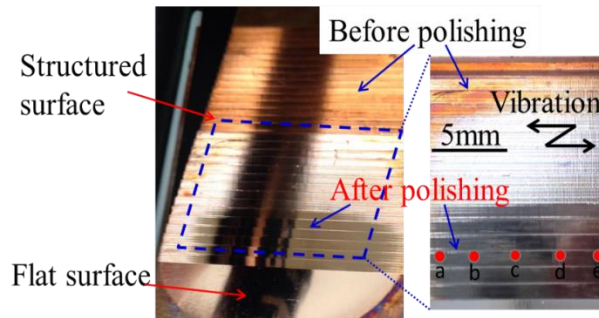
Polishing experiments were performed on the constructed experimental rig. The V-groove samples made of oxygen-free copper were used as the workpiece in experiments. The miniature V-groove with a height of $H=0.6$ mm, a pitch of $P=1.2$ mm and an included angle of $\alpha=75^\circ$ were prepared by flying cutting. The roughness of the sides of the V-grooves was in the range of 180-220 nmRa. The purpose of this research was to investigate the effects of process parameters including MCF slurry supplying amount V , workpiece oscillation parameter f/A_{p-p} and MCF carrier rotational speed n_c on work-surface roughness and form error. Therefore, the water-based MCF slurry was prepared with a given compositions as shown in Table 1. Table 2 lists the experimental parameters; polishing experiments were conducted at different values of f/A_{p-p} , V , and n_c but with a constant magnet revolution speed n_m and clearance Δ between the MCF carrier and the workpiece to study the effects of these process parameters on the

polishing characteristics.

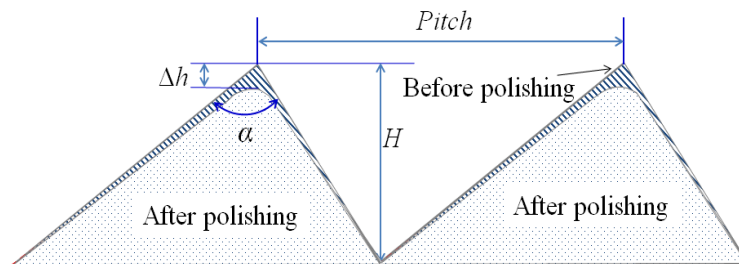
Figs. 4.3 (a) and (b) show the photo of a typical work-surface and the measured cross section profiles before and after 150 minutes polishing with 0.75 mL MCF slurry at 30Hz/4mm_{p-p}, respectively. Evidently, the mirror surface on both flat surface and structured surface were obtained after MCF slurry polishing. In order to investigate the polishing efficiency in term of the improvement of surface quality, the surface roughness were measured at five different positions (a-e in the right side of Fig.4.3 (a)) along the oscillation direction and the average value of them was obtained to be regarded as the surface roughness under the given conditions. In addition, as shown in Fig. 4.3 (b), the cross section profiles of the groove before and after polishing were measured and compared with each other to obtain the height decrease Δh , and then the form accuracy of the groove polished was evaluated in terms of the form error η which is defined as:

$$\eta = \frac{\Delta h}{H} \times 100\% \quad (4.1)$$

Where H is the initial height of the groove.



(a) Photo of a work-surface polished



(b) Cross section profile of grooves

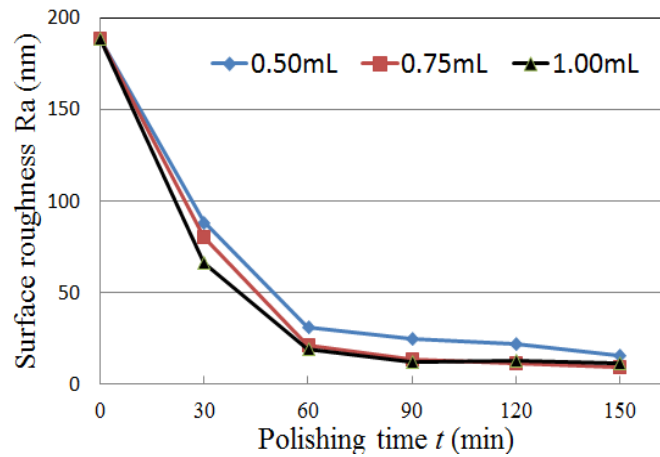
Figure 4.3 A typical work-surfaces polished for 150 min with 0.75ml MCF at 30Hz/4mm_{p-p}

Effect of MCF slurry supplying amount

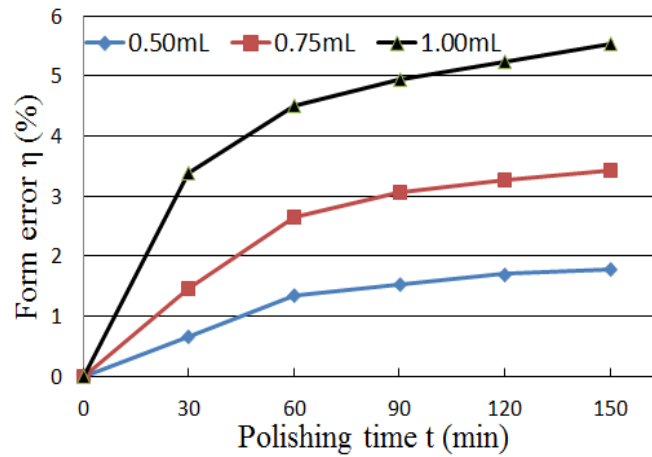
Polishing operations with different amounts of MCF slurry supplied were performed at $\Delta=1.0$ mm and $f/A_{p-p}=30\text{Hz}/4\text{mm}_{p-p}$. Figs.4.4 (a) and (b) show the variations of the surface roughness Ra and the form error η during polishing for different amounts of MCF slurry supplied, respectively. To begin with, as can be seen in Fig. 4.4 (a), at the first 60 minutes the Ra values decreased rapidly, and then the decrease rate got much low, eventually leading to little decline during polishing regardless of the amount of slurry supplied. However, shifting the attention into the final value of Ra after 150 min polishing revealed that the resultant surface roughness depends on the amount of MCF slurry supplied; the respective final values of Ra with 0.50 mL, 0.75 mL and 1.00 mL MCF slurry were reduced by 91.95%, 95.22% and 94.17%, respectively, after 150 min polishing. The smoothest work-surface with the roughness of 9.005 nmRa was achieved with 0.75 mL slurry supplied. On the other hand, as be observed in Fig. 4.4 (b) that the form error η increased with increasing polishing time monotonously irrespective of the amount of MCF slurry supplied. However, it is worthy to notice that the increase rate of the form error was significantly affected by the slurry supplying amount; the largest form error occurred with 1.0 mL MCF slurry, indicating that the smaller the amount of MCF slurry supplied was, the quicker the form error increased. In practical applications of molds/dies, it is said that the form error should be less than 5%. Thus, it is observed from Fig.4.4 (b) that as long as the amount of MCF slurry is below 0.75mL, the form error would never be over 5%.

The above mentioned results demonstrated that the amount of the slurry supplied should be determined at the value of 0.75 mL in the current work. When the amount of MCF slurry is less, the magnetic particles within the slurry gathered under the magnet center due to the high magnetic force. The less the slurry amount, the smaller the contact area, resulting in the lower roughness decreases rate and form error. By contrast, as the amount of MCF slurry is more, the movability of abrasive grains becomes better under

the magnetic field and the magnetic clusters are easy to be formed uniformly. The more amount of slurry is beneficial to form the longer cluster along the magnetic line of force and during polishing the clusters are compressed to strengthen the polishing force acting on the work surface. The more the slurry amount, the bigger the contact area, eventually resulting in the better work-surface and higher form error. These are considered to be the reason why the 0.75mL MCF has the best polishing performance.



(a)



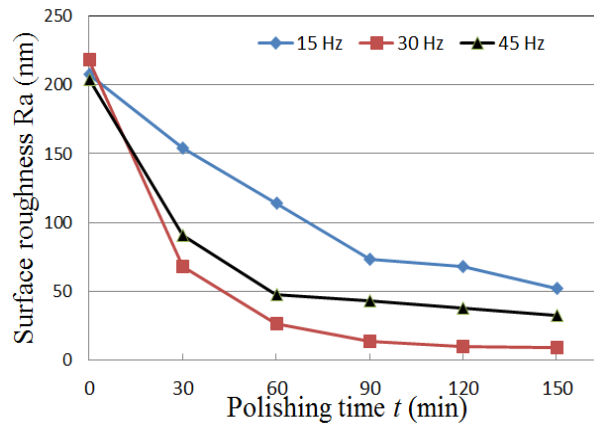
(b)

Fig 4.4 Effects of the slurry supply amount on (a) surface roughness and (b) form error.

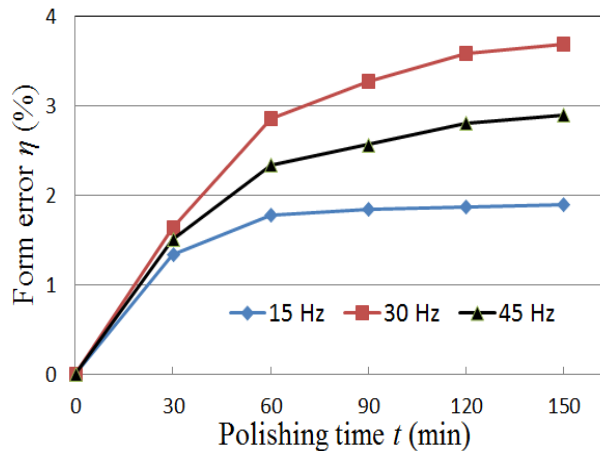
Effect of workpiece oscillation parameter

Figs. 4.5(a) and (b) show the effects of the oscillation parameter f/A_{p-p} on the

surface roughness and the form error at a given clearance of $\Delta=1.0$ mm with 0.75 mL MCF slurry, respectively. It is obviously observed that the variation tendencies of both the surface roughness and the form error during polishing were similar with those in Fig.4.4. It can be figured out from Fig. 4.5(a) that the highest roughness decrease rate and the smoothest work-surface were attained at the oscillation parameter of $f/A_{p-p}=30\text{Hz}/4\text{mm}_{p-p}$. The final surface roughness decreased from 207 nmRa, 212 nmRa and 205 nmRa to 52.225 nmRa, 9.005 nmRa and 32.433 nmRa, respectively, at $f/A_{p-p}=15\text{Hz}/5\text{mm}_{p-p}$, $30\text{Hz}/4\text{mm}_{p-p}$ and $45\text{Hz}/2\text{mm}_{p-p}$. As for the form error, as can be seen in Fig. 5(b) that the highest form error occurred also at $f/A_{p-p}=30\text{Hz}/4\text{mm}_{p-p}$. After 150 min polishing, the form error increased to 1.89%, 3.6% and 2.89%, respectively, at $f/A_{p-p}=15\text{Hz}/5\text{mm}_{p-p}$, $30\text{Hz}/4\text{mm}_{p-p}$ and $45\text{Hz}/2\text{mm}_{p-p}$.



(a)



(b)

Fig 4.5 Effects of oscillation parameter on (a) surface roughness and (b) form error.

According to the Preston hypothesis, the material removal is closely related to the pressure the polisher acts on the work-surface in the polishing zone and the relative velocity between the abrasive grains and the workpiece. In this part, as the composition of MCF slurry used and the clearance were kept constant, the polishing pressure would be independent of the parameter f/A_{p-p} and kept constant, meaning that the larger the relative velocity between the abrasive grains and workpiece was, the higher the material removal rate became. The maximum relative velocity reached 0.24 m/s, 0.38 m/s and 0.28 m/s, respectively, at $f/A_{p-p}=15\text{Hz}/5\text{mm}_{p-p}$, $30\text{Hz}/4\text{mm}_{p-p}$ and $45\text{Hz}/2\text{mm}_{p-p}$. This is the reason why the highest form error rate and the smoothest work-surface were obtained at $f/A_{p-p}=30\text{Hz}/4\text{mm}_{p-p}$.

4.4 Surface finishing of linear V-grooves (OFC)

4.4.1 Structure and dimensions of workpiece

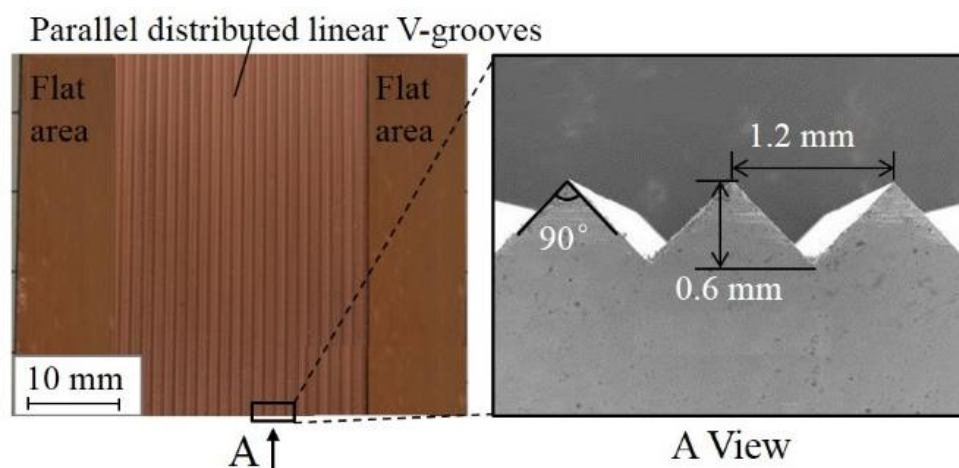


Fig. 4.6. Structure and dimensions of workpiece with miniature V-grooves

The structure and dimensions of the workpiece with miniature V-grooves are shown in Fig. 4.6. This workpiece was prepared by generating parallel distributed linear V-grooves on an OFC plate using a shaping technique on a numerical control milling machine (VHR-AN by Shizuoka Machine Tool CO.) using a superhard cutting tool.

The detailed dimensions of the miniature V-grooves generated were 0.6 mm in depth, 1.2 mm in pitch, and 90° in included angle (see the right side of Fig. 4.3). The original roughness values of the side surfaces of the V-grooves were in the range of 320–340 nm Ra.

4.4.2 Experimental conditions and procedure

The purpose of this study was to determine the feasibility of finishing V-grooves with an MCF slurry and elucidate the fundamental finishing characteristics, including the variations in the form accuracy and surface roughness during polishing. Therefore, the composition of the MCF slurry used and the experimental parameters (worktable vibration frequency/amplitude, magnet eccentricity, magnet revolutionary speed, MCF carrier rotational speed, amount MCF slurry supplied, and clearance) were kept constant, as listed in Table 4.1 and Table 4.3, respectively, based on the present author's previous work on surface finishing with an MCF slurry [25]. Subsequently, under these experimental conditions, the variations in the form accuracy and surface roughness values of the V-grooves during polishing were attained experimentally.

Based on previous results [19], a circular interacting area between the MCF slurry and the workpiece can be established in less than 3 s once the magnet begins to revolve and generate a rotary magnetic field, and the interacting area diameter D depends on the magnet diameter, magnet eccentricity, amount of MCF slurry supplied, and clearance. Therefore, in this work, the polishing area became elliptical (Fig. 4.7(a)), with a major diameter of $D+2A$ and a minor diameter of D because of the vibration of the workpiece at amplitude A along the X axis. The actually measured minor diameter was $D = 32$ mm, and the vibration amplitude was $A = 2$ mm under the current experimental conditions.

Table 4.3 Experimental parameters

Workpiece	Linear V-grooves (Pitch:1.2 mm, Depth:0.6 mm, Angle=90 °)
Frequency/Amplitude, f/A	30 Hz/2 mm B=0.45 T
Magnet	Eccentricity $r=4.5$ mm Rotational speed $n_m=1000$ rpm
MCF carrier	Rotational speed $n_c=10$ rpm
Supplying of MCF slurry, V	0.75 mL
Polishing time, t	30, 60, 90, 120, 150 min
Clearance, Δ	1.0 mm

When polishing with an MCF slurry, the material removal is attributed to the micro-cutting action of abrasive particles and depends on the relative velocity of the abrasive particles to the workpiece and the tangential polishing force imposed on the work surface [13]. It can be determined from Fig. 4.7(a) that the material removal rates at different locations in the polishing zone would be different because the relative velocity, composed of the work vibration speed and abrasive particle revolution speed, would be different at different locations. In turn, this would lead to the occurrence of differences in the form accuracy/surface roughness at different locations. In order to clarify this, the material removal, form accuracy, and surface roughness were investigated for eight different locations (P1 – P8 in Fig. 4.7(a)), which were aligned at equal intervals along a circle with a diameter of $D_L = 9.6$ mm. Additionally, given that the clearance between the MCF carrier and the work surface is the major factor affecting the work-surface roughness [19], the surface roughness values at different positions on both sides of a V-groove would be different owing to the difference between the clearances at different positions, as can be determined from the right portion of Fig. 4.1. Consequently, in this work the surface roughness values at four different position, i.e. the upper left, upper right, lower left, and lower right (see Fig. 4.7(b)), were measured for comparison.

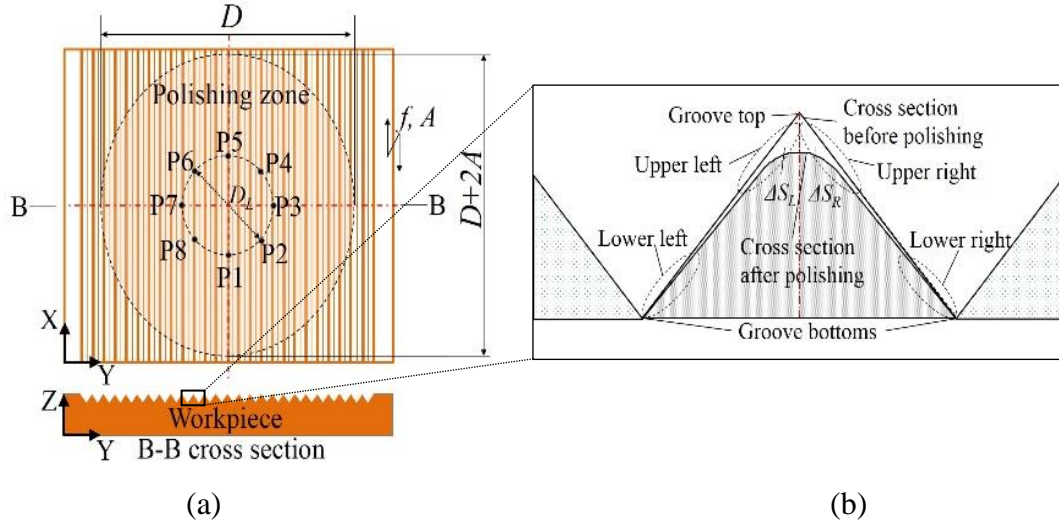


Fig. 4.7. Measuring locations and positions in polishing zone

Usually, the form accuracy was characterized using the form retention rate, but after MCF polishing, the unequal material removal was found on different sides of grooves. In order to clearly indicate this phenomenon the left-right symmetry error (ε) was defined to investigate the difference. They were introduced and respectively defined as follows:

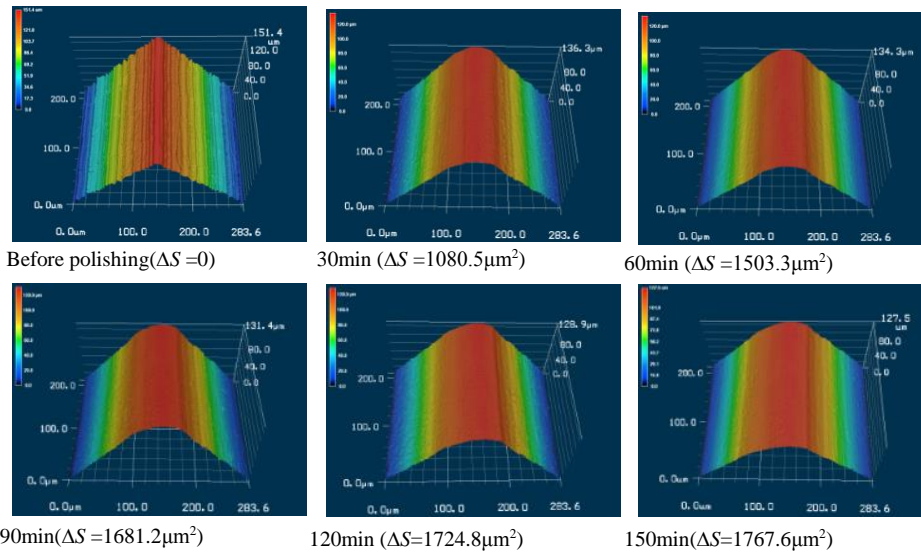
$$\eta = \frac{S}{S_0} \times 100\% \quad (4.2)$$

$$\varepsilon = \frac{\Delta S_L}{\Delta S_R} - 1 \quad (4.3)$$

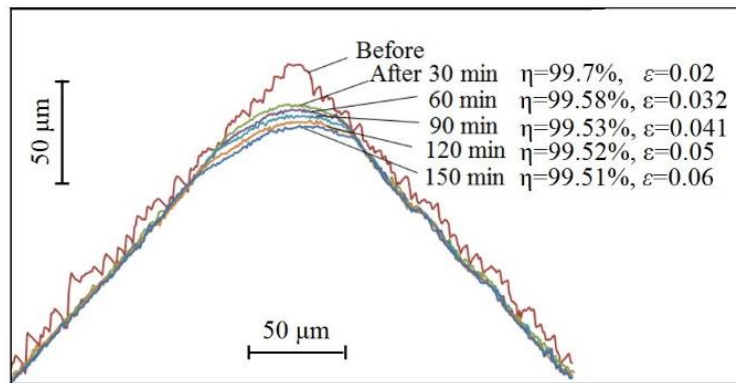
where S_0 and S are the cross-sectional areas of a single V-groove before and after polishing (see Fig. 4.4(b)), respectively. Thus, the decrease in cross-sectional area, $\Delta S = S_0 - S$, can be regarded as the material removal. ΔS_L and ΔS_R are the decreases in the areas on the left and right halves of the cross-sectional area, respectively, hence $\Delta S = \Delta S_L + \Delta S_R$. Accordingly, $\varepsilon = 0$, i.e. $\Delta S_L = \Delta S_R$, indicates that the same amounts of material are removed on both sides of the V-groove, showing that the V-groove exhibits an ideal left–right symmetry even after polishing; when $\varepsilon < 0$ (or > 0), i.e. $\Delta S_L <$ (or $>$) ΔS_R , the material removal on the left (or right) side is less than that on the right (or left)

side, indicating that the groove became asymmetric after polishing.

To obtain the surface roughness, 3D and cross-sectional profiles, and SEM images of the polished V-grooves using a white-light interferometer (Zygo Newview 600 by Zygo Corp.), 3D colour laser scanning microscope (VK-9700 by Keyence Corp.), and scanning electron microscope (ERA-8900 by Elionix), respectively.



(a) 3D laser microscopic images



(b) Cross-sectional profiles of a single linear groove

Fig. 4.8. (a) 3D laser microscopic images and (b) cross-section profiles at P2 before and after polishing for different times

4.4.3 Experimental results

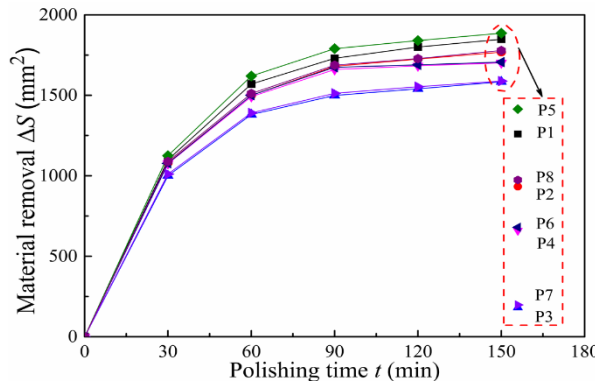
4.4.3.1 Form accuracy

The variations in the V-groove form accuracies during polishing were first investigated. Fig. 4.8(a) and (b) shows typical 3D laser microscopic images and cross-sectional profiles at location P2 before and after polishing for different polishing times, respectively. The material removal ΔS , form retention rate η , and left–right symmetry error ε were also obtained, as shown in the same figure. It can be observed in Fig. 4.8(a) that the surface became smooth gradually, and the material removal increased monotonically during polishing. However, it also seen in Fig. 4.8(b) that the material removal at a position close to the groove top was more than that at a position close to the groove bottom, and the form accuracy became increasingly worse during polishing. Nevertheless, after 150 min of polishing, the resultant form retention rate η and symmetry error ε were 99.51% and 0.06, respectively, showing that the resultant form accuracy satisfied the requirement for the injection mould of a sunlight concentration Fresnel lens.

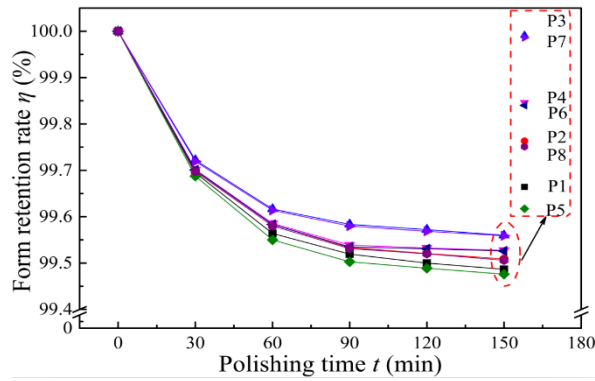
The variations in ΔS , η , and ε at different locations during polishing are compared in Fig. 4.6(a), (b), and (c), respectively. Similar variation tendencies can be observed for the values of ΔS and η and the absolute value of ε for different locations. At the beginning, they increase rapidly. Then, after a while, e.g. at around 30 min, the increase rate gradually declines, leading them to eventually reach their respective saturation values. However, it is worth noting that the saturation values at different locations were different from each other, indicating that not only the material removal but also the form accuracy would be different at different locations in the polishing zone.

In order to determine why the form accuracy and material removal values were different at different locations, i.e. P1 and P3, the attention is shifted to the 3D and cross-sectional profiles of the V-grooves at P1/P3 which were shown in Fig. 4.10. The

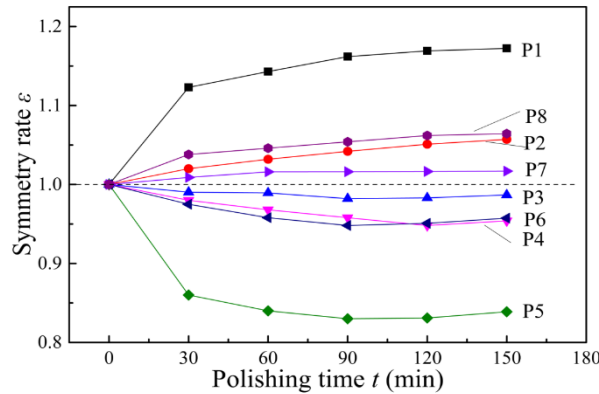
resultant material removals and form accuracies after polishing at different positions are shown in Fig. 4.8.



(a) Material removal increases with the increase of polishing time



(b) Form retention rate decreases with the increase of polishing time



(c) The absolute value of symmetry rate increases with the increase of polishing time
 Fig. 4.9. Variations in material removal ΔS , form retention rate η , and symmetry error ε during polishing

Fig. 4.10 (a) demonstrated that after polishing, although the side surfaces of the grooves at P1/P3 were smoother, the final cross-sectional profiles were different. This was probably owing to the difference between the material removal behaviours at the

different locations, which subsequently resulted in the occurrence of differences between the form retention rate η and the symmetry error ε at the different locations (Fig. 4.11). The reason for this phenomenon will be discussed in section 4.4.4.

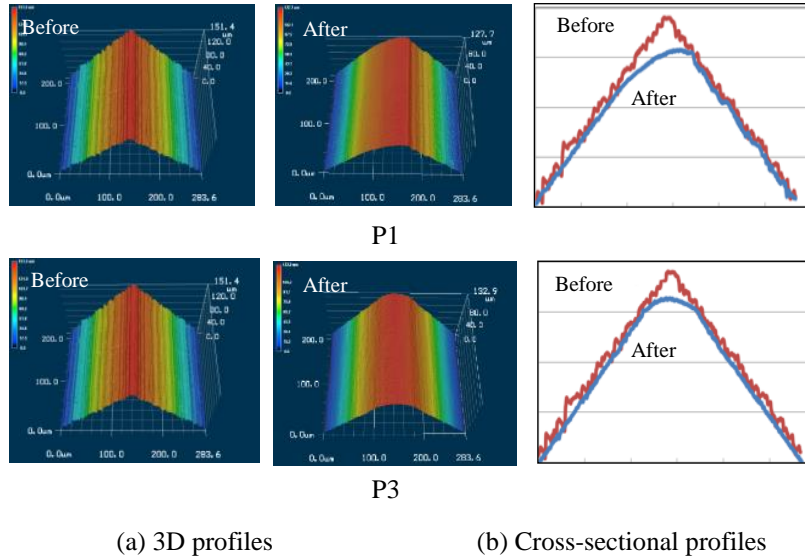


Fig. 4.7. 3D and cross-sectional profiles before and after 150 min of polishing at

P1/P3

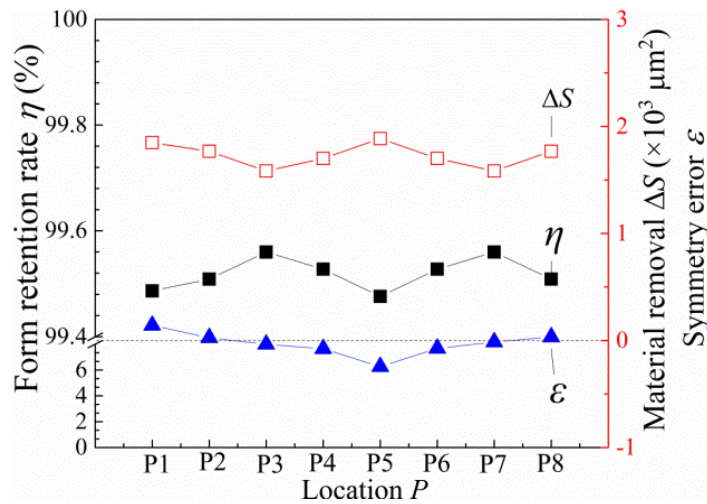


Fig. 4.11. Form retention rate, material removal, and symmetry error values after 150 min of polishing at different locations

4.4.3.2 Surface roughness

SEM observations and roughness measurements were carried out on the work surface before and after polishing for different times at different locations/positions. As an example, Fig. 4.12(a) and (b) shows SEM images of a single V-groove before and

after 150 min of polishing at four different positions at location P1, respectively. As can be observed in the figures, the parallel distributed cutting marks on the side surface of the groove generated in the previous machining process disappeared completely after 150 min of polishing. In addition, although there is a slight difference between the final surface roughness values at the different positions, the roughness values at the upper-left, upper-right, lower-left and lower-right positions significantly decreased from their initial values of 323.63, 325.63, 304.80 and 305.80 nm Ra to the final ones of 17.91, 75.57, 38.71 and 45.84 nm Ra, respectively, demonstrating that a mirror surface was attained for the V-grooves using the proposed polishing technique.

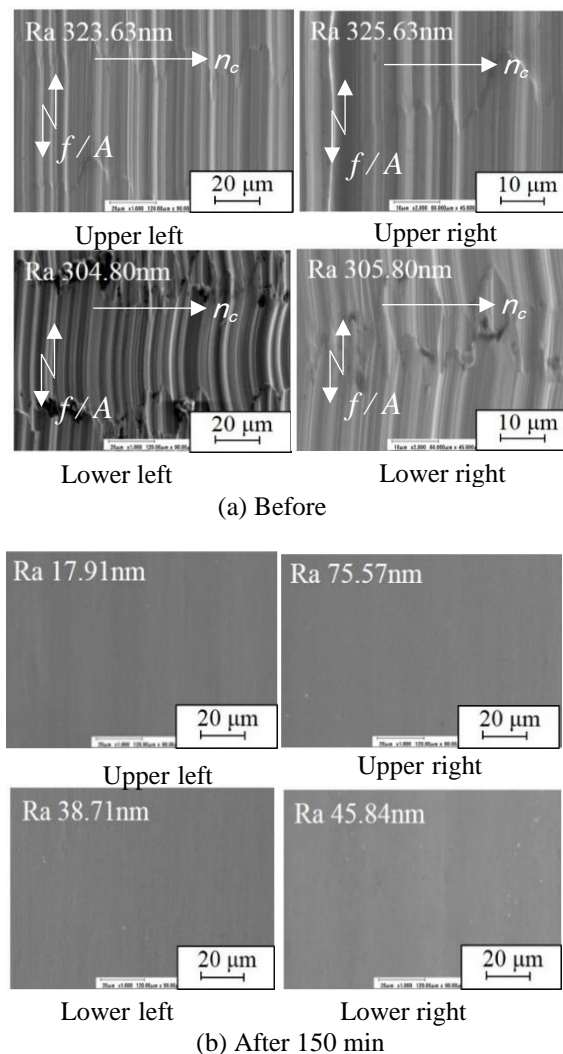


Fig. 4.12. SEM images of V-groove before and after 150 min of polishing at different positions for location P1

Table 4.4 lists the variations in the final normalized surface roughness at different locations at the upper-left, lower-left, upper-right, and lower-right positions, respectively. The normalized surface roughness, which was defined as $NRa = Ra/Ra_0$ (Ra_0 and Ra are the work-surface roughness values before and after 150 min polishing), was introduced to indicate the surface roughness improvement. It can be observed from Table 4.4 that for every location/position, the final normalized surface roughness NRa was different. According to the final normalized surface roughness NRa , the surface quality Ra can divide into two part: good ($NRa \leq 0.2$) and bad ($NRa > 0.2$).

Table 4.4 Variations of final normalized surface roughness NRa at different locations/positions

Location Position	P1	P2	P3	P4	P5	P6	P7	P8
Upper left	0.06	0.09	0.11	0.23	0.41	0.20	0.11	0.06
Upper right	0.34	0.21	0.11	0.06	0.09	0.11	0.11	0.22
Lower left	0.13	0.22	0.17	0.23	0.17	0.21	0.16	0.23
Lower right	0.20	0.15	0.19	0.14	0.16	0.24	0.16	0.23

The quality ranks are displayed in Fig. 4.13. It is worth noting that at P4, P5, and P6, the surface quality of Ra on the right side of grooves were better than those on the left sides, whereas at P1, P2, and P8, the phenomenon was the reverse. It can also be found that the surface quality of Ra at the upper positions of the locations, except the right side of P1 and left side of P5, were better than those at the lower positions. Furthermore, it can be seen that the surface quality of Ra at P3 and P7 were good. The reason for this phenomenon will be discussed in detail later in sub-section 4.4.4.3.

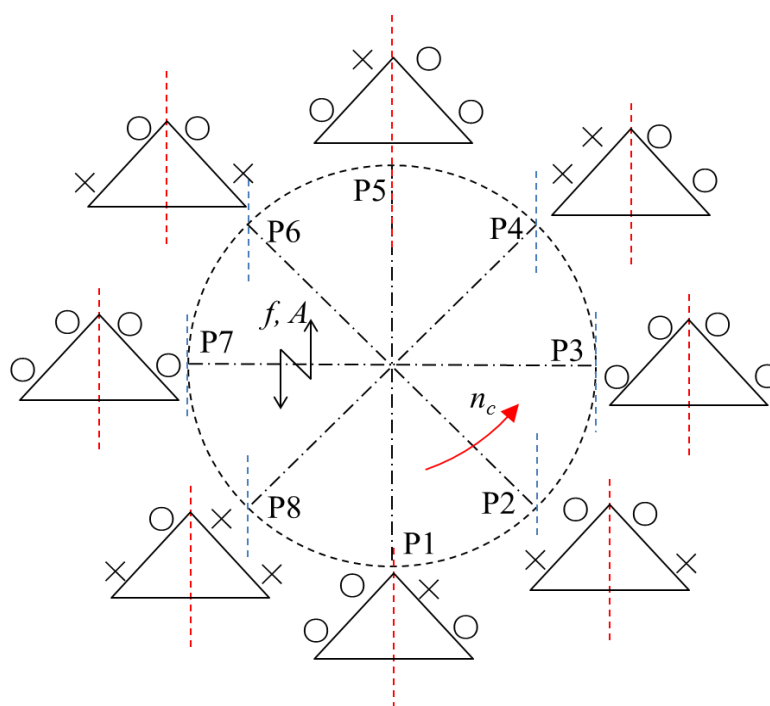


Fig. 4.13. Surface roughness values at different locations and positions

4.4.4 Discussions

As previously clarified in section 4.4.3, the form accuracy, i.e. the form retention rate and symmetry error, and surface roughness values were different at different locations/positions. These phenomena could be predominantly attributed to the following three reasons: 1) the distribution of abrasive particles was non-uniform in the polishing zone; 2) the clearances between the MCF carrier and the work surface were different at different positions; 3) the relative velocities of the abrasive particles to the work surface were different at different locations. This section discusses how the internal structure of the MCF slurry used was investigated using SEM observation to elucidate the abrasive particle distribution. Then, the effect of the clearance is discussed. Finally, the relative velocities of the abrasive particles to V-grooves at different locations are analyzed followed by a discussion of the dependence of the form accuracy and surface quality Ra on the velocity.

4.4.4.1 Internal structure of MCF slurry

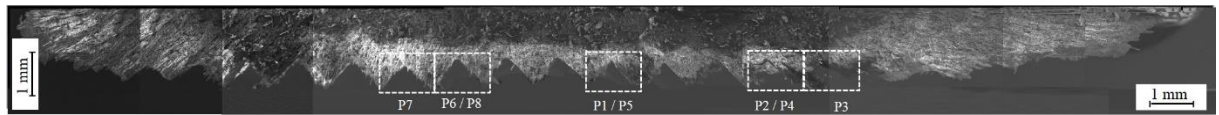
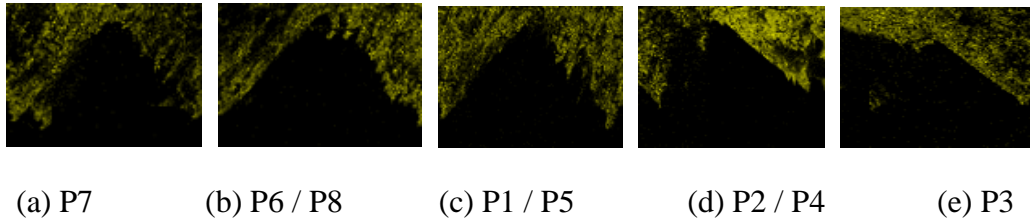


Fig. 4.14. SEM image of MCF cross-sectional profile during polishing process



(a) P7 (b) P6 / P8 (c) P1 / P5 (d) P2 / P4 (e) P3

Fig. 4.15. Aluminum element distributions of MCF slurry obtained with energy dispersive X-ray

For the SEM observation, an MCF slurry specimen was prepared by cutting off the MCF slurry used for 5 min along the line of B-B (see Fig. 4.4(a)). Thereafter, the specimen was placed into the SEM to observe its internal structure and investigate the distribution of the oxide aluminum (Al_2O_3) abrasive particles within the used MCF slurry. Fig. 4.14 shows the obtained SEM image of the entire B-B cross section of the MCF slurry used. Evidently, corresponding to the locations of the V-grooves on the work-surface, numerous V-shaped grooves were formed in the MCF slurry, correspondingly due to the replication principle, and their sizes, including the depth and pitch, were approximately the same as those of the V-grooves in the workpiece (see Fig. 4.3). This indicates that the MCF slurry reached the whole surface of the V-grooves during polishing, and all the locations of the V-grooves within the polishing zone could be polished, as long as the abrasive particles were uniformly distributed in the same zone.

In order to confirm this, the aluminum element distributions were obtained, and the typical ones for the areas corresponding to locations P7, P6/P8, P1/P5, P2/P4, and P3 (see Fig. 4.14) are shown in Fig. 4.15(a)–(e), respectively. From this figure, it can

be observed that the abrasive particles (Al_2O_3) were distributed evenly within the slurry. This fact excluded the possibility that the differences in the form accuracy and surface quality Ra values at different locations/positions were caused by an uneven distribution of the abrasive particles in the polishing zone.

4.4.4.2 Effect of clearance

According to Guo et al. [19], in the polishing of optical glasses using an MCF slurry under a rotary magnetic field, the material removal rate (MRR) depends significantly on the tangential polishing force, which is considerably affected by the clearance between the MCF carrier and the work surface. In this study, as shown in Fig. 4.1, the actual clearance between the MCF carrier and the work surface at a position closer to the groove top was smaller than that at a position closer to the groove bottom. Thus, the tangential polishing force on the upper position was higher than that at the lower position. This would, consequently, be one of the reasons why a larger amount of work material was removed at a position closer to the groove top (see Fig. 4.11(b)). The surface asperity of the V-groove at the upper position was hence more eliminated than that at the lower positions, resulting in the surface quality Ra values at most of the upper positions being better than those at the lower positions (see Fig. 4.16). Therefore, it is very important to make the clearance the same at every position to enhance the form accuracy and improve the uniformity of the surface quality Ra for the whole polishing work surface. A strategy to solve this problem will be developed in future work.

4.4.4.3 Effect of relative velocity of abrasive particles to V-groove

Guo et al. [19] also stated that besides the tangential polishing force, the relative velocity of the abrasive particles to the work surface greatly affects the material removal. In the current work, as illustrated in Fig. 4.16, the relative velocity V at arbitrary

location P, as determined by azimuth angle α and radius R , in the polishing zone was the combination of two velocities at the same location. The first was the vibration velocity of workpiece V_w on the X axis caused by the worktable oscillation, and the other was the tangential velocity of the abrasive particles V_{MCF} along the line tangent to a circle with radius R at location P. The value of V_{MCF} resulted from the MCF carrier rotational motion when assuming that all the abrasive particles within the MCF slurry revolved solidly following the rotation of the MCF carrier.

Let the amplitude, frequency, and phase of the worktable oscillation be A , f , and φ , respectively. Then, the workpiece vibration motion can be expressed as

$$x = A \cos(2\pi ft + \varphi) \quad (4.4)$$

The workpiece velocity is obtained by differentiating Eq. (3) with respect to time t as follows:

$$V_w = -2\pi f A \sin(2\pi ft + \varphi) \quad (4.5)$$

On the other hand, the value of the abrasive particle velocity at location P is given as follows:

$$V_{MCF} = 2\pi R n_c / 60 \quad (4.6)$$

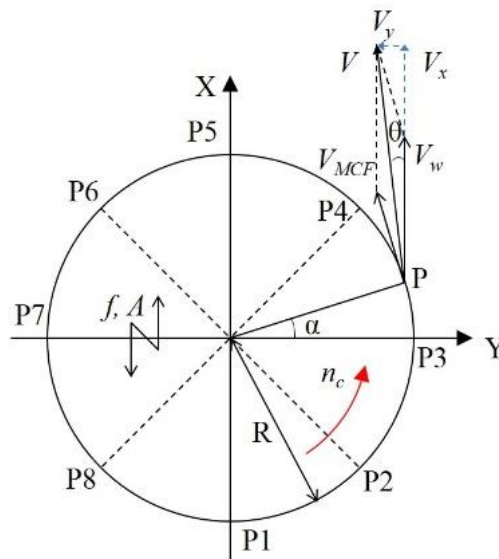


Fig. 4.16. Schematic diagram of relative velocity of abrasive particles to work surface

Subsequently, the X and Y components, V_x and V_y , of velocity V can be determined using Eqs. (4.7) and (4.8), respectively.

$$V_x = V_{MCF} \cos \alpha + V_w \quad (4.7)$$

$$V_y = V_{MCF} \sin \alpha \quad (4.8)$$

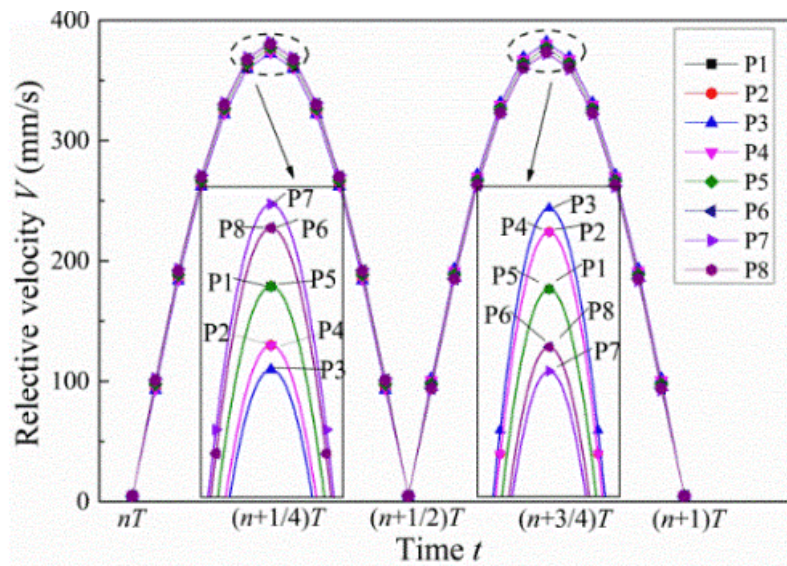
Eventually, an equation for calculating the value of V can be obtained from Eqs. (4.5) and (4.6), as follows:

$$V = \sqrt{V_x^2 + V_y^2} = 2\pi \sqrt{[Rn_c/60 - fA \sin(2\pi ft + \varphi) \cos \alpha]^2 + [fA \sin(2\pi ft + \varphi) \sin \alpha]^2} \quad (4.9)$$

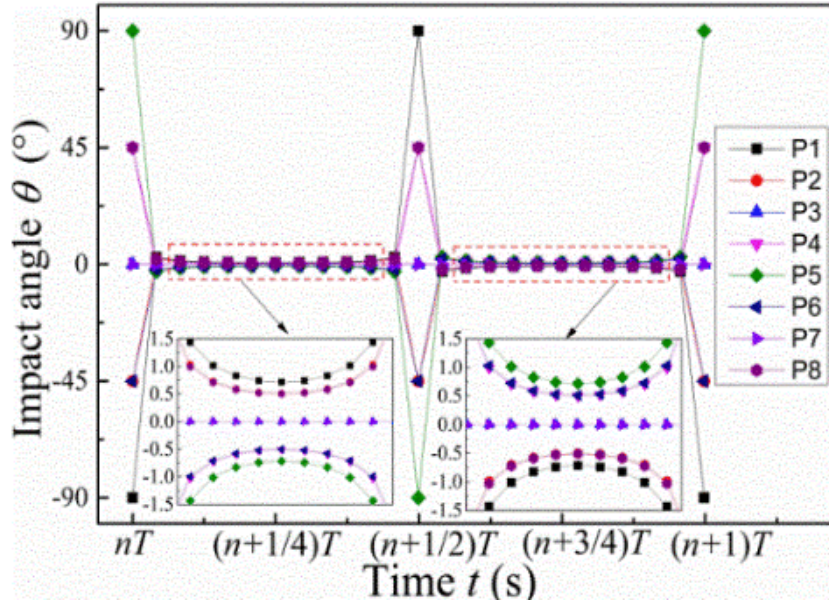
In addition, the angle θ between the relative velocity and the X axis is given as follows:

$$\theta = \arctan \frac{V_y}{V_x} = \arctan \frac{V_{MCF} \sin \alpha}{V_{MCF} \cos \alpha + V_w} \quad (4.10)$$

This determines the impact direction of the abrasive particles against the side surface of the V-grooves, and hereafter is called the impact angle.



(a)



(b)

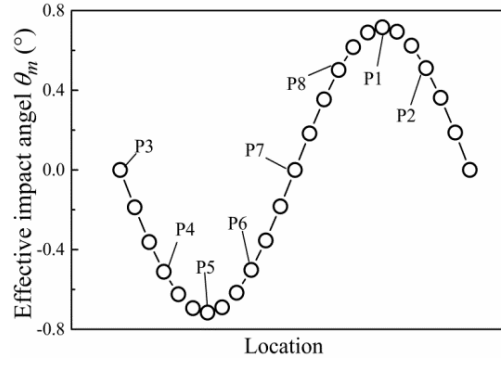
Fig. 4.17. Changes in (a) V and (b) θ at different positions during cycle period of workpiece

Fig. 4.17(a) and (b) shows the variations in the values of V and impact angle θ during an arbitrary vibration cycle of $t = nT \sim (n+1)T$ at locations P1–P8, respectively, calculated using Eqs. (4.9) and (4.10), where n is a natural number, i.e. 0, 1, 2... and T is the vibration period. In this calculation, the values of α were -90° , -45° , 0° , 45° , 90° , 135° , 180° , and -135° for the locations of P1–P8, respectively, and the value of R was 4.8 mm because the diameter of the circle with which P1–P8 was aligned was $D = 9.6$ mm, as previously mentioned in subsection 4.2.4. The values of the other parameters used for calculation are listed in Table 3. In addition, the phase was set at $\varphi = 0$ for simplicity, and the workpiece vibration period was determined to be $T = 1/f = 1/30$ Hz = 0.33 s.

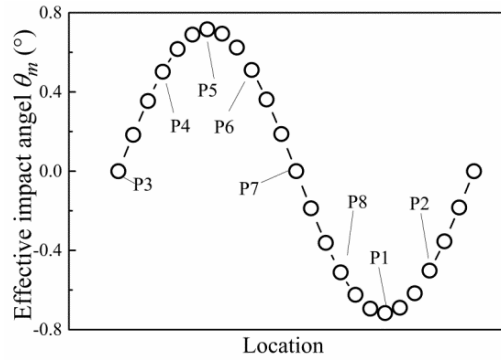
As can be seen in Fig. 4.17(a), either V or θ at all the locations varied periodically with the same period of $T/2$. V reached its respective peaks at the moments of $t = (n+1/4)T$ and $(n+3/4)T$, whereas it declined to its respective valleys at $t = nT$ and $t = (n+1/2)T$ (Fig. 4.17(a)). Compared to the peak values of V , which were in the range of 372–

382 mm/s, its valley values were 5.03 mm/s, which were less than 1.4% of the peak ones, i.e. the former was significantly larger than the latter, implying that the material removal was dominantly obtained at the moments of around $t = (n+1/4) T$ and $(n+3/4) T$. The same figure also shows that, although the peak values of V at different locations were different from each other, the difference between them was very small; for example, at the moment of $t = (n+1/4) T$ the highest relative velocity of $V = 382$ mm/s occurred at P7 and the lowest one of $V = 372$ mm/s occurred at P3. Thus, the difference between them was just about 2.4%. This suggests that the difference between the material removals at different locations was hardly caused by the difference in the peak values of V .

The impact angle θ (Fig. 4.17(b)) reveals that at the moments of around $t = n T$ and $(n+1/2) T$, the absolute value of θ reached much greater values. However, at other moments, it became very small, less than 2.76° . As previously stated, the materials were dominantly removed at the moments of around $t = (n+1/4) T$ and $(n+3/4) T$ when V reached its maximum, rather than at the moments of around $t = n T$ and $(n+1/2) T$, when V was at its minimum. Hereinafter, the impact angle θ at the moments of $t = (n+1/4) T$ and $(n+3/4) T$ are defined as the effective impact angle θ_m . The values of θ_m were obtained for different locations at the two moments. Fig. 4.18(a) and (b) shows the obtained θ_m for the P1–P8 locations at the moments of $t = (n+1/4) T$ and $(n+3/4) T$, respectively, revealing that θ_m varied in the range of -0.72° – 0.72° between the locations, regardless of the moment. However, at the same location, the absolute value of θ_m is found to be independent of the moment, whereas its sign at $t = (n+1/4) T$ was the opposite to that at $t = (n+3/4) T$, indicating that although the value of the effective impact angle remained constant, the impact direction was reversed periodically during polishing. This phenomenon might significantly affect the material removal and form accuracy, as well as the work-surface quality.

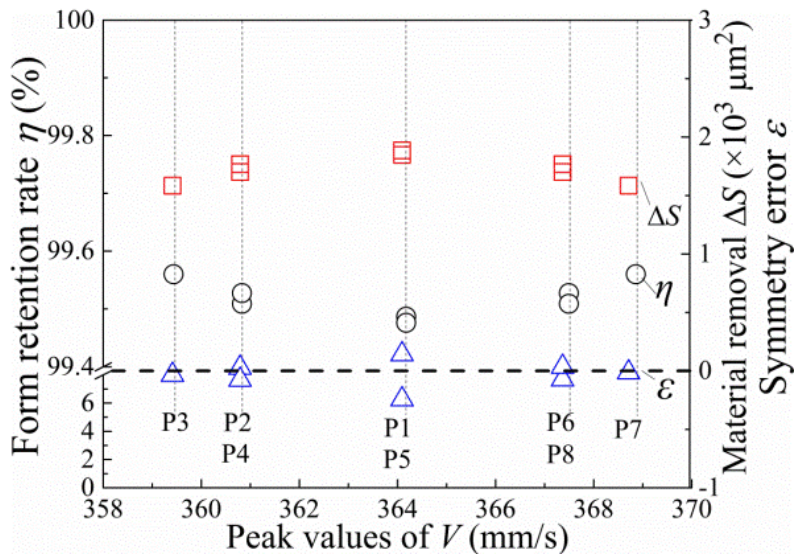


(a) $(n+1/4) T$

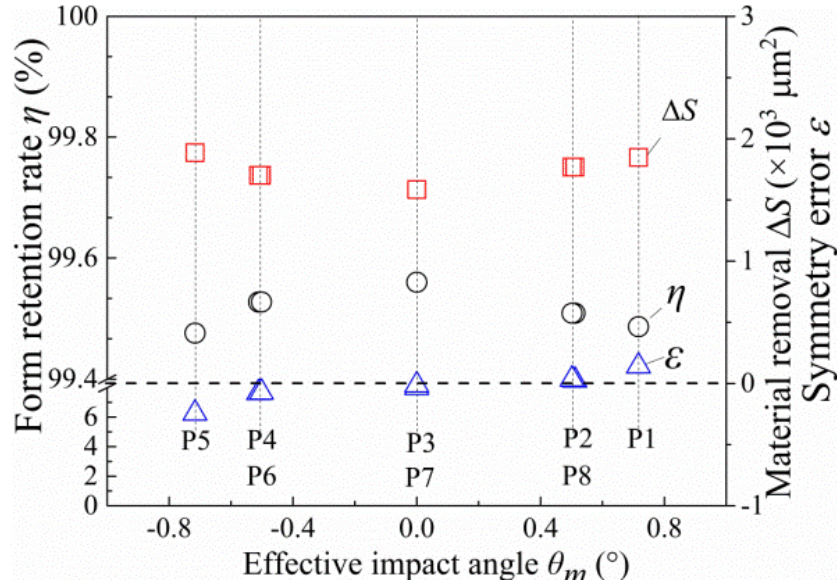


(b) $(n+3/4) T$

Fig. 4.18. Changes in θ_m at different positions



(a)



(b)

Fig. 4.19. Peak values of V /effective impact angle θ_m vs. material removal/form accuracy at $(n+1/4)T$

In order to confirm the previous discussion, the experimentally obtained material removal ΔS , form retention rate η , and symmetry error ϵ were plotted against the calculated peak values of V and θ_m for the moment of $t = (n+1/4)T$, as shown in Fig. 4.16(a) and (b), respectively. The dependence of ΔS , η , and ϵ on the peak values of V (Fig. 4.16(a)) is hardly observed, demonstrating that the difference between the material removal and form accuracy values at different locations could not be attributed to the difference in the peak values of V . In contrast, as can be seen in Fig. 4.16(b), a larger absolute value of θ_m resulted in higher values for ΔS and the absolute value of ϵ , whereas a lower value of η , indicating an increase in the absolute value of θ_m , produced an increase in the material removal, but a decrease in the form accuracy. In particular, it should be noted that $\epsilon < 0$ when $\theta_m < 0$ (at P4, P5, and P6), and $\epsilon > 0$ when $\theta_m > 0$ (at P1, P2, and P8). According to Eq. (4.2), $\epsilon < (\text{or } >) 0$, i.e. $\Delta S_L < (\text{or } >) \Delta S_R$, indicates that the material removal on the left side of the V-groove is less (or more) than that on the right side; in other words, at P4, P5, and P6, the material removal values

on the left side were less than those on the right side, while at P1, P2, and P8, this was reversed. These results mean that the material removal and form retention rate are independent of the sign of θ_m , but the symmetry is affected not only by the absolute value but also by the sign of θ_m , i.e. the impact direction of the abrasive particles to the side surface of the V-grooves. Subsequently, the reason why this phenomenon occurred was analysed, and a way to deal with it was investigated, as described below.

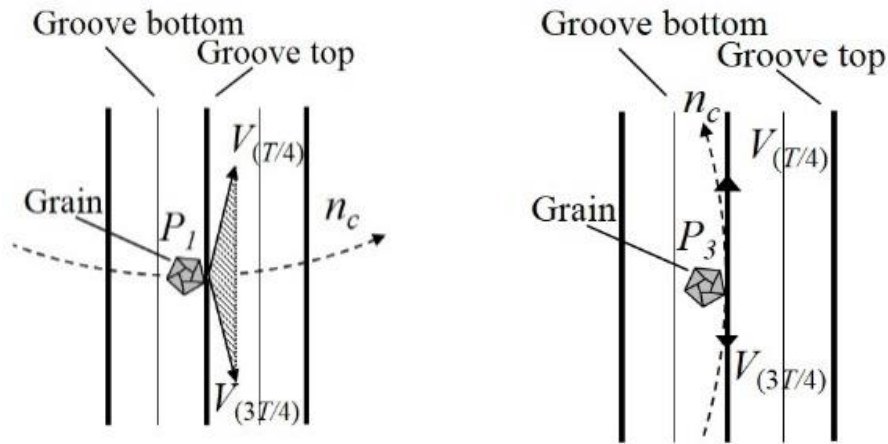


Fig. 4.20. Relative speed vectors of abrasive particles to grooves at P1/P3 during cycle period of workpiece

Based on the data in Fig. 4.18, the distribution of the relative velocity vectors at locations P1/P3 in the polishing zone during cycle period of workpiece is visually displayed in Fig. 4.20. It is interesting to note that the velocity vectors at P1 are always oriented from left towards the right, whereas that at P3 are always along the grooves, i.e. the X axis ($\theta = 0^\circ$), without abrasive particles crosscutting the V-grooves. This phenomenon suggests that the abrasive particles impact the V-grooves with different orientations at different moments. At P1, the abrasive particles first move right towards impact on the left-side surface of the V-groove. Hence, the work material on the right side is removed by the micro-cutting action of the abrasive particles. However, after impacting the right side, the majority of the abrasive particles would move upward due to the repulsion from the right side, which would make it difficult for them to reach the

left side of the V-groove. Thus, little work material would be removed on the left side. At P3, the number of active abrasive particles acting on the left/right side is almost the same as that on right/left side because the particles are distributed uniformly within the MCF slurry. This in turn results in the same material removal, which leads to $\varepsilon = 0$ and the same surface quality of Ra on both sides at the two locations. The phenomenon on other locations can also explain using this method. This fact demonstrates that the relative velocity should be along the V-grooves as much as possible to enhance the form accuracy and reduce the surface quality Ra difference at different positions.

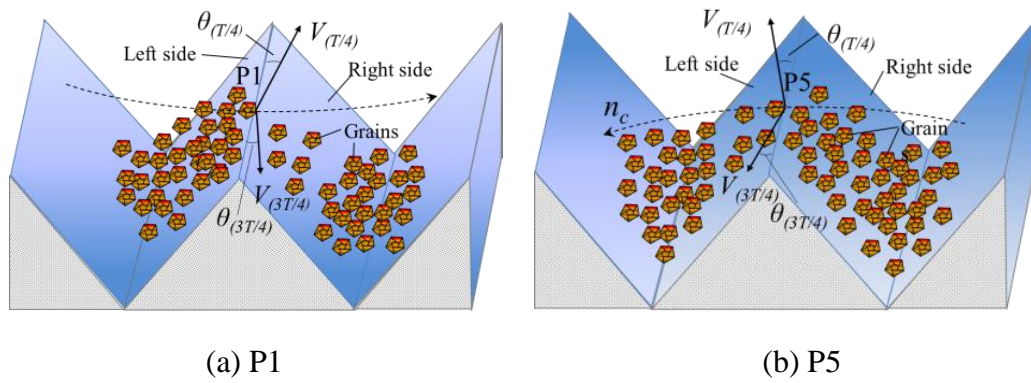


Fig. 4.21. Velocity orientation at polishing locations of P1 and P5

As previously shown in Fig. 13, the surface quality Ra values at the upper positions were better than those at the lower ones for the majority of locations. The exception was the right side at P1 and left side at P5, where this tendency was reversed, i.e. the surface quality Ra values at the lower-right position at P1 and lower-left position at P5 were better than those on the upper-right side at P1 and upper-left side at P5. In order to explore the reason for this phenomenon, the motions of the abrasive particles at P1 and P5 are further discussed in detail in the following.

Fig. 4.21(a) and (b) schematically illustrates the distributions of the abrasive particles and their relative typical velocities at P1 and P5 for the moments of $t = (n+1/4) T$ and $(n+3/4) T$, respectively. As shown in Fig. 4.21(a), at P1, the abrasive particles previously located on the left side of the V-groove move towards the right side with the relative velocities $V_{(T/4)}$ and $V_{(3T/4)}$ alternately at the moments of $t = (n+1/4) T$ and

$(n+3/4)T$. Along with their left-to-right motion, the abrasive particles impact the right side and remove work material at the same side as a result of their micro-cutting actions. Immediately after this, the majority of particles move upward due to the repulsion from the right side of the V-groove, resulting in a reduction in the number of abrasive particles actively acting on the upper-right position of the V-groove. However, at the lower-right position of the groove, this upward movement of the abrasive particles would hardly occur, and thus the number of abrasive particles actively acting there would be maintained. In general, a larger number of active abrasive particles will remove a larger amount of material, implying that at P1, the material removal at the upper-right position is less than that at the lower-right position. A similar phenomenon can be observed on the left side at P5 (Fig. 4.21(b)).

4.4.4.4 Effect of MCF carrier rotation speed

As previously clarified, it is crucial to decrease the effective impact angle θ_m as much possible to obtain a higher form accuracy and better surface quality Ra, as well as a smaller difference in the surface quality Ra values at different locations/positions in the grooves.

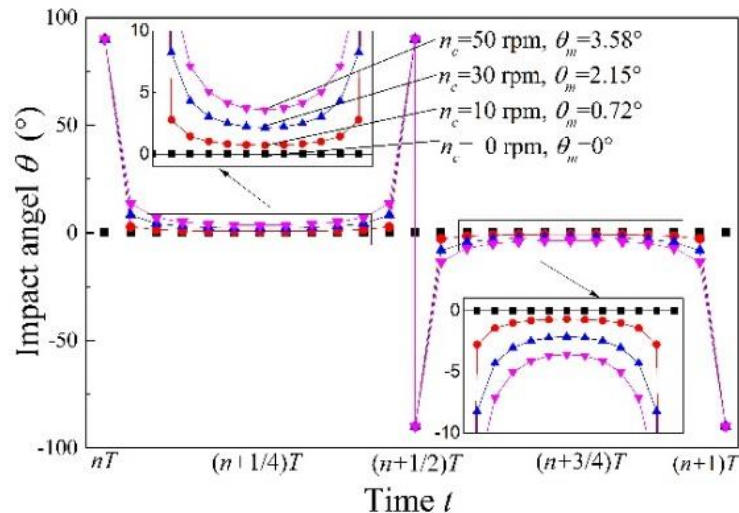


Fig. 4.22. Changes in θ at different MCF rotational speeds during workpiece cycle period

According to Eq. (4.10), the impact angle θ depends on the MCF carrier rotational speed and the work vibration speed. As previously mentioned in section 4.2.1, the MCF carrier is rotated just to prevent the active abrasive particles from always acting on the same polishing area during polishing. Therefore, the MCF carrier rotation speed n_c should be set at an appropriate value. However, based on the variation in the impact angle with time for different values of n_c calculated using Eq.(4.10) (Fig. 4.22), it can be found that a higher rotation speed n_c would result in a larger effective impact angle θ_m , implying that the form accuracy would be deteriorated as n_c increases, according to the discussion in section 4.4.4.3. In order to confirm this implication, polishing experiments were carried out to reveal the actual effects of the MCF carrier rotational speed on the material removal and form accuracy of the V-grooves.

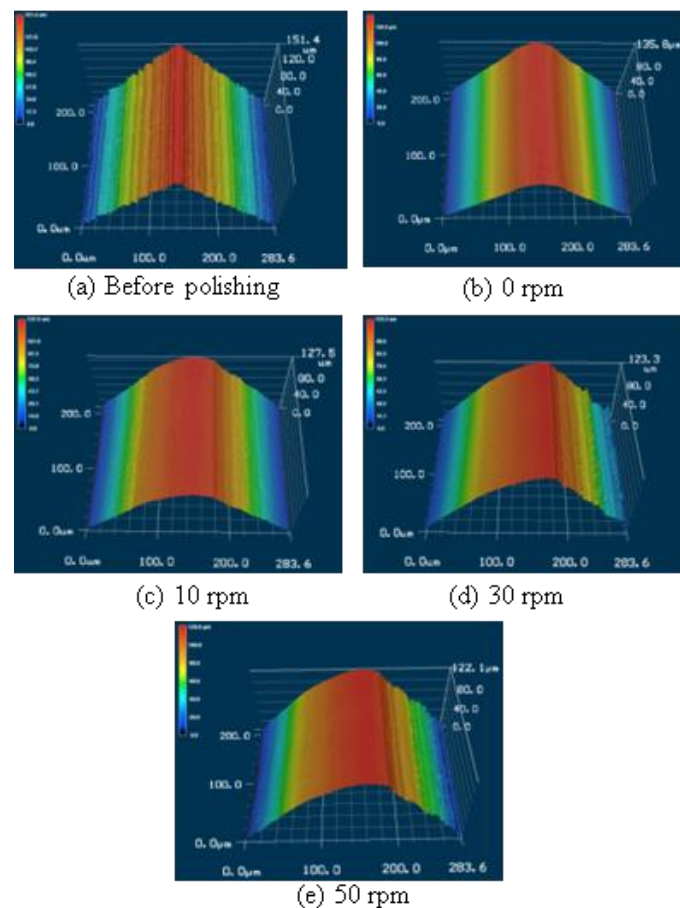


Fig. 4.23. 3D laser microscopic images of V-groove at P1 before and after 150 min of polishing at different MCF carrier rotational speeds

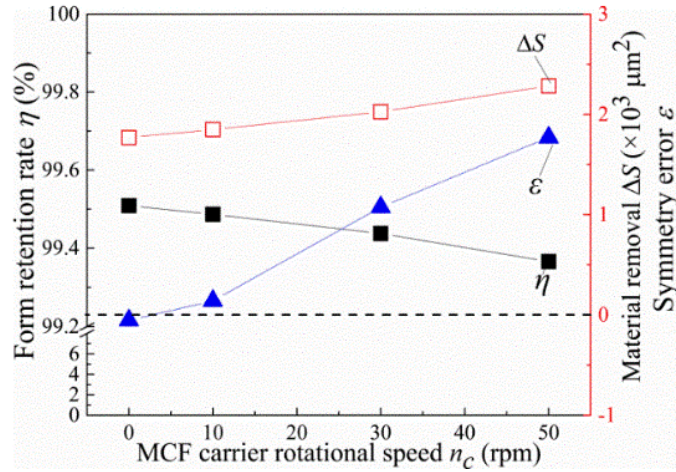


Fig. 4.24. Form retention rate, material removal, and symmetry error after 150 min of polishing at different MCF carrier rotational speeds

As typical experimentally obtained results, Fig. 4.20(a)–(e) shows 3D laser microscopic images of the V-groove at location P1 before and after 150 min of polishing at different MCF carrier rotational speeds, i.e. $n_c = 0, 10, 30,$ and 50 rpm, respectively. A comparison of the image in Fig. 4.20(a) with those in Fig. 4.20(b)–(e) indicates that although, after 150 min of polishing, the side surfaces of the V-groove at all the positions were significantly smoothed, the material removal and form accuracy were different for different values of n_c . In particular, the difference in the surface quality Ra values at the different positions seemingly became greater as the value of n_c increased. Subsequently, the effect of n_c on the material removal and form accuracy were quantitatively obtained from the data, like those in Fig. 4.20, and plotted in Fig. 4.21. It can be observed in this figure that the material removal ΔS increased linearly, and the form accuracy, i.e. the form retention rate η and symmetry error ε , gradually deteriorated as the MCF carrier rotational speed increased. These results confirmed the aforementioned implication that the form accuracy deteriorated as n_c increased, and suggested that the MCF carrier should be rotated as slowly as possible to enhance the form accuracy.

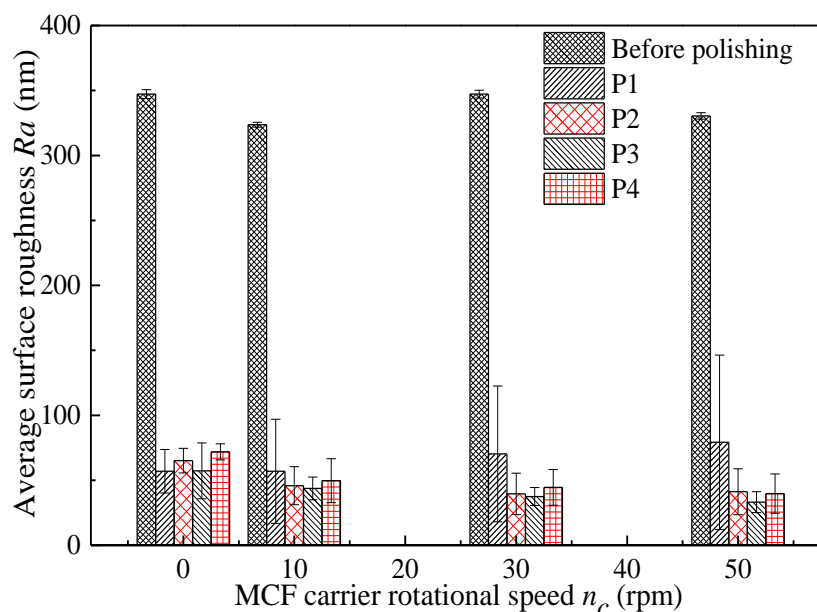


Fig. 4.25. Effects of MCF carrier rotational speed on final surface roughness after 150 min of polishing at different locations

On the other hand, the effects of n_c on the final surface roughness values at different locations were obtained, as exhibited in Fig. 4.25. Herein, the final surface roughness at each location was the average value of four measurements of the surface roughness after 150 min of polishing at four different positions, i.e. the upper left, upper right, lower left, and lower right (see Fig. 4.7(b)), at the corresponding location. For comparison, the initial surface roughness values before polishing at the different locations are also presented in the same figure. As demonstrated by Fig. 4.25, for any value of n_c , the surface roughness values at all the locations were considerably decreased after 150 min of polishing. However, the final surface roughness values were different, not only at different locations, but also at different values of n_c . Although the average values for the four final surface roughness values at the four locations seemingly tended to decrease as n_c increased, once the MCF carrier rotational speed was greater than $n_c = 10$ rpm, n_c seemed to have little influence on any further decrease in the final surface roughness.

When $n_c = 0$ rpm, the surface quality Ra was the worst and the form accuracy was the best compared to those at other values of n_c . This was probably because the active

abrasive particles were always acting on the same polishing area during polishing, which resulted in the least material removal but the best form accuracy (see Fig. 24). Subsequently, taking into account the balance between the form accuracy and the surface quality R_a indicates that the MCF carrier rotation speed should be set at $n_c = 10$ rpm under the experimental conditions used in the current work.

4.5 Ni-P plated surface polishing

The surface of linear V-grooves generated on an oxygen-free copper substrate has been polished to mirror surface using MCF slurry, in addition, the form accuracy of the V-grooves is more than 99.4% which accords with the use requirements in the manufacturing process. Subsequently, the Ni-P plating is particularly useful for hot embossing metal molds/dies and injection metal molds/dies because it extends the working life of the molds/dies, thus reducing production costs on account of its ability to produce coatings with excellent corrosion resistance, wear properties, hardness, and abrasion resistance. Hence, it is difficult to finish Ni-P-plated surfaces via conventional polishing processes. Consequently, to improve the surface quality, it is imperative to develop a novel polishing method that effectively eliminates the excess material while preventing tool marks. In order to investigate the potential ability of polishing the Ni-P plated STAVAX with linear miniature grooves using MCF slurry, the fundamental research on the new material was carried out.

4.5.1 Ni-P plated STAVAX workpiece with linear V-grooves

In this part, for the workpiece shown in Fig.4.26, disc-shaped STAVAX steel (3 mm thick) whose upper surface was coated with an electroless Ni-P-plated layer 1 mm thick was used. The dimensions of the miniature linear V-grooves is as same as the used workpiece in section 4.4. The detailed dimensions of the miniature V-grooves generated

were 0.6 mm in depth, 1.2 mm in pitch, and 90° in included angle. The SEM images of the Ni-P plated STAVAX workpiece with linear V-grooves is shown in Fig.4.27. It can be observed from this figure that the surface topography of the Ni-P plated surface is smoother than that on the oxygen-free copper. For the value of the surface roughness of the grooves surface, the optical surface profiler was used to measure the surface quality.

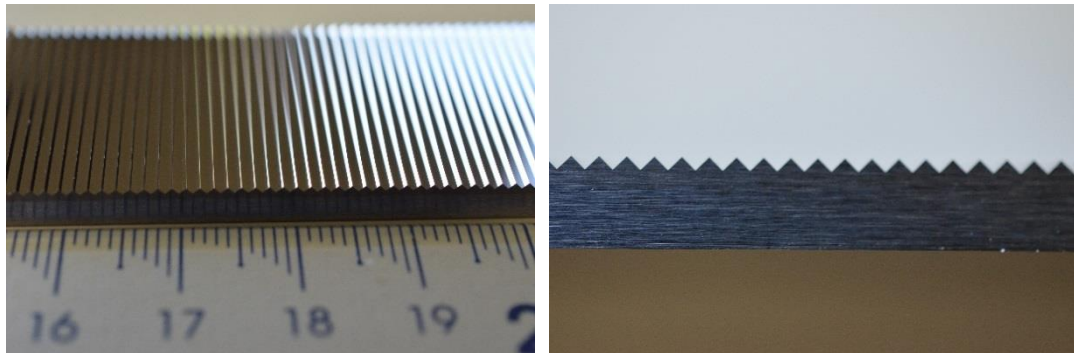


Fig.4.26 Ni-P plated STAVAX workpiece with linear V-grooves

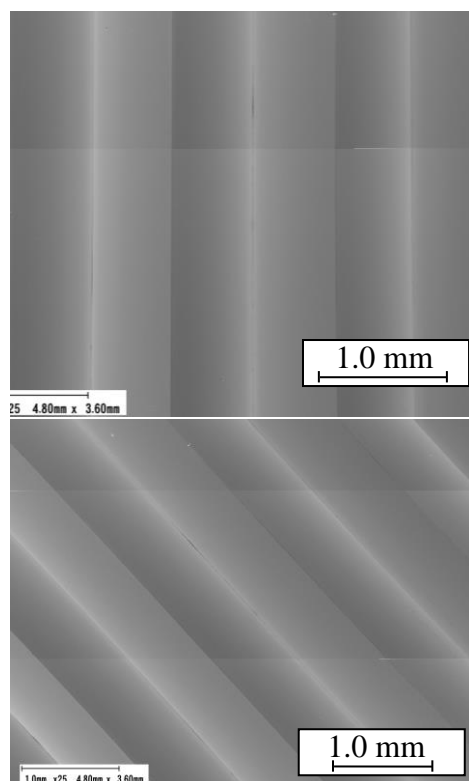


Fig.4.27 SEM images of the linear V-grooves

4.5.2 Experimental conditions

The purpose of this study was to determine the feasibility of finishing V-grooves on Ni-P plated STAVAX with an MCF slurry and elucidate the fundamental finishing characteristics, including the variations in the form accuracy and surface roughness during polishing. Therefore, the composition of the MCF slurry used and the experimental parameters (worktable vibration frequency/amplitude, magnet eccentricity, magnet revolutionary speed, amount MCF slurry supplied, and clearance) were kept constant, as listed in Table 4.1 and Table 4.3, respectively, based on the present author's previous work on surface finishing oxygen-free copper grooves in section 4.4. Subsequently, under these experimental conditions, the variations in the form accuracy and surface roughness values of the V-grooves during polishing were attained experimentally.

4.5.3 Experimental

4.5.3.1 Form accuracy

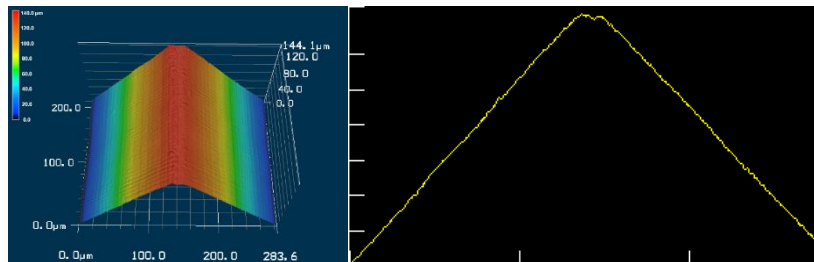


Fig.4.28 3D image and cross section profile of a single groove

Before polishing, the 3D morphology of the miniature grooves was measured and shown in Fig.4.28. The design angle of the single V-grooves is 90 degree, and that of the processed grooves is about 89.48 degree. It can be observed that the shape of the top of the miniature V-grooves keep well. A mount of the cutting marks remain on the side surface of the linear grooves and these marks rough the surface roughness.

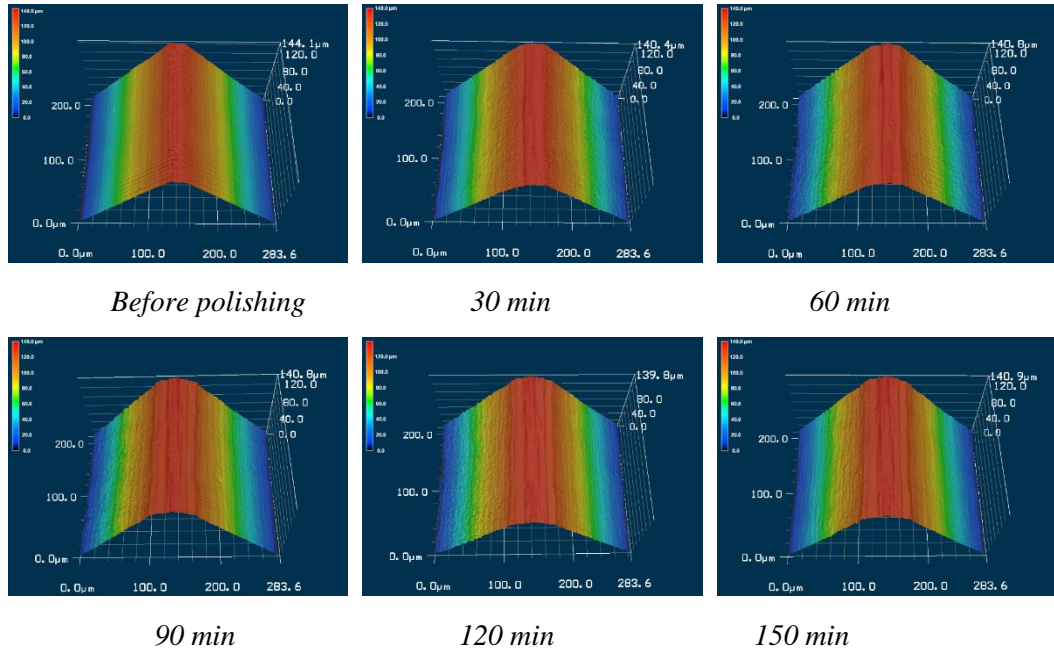
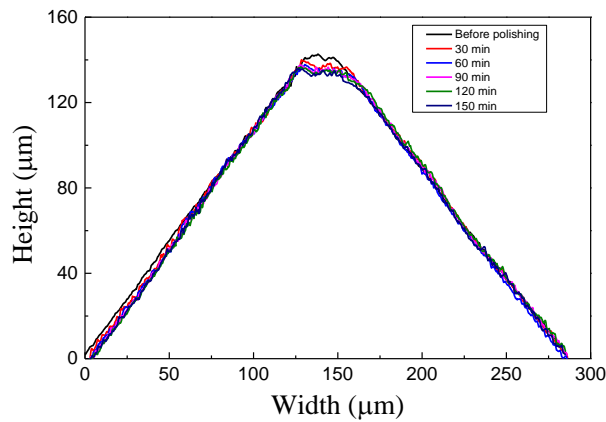


Fig.4.28 3D laser microscopic images with $n_c=50$ rpm

It can be seen in Fig. 4.28 that the material removal at a position close to the groove top was more than that at a position close to the groove bottom, and the form accuracy became increasingly worse during polishing regardless of the MCF carrier rotational speed. However, it can be observed in Fig. 4.29 that the surface became smooth gradually, and the material removal increased monotonically during polishing. Fig.29 (a) shows the changes of the cross section profiles with the polishing time with a lower MCF rotational speed 10 rpm, whereas with the higher rotational speed 50 rpm is shown in Fig.29 (b).



(a) MCF carrier rotational speed $n_c = 10$ rpm

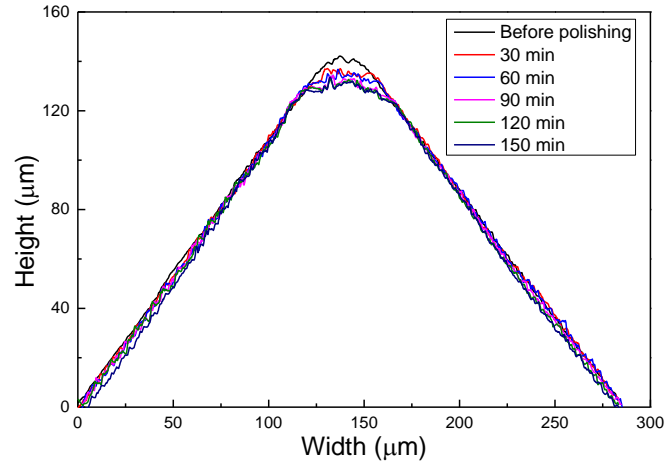
(b) MCF carrier rotational speed $n_c=50$ rpm

Fig.4.29 Cross section profile of a single groove before and after every 30 mins under the given experimental conditions

According to the cross section profile of the grooves before and after MCF slurry polishing, the material removal and the form error were obtained by the decreased height of the groove in the cross section profile. The changes of the value of material removal and form error with the polishing time are shown in Fig.4.30.

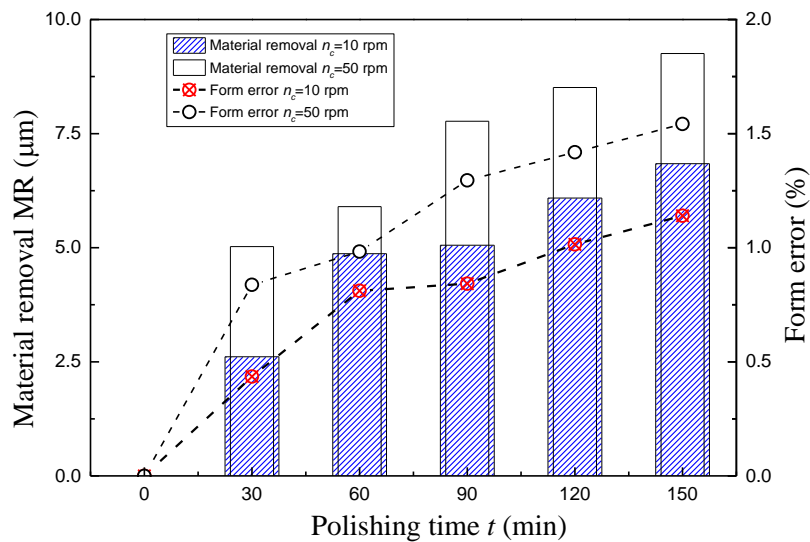


Fig.4.30 Changes of the material removal and form error with the polishing time

From Fig.4.30, it can be found that there is a difference in material removal and form error after MCF slurry polishing with different MCF carrier rotational speeds. The column chart shows the material removal after 150 min of polishing. It demonstrates the

material removal increases with the increasing of polishing time regardless of the MCF carrier rotational speed. However, it is worthy of that the material removal is more with higher MCF carrier rotational speed than that with lower speed and the maximum value of the material removal is less than $10\ \mu\text{m}$ after 150 min MCF polishing process at $=50$ rpm. This difference in material removal results the different of the form error during the polishing process. The form error of the miniature V-grooves increases with the increase of the polishing time. In addition, the form error becomes worse with higher MCF carrier rotational speed than that with lower rotational speed. The notable of that it is less than 1.6% in form error after MCF slurry polishing regardless of the MCF carrier rotational speed. In order to evaluate the r of the miniature V-grooves during the polishing process, the form retention rate of the single grooves is used by the reduced areas of the cross section profiles. Then the changes of form retention rate of the miniature grooves with polishing time is shown in Fig. 4.31.

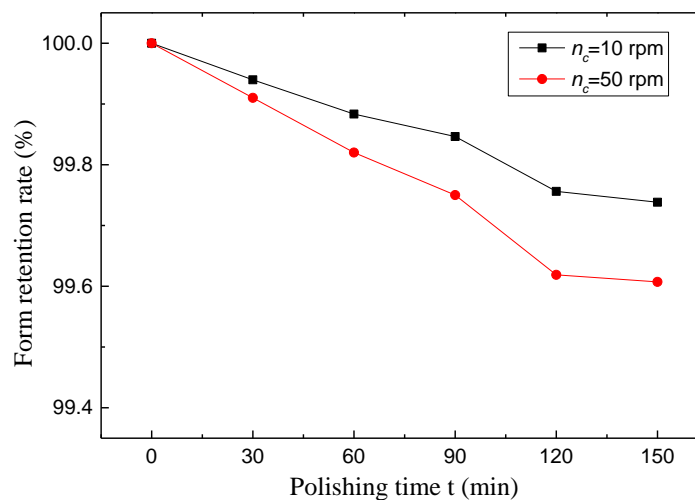


Fig.4.31 Changes of the form retention rate with the polishing time

From Fig.4.31, it can be found that the form retention rate decreases with the increase of the polishing time. In addition, they have the same decrease trend during the polishing process with both the MCF carrier rotational speed. However, the form retention rate decreases more quickly with a higher MCF carrier rotational speed. Most

noticeably of all, the form retention rate is higher than 99.6% regardless of the MCF rotational speed which can meet the requirement in the manufacturing process.

4.5.3.2 Surface roughness

The initial and final workpiece surface roughness after 150 min polishing with MCF slurry for various values of the clearances were measured using the scanning white-light interferometer. The results indicated that the value of the surface roughness is dependent on the MCF carrier rotational speed. In addition, the surfaces are more smooth where the material of the polished area removed more. Fig. 4.32 shows the initial and final work-surfaces with different MCF carrier rotational speeds with MCF slurry. It is obvious that the initial work-surface was improved significantly after polishing with two different rotational speeds; the polished surface roughness decreased, from the initial R_a value of 9.1 nm to the final R_a value of 2.9 nm and R_a 3.9 nm, respectively, at $n_c=50$ rpm and $n_c=10$ rpm with MCF slurry.

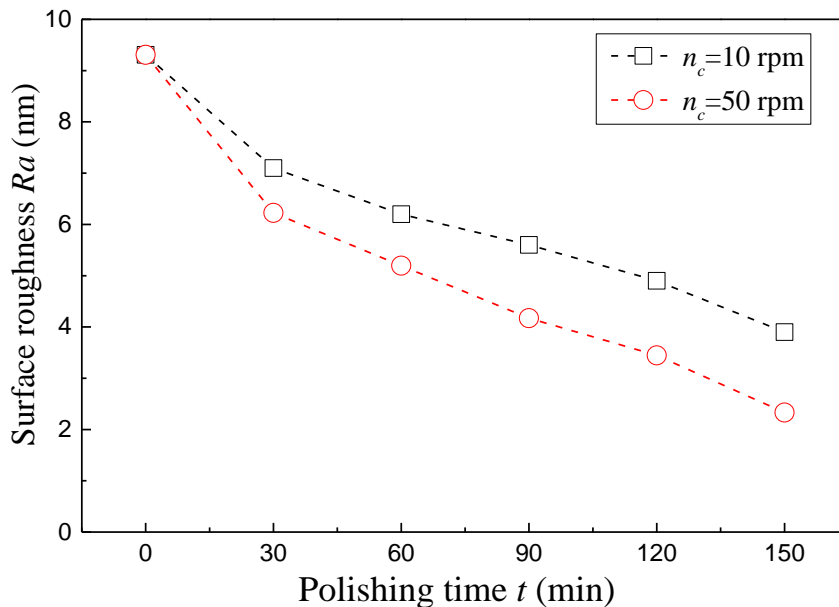


Fig.4.32 Surface roughness before and after polishing

4.6 Conclusions

Aiming at the development of a novel polishing technique for the high-precision surface finishing of structured surfaces with miniature V-grooves, a feasibility study was performed on the surface finishing of linear V-grooves generated on an oxygen-free copper substrate using an MCF slurry. First, a polishing apparatus was constructed by installing an MCF unit produced in-house for the generation of a rotary magnetic field and the rotation of the MCF carrier and a commercially available wavemaker used for vibrating the workpiece onto an existing polisher. Then, polishing experiments were performed to clarify the fundamental polishing characteristics, including the variations in the material removal, form accuracy (i.e. form retention rate and symmetry error), and surface roughness at different polishing areas during polishing. Thereafter, the fundamental characteristics were determined by investigating the distribution of the abrasive particles in the polishing zone, relative velocity of the abrasive particles compared to the V-groove, and impact angle of the abrasive particles against the V-groove side surface. Finally, the effect of the MCF carrier rotation speed n_c on the characteristics was elucidated, and an appropriate value for n_c was proposed from the viewpoint of the balance between the form accuracy and surface quality Ra. The obtained results can be summarized as follows.

- (1) Regardless of the process parameters, the work-surface roughness decreases monotonously with polishing time; although the final roughness depends on the polishing conditions, the roughness of the smoothest work-surface attained in the current work was less than 10 nm Ra. The oscillation parameter f/A_p is one of the important factors which does greatly influence the surface roughness. The final surface roughness decreased to 52.225 nmRa, 9.005 nmRa and 32.433 nmRa, respectively, at $f/A_p=15\text{Hz}/5\text{mmp}$, $30\text{Hz}/4\text{mmp}$ and $45\text{Hz}/2\text{mmp}$.
- (2) The form error increases during polishing regardless of the process parameters. The

MCF slurry amount deeply affected the form error, and it was more than 5% when the value was 1.00 mL in this experiment. The better surface roughness and smaller form accuracy were obtained at $f/A_{p-p}=30$ Hz/4 mm, $n_c=0$ rpm with 0.75 mL MCF slurry.

- (3) The impact angle θ was determined based on the MCF carrier rotational speed and workpiece vibration speed, and varied periodically with time; the form accuracy was greatly affected by the effective impact angle θ_m , which was the value of θ at the moment when the relative velocity peaked.
- (4) The V-groove form accuracy, i.e. the form retention rate η and symmetry error ε , deteriorated during polishing, and the final form accuracy differed with the location in the polishing zone, which was attributed to the different θ_m values at different locations. The form accuracy was worse at a location where the absolute value of θ_m was larger. Nevertheless, the form retention rate η and symmetry error ε at the location where the form accuracy was the lowest were more than 99.47% and less than 0.17, respectively, which satisfied the requirements for the injection mould of a sunlight concentration Fresnel lens.
- (5) At the majority of locations, the surface quality Ra values at the upper positions of the V-grooves were better than those at the lower ones. At the locations where the motion of the abrasive particles was from the right/left side to the left/right side of the grooves, the surface quality Ra values at the right/left side were better than those at the left/right side. The differences in the surface quality Ra values at the different positions were different at different locations, and the difference was larger at a

location where θ_m was larger. The final surface roughness values after 150 min of polishing were in the range of 15–50 nm Ra at all the discussed locations/positions, indicating that a mirror-like surface could be successfully achieved for a miniature V-groove.

(6) Increasing the MCF carrier rotational speed n_c led to an increase in θ_m and hence deteriorated the form accuracy, but improved the surface quality Ra. Taking into account the balance between the form accuracy and the surface quality Ra, n_c should be set at 10 rpm under the experimental conditions in the current work.

These results demonstrated that this novel MCF polishing process is a feasible method for the ultra-fine surface finishing of miniature V-grooves.

References

- [1] Erik Pihl, Concentrating Solar Power, Report of the Royal Swedish Academy of Sciences, 2009.
- [2] Zuo Chun Shen, Yu Lu, Jian Ye Lu. Fresnel lens solar concentrator design and spectral distribution on focus surface. *Optical Review*.2011; 18; 398-402.
- [3] Chien-Yao Huang, Chun-Chieh Chen, Hsiao-Yu Chou, Chang-Pin Chou. Fabrication of Fresnel lens by glass molding technique. *Optical Review*. 2013; 20; 202-204.
- [4] Y. Tanigawa, N. Nakamura, M. Uchino, M. Sugimoto, T. Maruo, Z. Haga, et al. Development of mold manufacturing technique using atranscription method for LED. *Die Mould Technol*. 2009; 24; 140-141. (in Japanese)
- [5] H. Ohmori, Y. Hachisu, K. Maekawa, N. Tone, Y. Uehara and Y. Takizawa. Ultra fabrication technologies of large Telescope Lenses for JEM-EUSO creating new astronomy, *JSPE 77*, 2011, 16-20. (in Japanese)
- [6] Brinksmeier E, Riemer O. Deterministic production of complex optical elements. *Int J Prod Eng Comput*. Special Issue on CAPP and Advances in Cutting Technology.2002; 4; 63-72.
- [7] A Gessenharter, O Riemer, E Brinksmeier. Polishing processes for structured surfaces. *Proceedings of the 18th ASPE*, 2003.
- [8] Ekkard Brinksmeier, Oltmann Riemer, Alexander Gessenharter. Finishing of structured surfaces by abrasive polishing. *Precision Engineering*.2006; 30; 325-36.
- [9] Wook-Bae Kim, Seung-Hwan Lee and Byung-Kwon Min. Surface Finishing and

- Evaluation of Three-Dimensional Silicon Microchannel Using Magnetorheological Fluid. *J. Manuf. Sci. Eng.* 2005; 126; 772-78.
- [10] Lim, C.H.; Kim, W.B.; Lee, S.H.; Lee, J.I. Surface polishing of three dimensional micro structures. *Micro Electro Mechanical Systems. 17th IEEE International Conference on (MEMS).* 2004; 709-12.
- [11] Masayuki Natsume, Takeo Shinmura and Katsumi Sakaguchi. Study of magnetic abrasive machining by use of work vibration system (characteristics of plane finishing and application to the inside finishing of groove). *The Japan Society of Mechanical Engineers.* 1998; 64; 4447-52.
- [12] Hideki Kawakubo and Tatsuya Yomogida. Finishing Characteristics of R-Groove Using Magnetic Filed Assisted Machining Mechod. *The Japan Society for Precision Engineering.* 2006; J07; 733-34.
- [13] Hideki Kawakubo and Masaki Sato. Polishing in Groove using Workpiece Oscillation Type Magnetic Field Assisted Machining. *The Japan Society for Precision Engineering.* 2008; E47; 375-76.
- [14] Hideki Kawakubo and Masaki Kamijima. Polishing for Ferromagnetic Materials using Workpiece Oscillation Type Magnetic Polishing Method. *The Japan Society for Precision Engineering.* 2010; B43; 139-40
- [15] Kunio Shimada, Yongbo Wu and Yat Choy Wong, Effect of magnetic cluster and magnetic field on polishing using magnetic compound fluid (MCF), *Jouranal of Magnetism and Magnetic Materials,* 2003;262;242-47.
- [16] Shimada, K., Akagami, Y., Kamiyama, S., Fujita, T., Miyazaki, T., Shibayama, A.

- New microscopic polishing with magnetic compound fluid (MCF). *J. Intell. Mater.Syst. Struct.* 2002; 13; 405-08.
- [17] Huiru Guo, Yongbo Wu, Dong Lu, Masakazu Fujimoto, Mitsuyoshi Nomura, Ultrafine Polishing of Electroless Nickel-Phosphorus Plating Mold with Magnetic Compound Fluid Slurry), *Materials and Manufacturing Processes*. 2014; 29; 1502-09.
- [18] H.R. Guo, Y. Wu, Y.G. Li, J.G. Cao, M. Fujimoto and S.D. Jacobs. Technical performance of zirconia-coated carbonyl-iron-particles based magnetic compound fluid slurry in ultrafine polishing of PMMA. *Key Engineering Materials*. 2012; 523-524; 161-66.
- [19] Huiru Guo, Yongbo Wu, Dong Lu, Masakazu Fujimoto, Mitsuyoshi Nomura. Effects of pressure and shear stress on material removal rate in ultra-fine polishing of optical glass with magnetic compound fluid slurry. *Journal of Materials Processing Technology*. 2014; 214; 2759-69.
- [20] Youliang Wang, Yongbo Wu, Huiru Guo, Masakazu Fujimoto, Mitsuyoshi Nomura and Kunio Shimada, A new magnetic compound fluid slurry and its performance in magnetic field-assisted polishing of oxygen-free copper, *J. Appl. Phys.* 2015;117; 17D712-1-12-4.
- [21] Yongbo Wu, Youliang Wang, Masakazu Fujimoto, Mitsuyoshi Nomura. Nano-precision polishing of CVD SiC using magnetic compound fluid slurry, *Journal of the Korean Society of Manufacturing Technology Engineers*. 2014; 23; 547-54.
- [22] Wu Y., Sato T., Lin W., Yamamoto K., Shimada K., Mirror surface finishing of

acrylic resin using MCF-based polishing liquid, *Int. J. Abras. Technol.* 2010; 3; 11-24.

[23] T. Furuya, Y. Wu, M. Nomura, K. Shimada, K. Yamamoto, Fundamental performance of magnetic compound fluid polishing liquid in contact-free polishing of metal surface, *Journal of Materials Processing Technology.* 2008; 201; 536-41.

[24] Ryutaro Mori, YongboWu, Masakazu Fujimoto and Weimin Lin. Nano MCF polishing of 3D Microstructure using Low-Frequency Oscillation. *The Japan Society for Precision Engineering.* 2010; J44; 669-70.

[25] Youliang Wang, Yongbo Wu, Masakazu Fujimoto and Mitsuyoshi Nomura. Ultra precision polishing of polymer lens mold steel using MCF slurry. *ABTEC2014.*

This page intentionally left blank.

Chapter V Finishing of circular V-groove using MCF slurry

5.1 Introduction

Fresnel lens a kind of optical elements which can be used for convergence or divergence of the light. It can be made much thinner than a comparable conventional lens due to the design allows the lens without the mass and volume of material that would be required by the conventional lens. There are two main types of Fresnel lens: linear and circular lens. Fresnel lenses are utilized in the optical landing system for aircraft carriers, where the light assists the pilots in performing proper landings. Another application for a Fresnel lens is enhancing reading lights, for passengers, on Airbus aircrafts so that the focused light beam does not impinge on neighboring passengers. Other applications, where Fresnel lenses are used, include: overhead projectors, railroad and traffic lights, projection televisions, spotlights, floodlights, decorative lights, and cameras. Recently, Fresnel lenses are becoming prevalent in the field of solar energy, where the lens is applied for the purpose of collecting and concentrating sunlight onto solar cells. As a result, the active solar cell area can be dramatically reduced, compared to conventional solar cells, which, in turn, will provide a significant reduction of budget spending due to lowered material consumption [Fresnel lens dimension with 3D profilometry, by Benjamin Mell]. Recently, Fresnel lenses are becoming dominant in the field of solar energy, where the lens is used for the purpose of gathering and concentrating sunlight onto solar cells. As a result, the active solar cell area can be dramatically reduced, compared to conventional solar cells, which, in turn, will provide a significant reduction of budget spending due to lower material consumption. The supply of the Fresnel lens shows an increasing rate, following the increasing in the development and application of clean energies. The Fresnel lens is injection molded with a copper mold insert which may be the most simple and cost-effective method.

In the present, high precision molds for the structured optical elements like Fresnel lenses are generated by precision grinding or diamond machining, abrasive flow machining. In order to produce the plastic lens which have high precision surface, the mold for the lens should have a higher precision. In some cases the surface quality of the high precision molds is not sufficient to satisfy the increasing requirements concerning surface roughness and form accuracy for optical applications.

Under an applied magnetic field, the particles magnetize and attract to another along the field lines and form a cluster with a certain strength. A multitude of clusters and the abrasive particles distributed within the clusters together form some stronger magnetic brush. When a relative motion is given between the work-surface and abrasive grains, a polishing force is imposed on the workpiece owing to the induced friction between the workpiece and abrasive grains, and the micro-cutting action of abrasive particles occurs to remove materials. As mentioned in Chapter 4, the Fresnel lens with linear grooves has been successfully polished to mirror surface using MCF slurry. However, the circular grooves polishing process is not known. This chapter will discuss the fundamental study of the precision polishing of miniature circular grooves using MCF slurry

5.2 Surface finishing of circular V-grooves (OCF)

5.2.1 Experimental details

An experimental apparatus was constructed in the laboratory, as shown in Fig. 5.1(a). A polishing unit composed of a magnet holder, an MCF carrier, and two motors, together with a belt/pulley set (Fig. 5.2(a)), was mounted on the Z-axis linear actuator of an existing polisher, allowing Z-axis motion. In addition, a rotary work-table was installed on the worktable of the same polisher to provide the workpiece with an oscillating motion in the X direction. In the MCF unit, a disc-shaped neodymium

permanent magnet with a magnetic field strength of 0.45 T was set at an eccentricity of $r = 4.5$ mm. Motor 1 was connected to the magnet holder through a flexible coupling and used to give the magnet a revolutionary motion around its holder's axis. Motor 2 was connected to the MCF carrier through the belt/pulley and used to rotationally drive the carrier. Motor 3 was connected to the work-table through the belt and used to rotationally drive the work-table. The carrier ($82 \text{ mm} \times 82 \text{ mm} \times 1 \text{ mm}$) was made of a non-magnetic material (aluminium in this work). Below the MCF carrier, a piece of oxygen-free copper (OFC) substrate with circular V-grooves was fixed on the work-table as the workpiece. This arrangement allowed the workpiece to rotate in a given viscosity. Thus, it allowed the relative velocity of the abrasive particles to the work surface. In addition, the clearance Δ could be varied by adjusting the vertical position of the MCF unit through the Z-axis linear actuator.

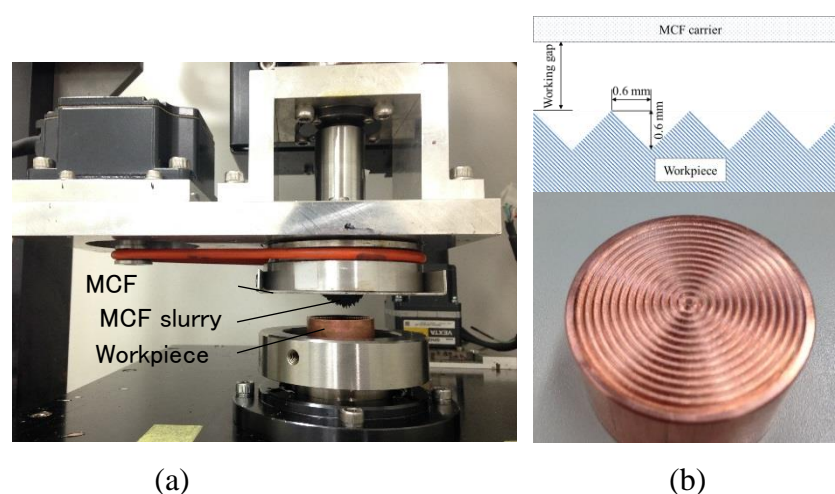


Fig. 5.1 Experiment setup and workpiece

The structure and dimensions of the workpiece with miniature V-grooves are shown in Fig. 5.1(b). This workpiece was prepared by generating distributed circular V-grooves on an OFC plate using a shaping technique on a numerical control milling machine (VHR-AN by Shizuoka Machine Tool CO.) using a superhard cutting tool. The detailed dimensions of the miniature V-grooves generated were 0.6 mm in depth, 1.2 mm in pitch, and 90° in included angle (see the upper side of Fig. 5.3). The original roughness values of the side surfaces of the V-grooves were 355 nm Ra.

The purpose of this study was to determine the feasibility of finishing circular V-grooves with an MCF slurry and elucidate the fundamental finishing characteristics, including the variations in the form accuracy and surface roughness during polishing. Therefore, the composition of the MCF slurry used and the experimental parameters (magnet eccentricity, magnet revolutionary speed, MCF carrier rotational speed, amount MCF slurry supplied, and clearance) were kept constant, as listed in Table 5.1 and Table 5.2, respectively. Subsequently, under these experimental conditions, the variations in the form accuracy and surface roughness values of the V-grooves during polishing were attained experimentally.

Table 5.1 Experiment conditions

Workpiece	Miniature circular V-grooves
Rotation speed of the workpiece	$n_w=200$ rpm, 600 rpm Nd-Fe-B: B=0.45T
Magnet	Revolution radius: $r=4.5$ mm Rotational speed: $n_m=1,000$ rpm
MCF carrier	Rotational speed: $n_c=10$ rpm
Supply of MCF slurry	1 mL
Polishing time	90min($n_w=200$ rpm)+60min ($n_w=600$ rpm)
Clearance	$\Delta=1$ mm

Table 5.2 Composition of MCF slurry used

Carbonyl iron powder	Mean diameter	7 μm
	Concentration	45 wt. %
Abrasive particle (Al_2O_3)	Mean diameter	1 μm
	Concentration	12 wt. %
Water-based magnetic fluid (MF)	Mean diameter	10 nm
	Concentration	40 wt. %
α -cellulose	Concentration	3wt. %

5.2.2 Results and Discussion

5.2.2.1 Surface roughness

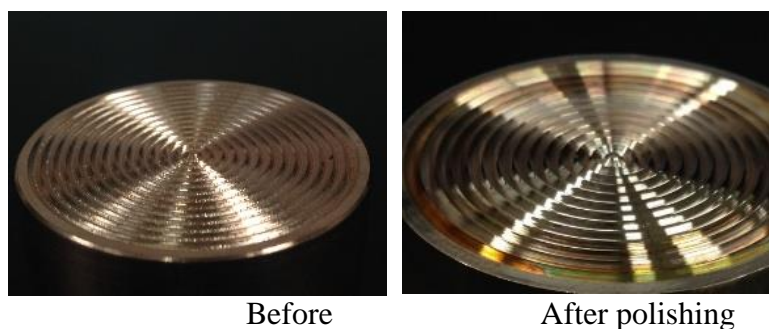


Fig. 5.2 Image of the circular grooves before and after polishing

Fig. 5.2 shows the images of the circular grooves before and after polishing using MCF slurry. It can be observed that the V-grooves before polishing have a rough surface and a lot of burr. After polishing, the V-grooves surface quality are obviously improved which show a mirror surface. The work-surface roughness was characterized with an optical surface profiler (Newview 600 by Zygo Corp.). The surface roughness before and after polishing are shown in Fig. 5.3.

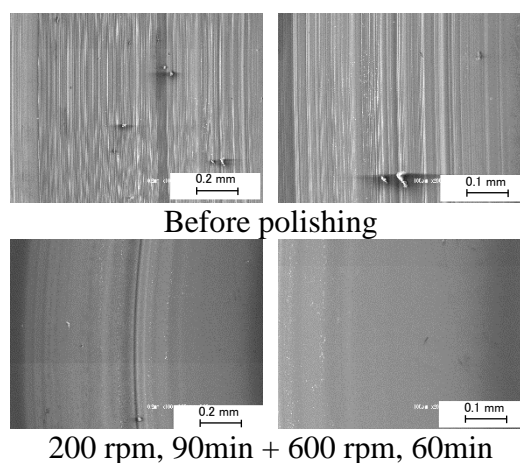


Fig. 5.3. SEM images before and after polishing

The SEM images of the miniature V-groove surface before and after polishing are shown in Fig.5.3. These images also investigate that the surface quality improve with the MCF polishing. The cutting marks and burrs distributes on the circular grooves surface lead to the rough surface. After polishing with MCF slurry, the marks and burrs removed and the smooth surface is observed.

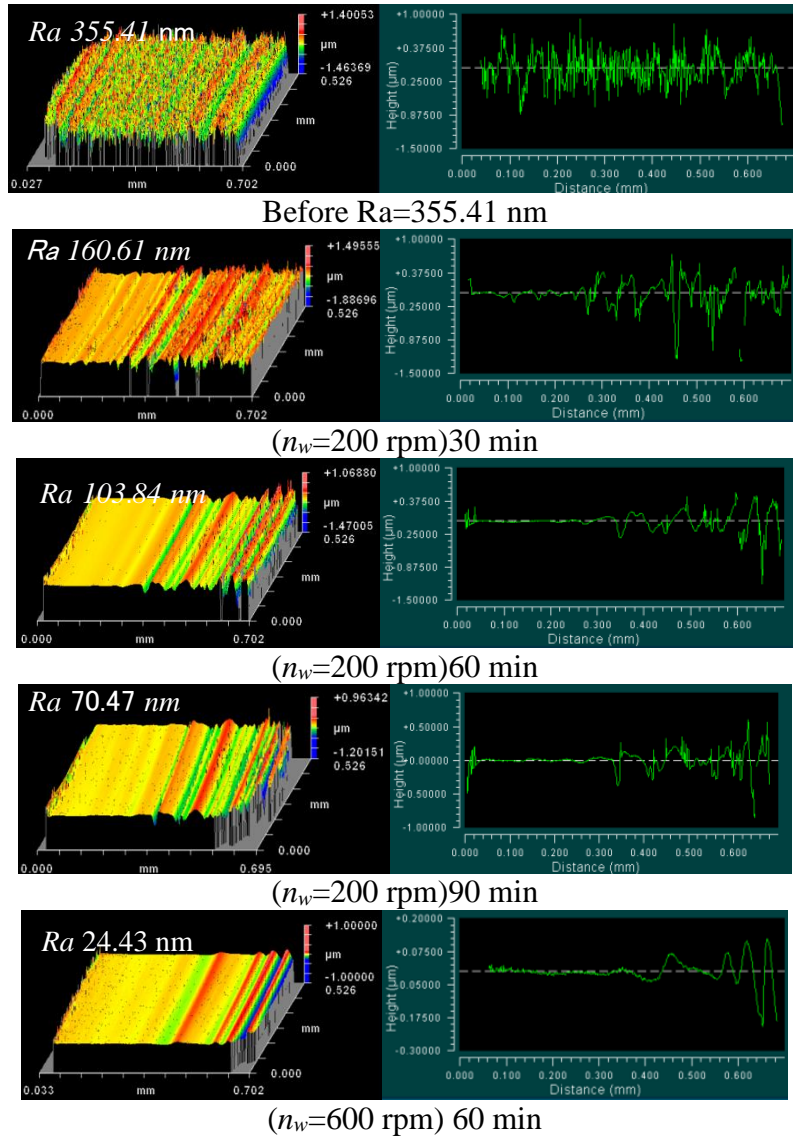


Fig. 5.4 Surface quality and cross section profiles with the polishing time at different n_w

Fig.5.4 shows the surface quality and cross section profiles during the polishing process. It can be observed that the groove surfaces smooth after MCF slurry polishing. The surface on the left is better than that on the right. The cross section profiles investigate that the distance of the smooth surface on the left increase with the increasing of polishing time. The results are shown in Fig. 5.5. The surface roughness decrease with the increasing of polishing time regardless of the rotary work-table speed n_w . It shout notice that the surface roughness decrease rapidly at the first 30 mins, and then the decrease tends become slow.

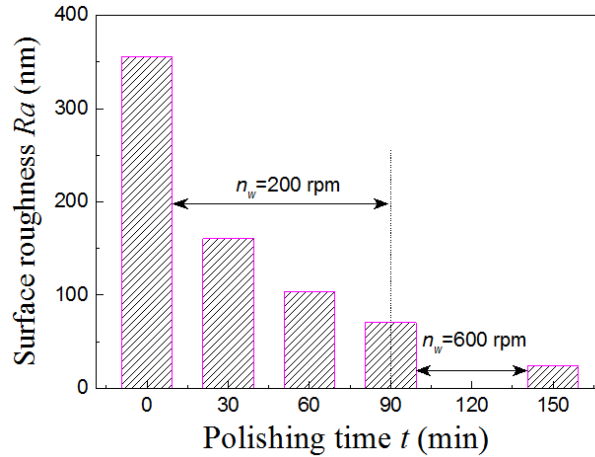


Fig. 5.5. Changes of surface roughness with the polishing time

In order to study the difference of surface roughness on the top and bottom of the groove. The surface roughness on both positions are shown in Fig. 5.6. It reveals that the surface roughness on the top is better than that on the bottom after polishing with the same time polishing. In addition, the final surface roughness achieves 24 nm Ra on the top and 45 nm Ra on the bottom. The results are shown in Fig.5.7.

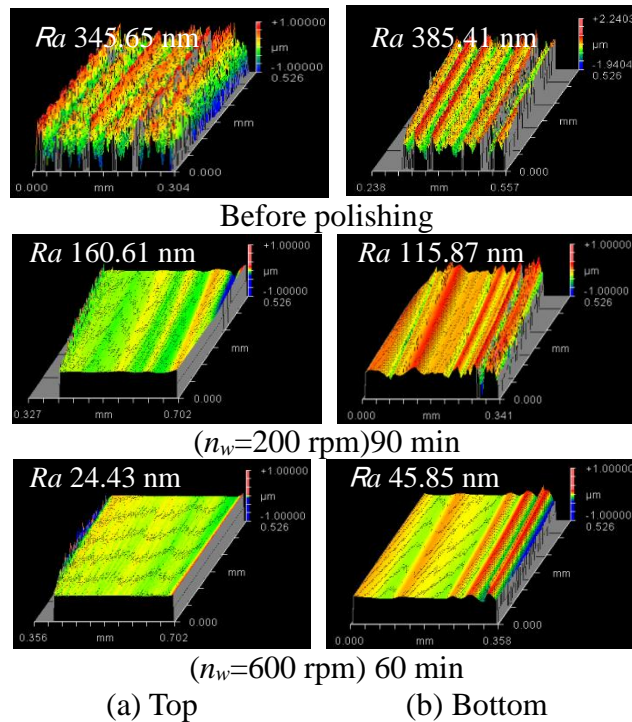


Fig. 5.6. The surface quality at different positions various with the polishing time

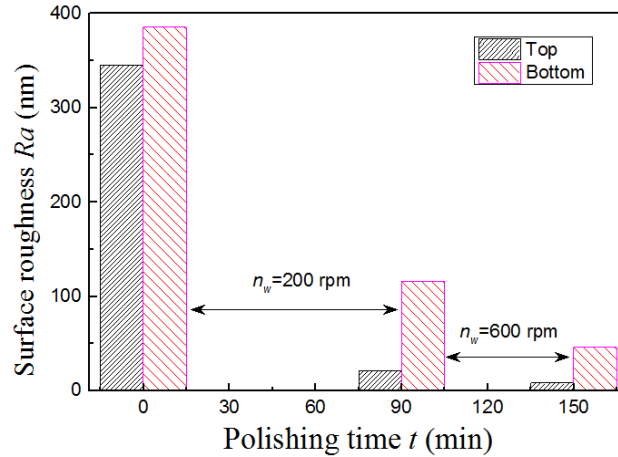


Fig. 5.7. Changes of the surface roughness at top and bottom with the polishing time

5.2.2.2 Form accuracy

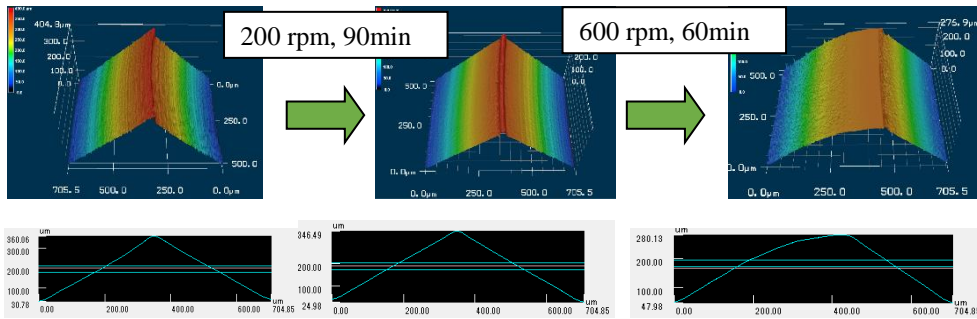


Fig. 5.8. The 3D images and cross section profiles of groove before and after polishing

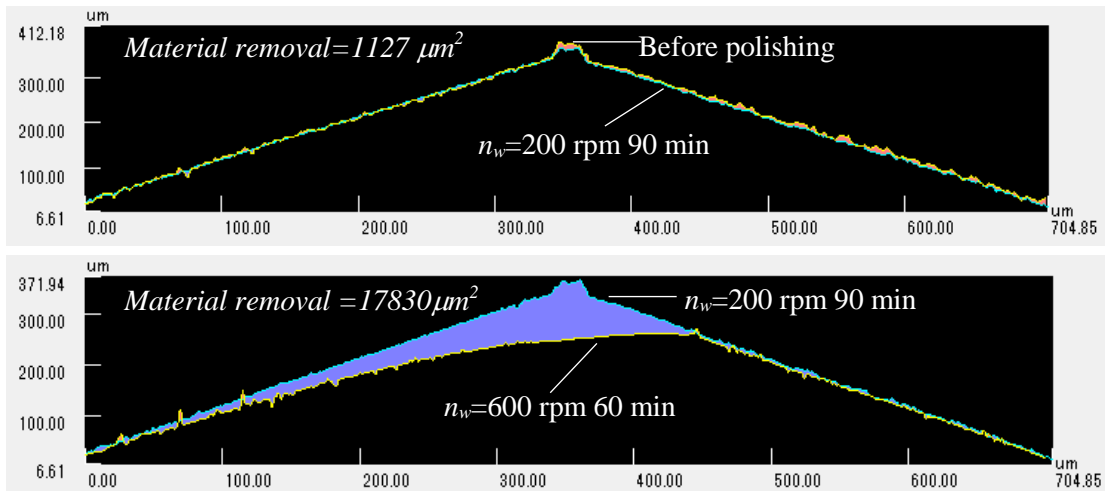


Fig. 5.9. The material removal after polishing with different n_w

In the finishing of miniature V-grooves, the form accuracy is important. The 3D images of the miniature groove before and after polishing with different work-table rotational speed are shown in Fig. 5.8. It can be found that the groove morphology

changes a little after 90 min polishing with workpiece rotational speed $n_w = 200\text{rpm}$. And then the morphology changes obviously on the top of miniature circular V-grooves with workpiece rotational speed $n_w = 600\text{rpm}$. The material removal area is $1127\ \mu\text{m}^2$ and $17830\ \mu\text{m}^2$. The higher workpiece rotational speed is, the more the material removal becomes.

5.3 Ni-P plated circular grooves polishing

5.3.1 Experimental conditions

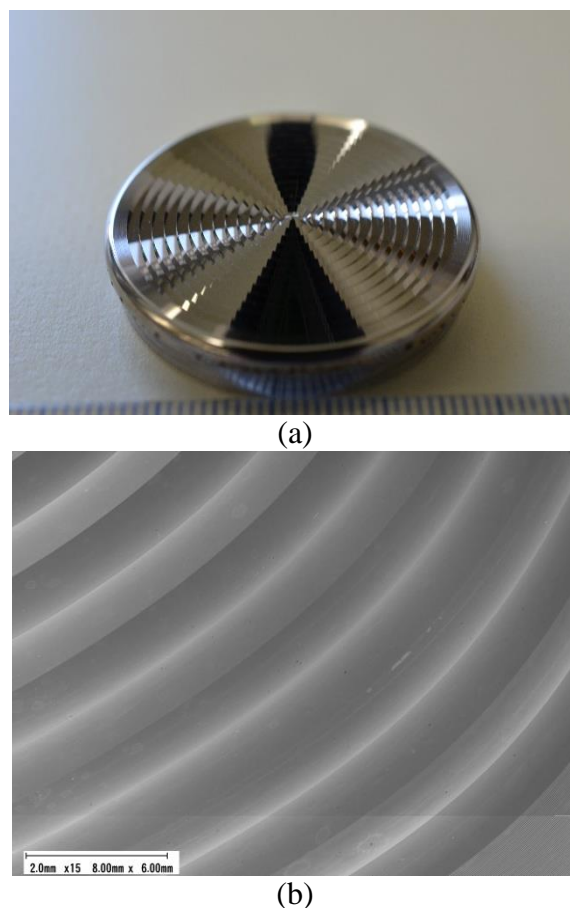


Fig. 5.10. Ni-P plated circular grooves

As shown in Fig.5.10, disc-shaped STAVAX steel (3 mm thick) whose upper surface was coated with an electroless Ni-P-plated layer 1 mm thick was used. The dimensions of the miniature circular V-grooves is as same as the used workpiece in section 5.2. The detailed dimensions of the miniature V-grooves generated were 0.6

mm in depth, 1.2 mm in pitch, and 90° in included angle. The SEM images of the Ni-P plated STAVAX workpiece with circular V-grooves is shown in Fig.5.10 (b).

When the circular grooves (OFC) were polished with a higher workpiece rotational speed, the material removal increase quickly and the form accuracy of miniature grooves decrease significantly. Therefore, the rotation speed of the workpiece was set as 500 rpm instead of 600 rpm in this section. The detail of experimental conditions is shown in Table 5.3.

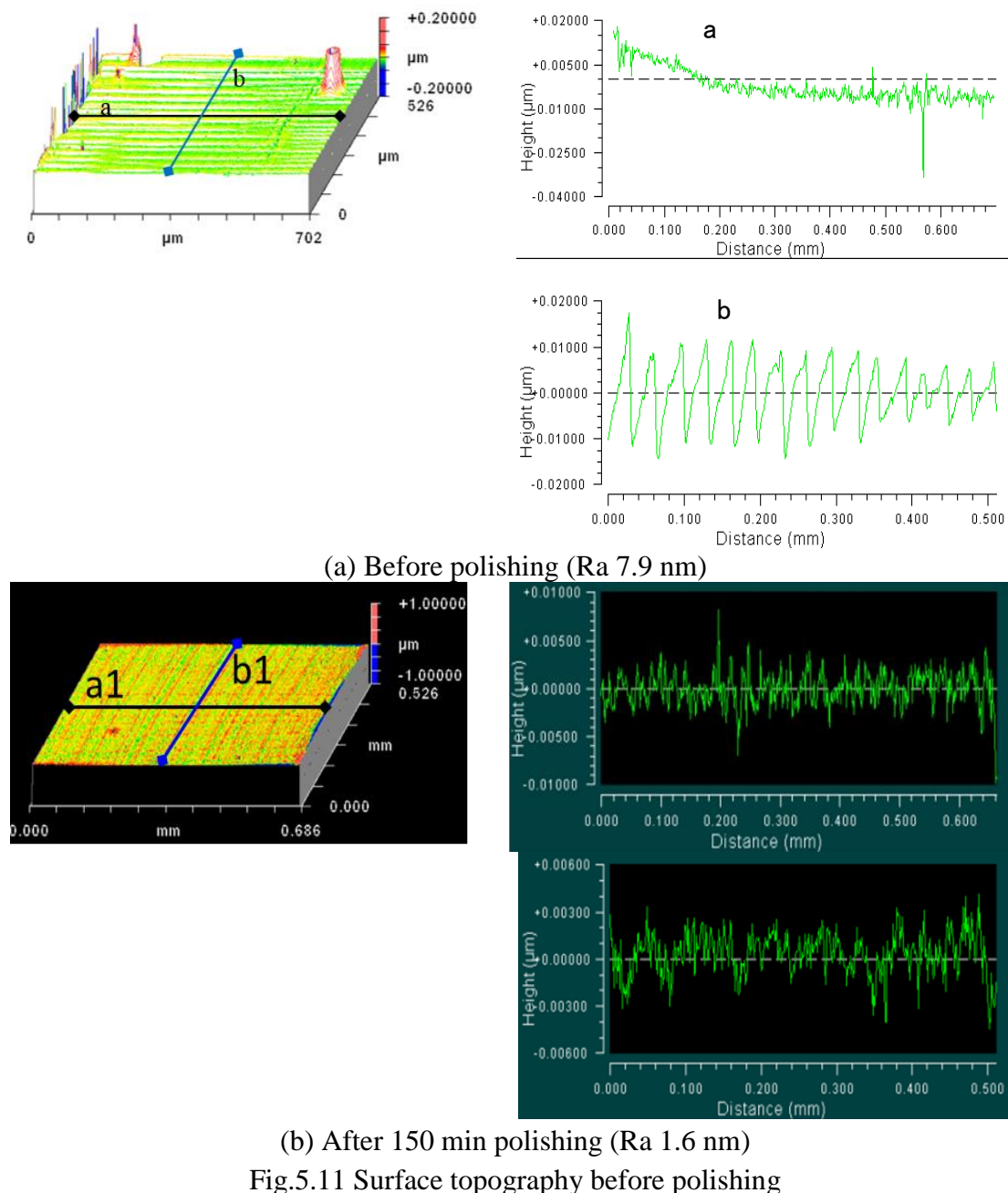
Table 5.3 Experiment conditions

Workpiece	Circular V-grooves
Rotation speed of the workpiece	$n_w=500$ rpm Nd-Fe-B: B=0.45T
Magnet	Revolution radius: $r=4.5$ mm Rotational speed: $n_m=1,000$ rpm
MCF carrier	Rotational speed: $n_c=10$ rpm
Supply of MCF slurry	1 mL
Clearance	$\Delta=1$ mm

5.3.2 Results and discussion

5.3.2.1 Surface roughness

The initial and final workpiece surface roughness after 150 min polishing with MCF slurry for various values of the clearances were measured using the scanning white-light interferometer. The surface topography before and after 150 min polishing using MCF slurry shown in Fig.5.11, which indicates the changes of the surface roughness after polishing process. It can be observed from Fig.5.11 (a) that the cutting marks on the surface on one direction results the surface is rough before polishing. It is obvious that the initial work-surface was improved significantly after polishing with MCF slurry; the polished surface roughness decreased greatly, from the initial R_a value of 7.9 nm to the final R_a value of 1.6 nm.



The changes of the surface roughness with the polishing time are shown in Fig.5.12. This figure indicates that the surface roughness decreases with the increasing of polishing time using MCF slurry. It is worth noting that the surface roughness decrease very quickly at the first 30 min during the whole polishing process. And then the surface roughness changes slowly. It indicates that the material removes effectively on the miniature V-grooves surface using MCF slurry. The results reveal the MCF slurry can be applied to the mirror surface finishing of circular V-grooves.

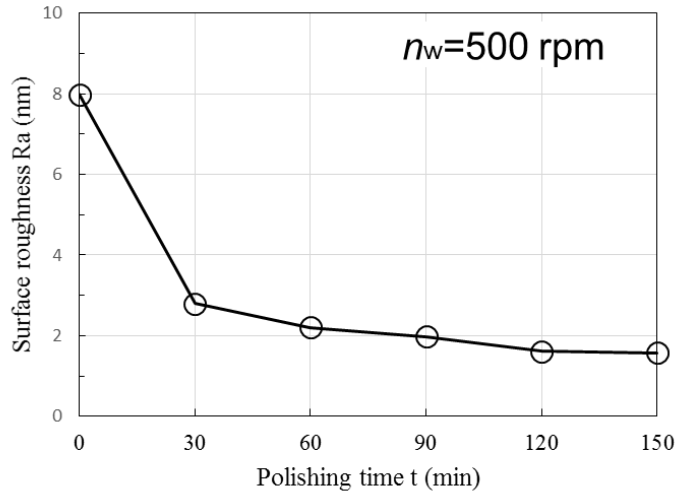


Fig.5.12 Changes of the surface roughness with the polishing time during the polishing process

5.3.2.2 Form accuracy

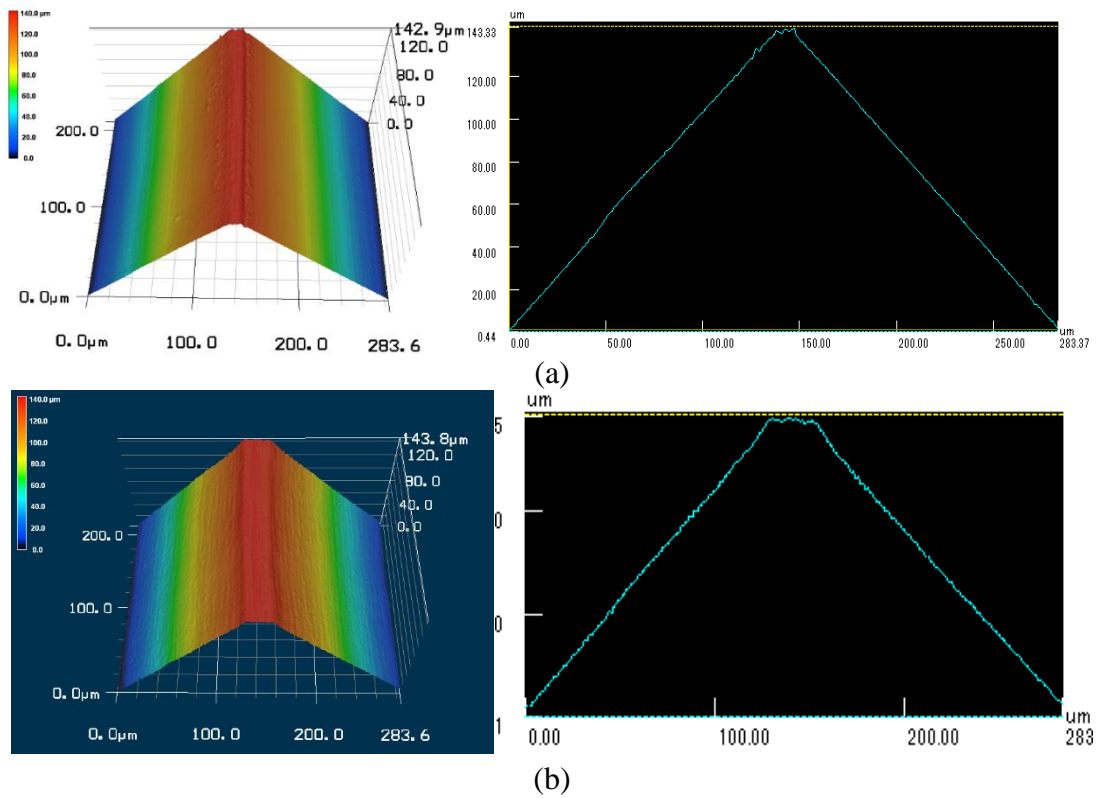


Fig.5.11 3D photographs of the top of miniature V-groove (a) before polishing, (b) polished for 150 min

Fig. 5.11 shows 3D photographs of the top of miniature V-groove before and after polishing for 150 min. Comparing Fig. 5.11(a) and (b) indicates that the form accuracy grow worse than the initial value along with the polishing time. The material removal

appears on the top of the groove using MCF slurry. From the cross section profiles of the V-grooves before and after polishing, the height of the grooves decrease only a little after MCF polishing

5.4 Conclusion

To develop a novel polishing method for the mirror surface finishing of miniature circular V-grooves. A feasibility study was performed on the surface finishing of circular V-grooves generated on an oxygen-free copper and Ni-P plated surface using an MCF slurry. The obtained results can be summarized as follows.

- (1) Regardless of the workpiece rotational speed, the surface roughness decreases with the increasing of polishing time during the polishing process. However, the surface roughness decreases quickly with a higher workpiece rotational speed.
- (2) The form accuracy decreases during polishing regardless of the process parameters. The workpiece rotational speed deeply affected the form accuracy in this experiment.

This page intentionally left blank.

Chapter VI Conclusions and Future Suggestions

A novel magnetic compound fluid (MCF) is proposed by mixing a magnetic field (MF) and a magnetorheological (MR) fluid. The MCF slurry contains μm -sized iron powders and nm-sized magnetite particles. Under a given magnetic field, the MCF slurry exhibit higher magnetic pressure and viscosity than MF and a more stable distribution of particles within slurry than MR fluids. The MCF slurry is usually contains carbonyl-iron-powder (CIP), water based MF, abrasive particles and α -cellulose. In this study, a rotary magnetic field was employed. In the rotary magnetic field, the magnetic flux density is constant, but the magnetic lines of force constantly revolve around the magnet holder axis. The objectives of this thesis research work are to clarify the useful life of the MCF slurry and the distribution of the particles within slurry under a rotary magnetic field, to smooth miniature V-grooves surface finishing with MCF slurry.

A novel polishing method using MCF slurry was proposed for the nano-precision surface finishing of OFC materials. Experimental investigations on the effects of process parameters on surface roughness Ra and material removal MR were performed. Regardless of the process parameters, the work-surface roughness decreases monotonously with polishing time; although the final roughness depends on the polishing conditions, the roughness of the best work-surface attained in the current work was less than 5 nm Ra. The relationship between the MR and polishing time t is linear under the given conditions. Moreover, the MR s, i.e., the polishing depths, obtained with different parameters; the highest MR s, i.e., the greatest depths, were obtained at $f=30$ Hz, $A_{p-p}=4$ mm, $\Delta=0.6$ mm with a MCF slurry (45 wt.% of CIP, 12 wt.% of abrasive particle, 3 wt.% of α -cellulose, 40 wt.% of MF). In addition, the best surface was obtained in the polished region where the polished area was the deepest.

The effects of the magnetic and gravitational forces acting on naked CIPs and APs were investigated and the behaviors of the CIPs and APs in the presence of an external magnetic field were qualitatively discussed. Then, the distributions of CIPs and APs on the working surfaces of MCF slurries were experimentally investigated with both magnetic and non-magnetic work surfaces. Finally, polishing experiments were performed on the magnetic workpiece, a Ni–P-plated STAVAX steel specimen, using MCF slurries containing CIPs and APs with different diameters at different working gaps to confirm the discussion on the particle distribution. The resultant vertical force acting on the naked CIPs was due to the magnetic and gravitational forces, and it significantly increased with increasing CIP diameter. With the magnetic workpiece, the resultant vertical force attracted the CIPs towards the work surface, whereas APs were pushed away from the work surface. Both the CIPs and the APs showed opposite behaviors with the non-magnetic workpiece. The percentage of active APs distributed on the working surface of an MCF slurry increased and the distributions became more even as either the diameter of the CIPs or the working gap increased. On the other hand, the distribution of CIPs was opposite that of APs. The percentage of active APs was beyond 25% with the non-magnetic workpiece, whereas it was less than 25% with the magnetic workpiece. The MCF slurry containing CS CIPs 7 μm in diameter and APs 1 μm in diameter should be employed and that the working gap Δ at 1 mm should be set in order to perform mirror surface finishing of magnetic Ni–P-plated STAVAX steel using the naked CIP-based MCF slurry. Under the experimental conditions in this work, the Ni–P-plated surface quality was significantly improved and a mirror surface roughness of $R_a = 4$ nm was successfully achieved without leaving scratches or particle adhesion with an MCF slurry containing CIPs 7 μm in diameter and APs 1 μm in diameter.

Aiming at the development of a novel polishing technique for the high-precision surface finishing of structured surfaces with miniature V-grooves, a feasibility study

was performed on the surface finishing of linear V-grooves generated on an oxygen-free copper substrate using an MCF slurry. First, a polishing apparatus was constructed by installing an MCF unit produced in-house for the generation of a rotary magnetic field and the rotation of the MCF carrier and a commercially available wavemaker used for vibrating the workpiece onto an existing polisher. Then, polishing experiments were performed to clarify the fundamental polishing characteristics, including the variations in the material removal, form accuracy (i.e. form retention rate and symmetry error), and surface roughness at different polishing areas during polishing. Thereafter, the fundamental characteristics were determined by investigating the distribution of the abrasive particles in the polishing zone, relative velocity of the abrasive particles compared to the V-groove, and impact angle of the abrasive particles against the V-groove side surface. Finally, the effect of the MCF carrier rotation speed n_c on the characteristics was elucidated, and an appropriate value for n_c was proposed from the viewpoint of the balance between the form accuracy and surface quality Ra. The impact angle θ was determined based on the MCF carrier rotational speed and workpiece vibration speed, and varied periodically with time; the form accuracy was greatly affected by the effective impact angle θ_m , which was the value of θ at the moment when the relative velocity peaked. The V-groove form accuracy, i.e. the form retention rate η and symmetry error ε , deteriorated during polishing, and the final form accuracy differed with the location in the polishing zone, which was attributed to the different θ_m values at different locations. The form accuracy was worse at a location where the absolute value of θ_m was larger. Nevertheless, the form retention rate η and symmetry

error ε at the location where the form accuracy was the lowest were more than 99.47% and less than 0.17, respectively, which satisfied the requirements for the injection mould of a sunlight concentration Fresnel lens. At the majority of locations, the surface quality Ra values at the upper positions of the V-grooves were better than those at the lower ones. At the locations where the motion of the abrasive particles was from the right/left side to the left/right side of the grooves, the surface quality Ra values at the right/left side were better than those at the left/right side. The differences in the surface quality Ra values at the different positions were different at different locations, and the difference was larger at a location where θ_m was larger. The final surface roughness values after 150 min of polishing were in the range of 15–50 nm Ra at all the discussed locations/positions, indicating that a mirror-like surface could be successfully achieved for a miniature V-groove. Increasing the MCF carrier rotational speed n_c led to an increase in θ_m and hence deteriorated the form accuracy, but improved the surface quality Ra. Taking into account the balance between the form accuracy and the surface quality Ra, n_c should be set at 10 rpm under the experimental conditions in the current work.

Future work should be done in order to clarify the polishing force of MCF slurry during the miniature V-grooves polishing process. In addition, the working life of the MCF slurry should be clarified and prolonged to polish the workpiece in the modern industry manufacturing.

Acknowledgements

The three and a half years in Japan has enriched my experience and will impress me forever. Many kinds person must be gratefully thanked to accomplish my thesis work.

My deepest gratitude goes first and foremost to Professor Wu, my supervisor, for his constant encouragement and guidance. Professor Wu has walked me through all the stages of the writing of this thesis. I have studied much about polishing various workpieces using magnetic compound fluid (MCF) slurry form the innumerable discussions with him. Without his consistent and illuminating instruction, this thesis could not have reached its present form. His rigorous attitude towards scientific research will guide me for the rest of my life and future research work.

I would like to express my heartfelt gratitude to Prof. Kunio Shimada of Fukushima University, Prof. Mamoru Mizuno and Prof. Teruo Bitoh of Akita Prefectural University for their willingness to serve as members of my thesis defense committee.

I am very grateful to Prof. Mitsuyoshi Nomura, Dr. Masakazu Fujimoto, Dr. Tatsuya Fujii and Mr. Kimura and Miura for their kind helps, advice and assistance in my work. After discussing with them always made a light breaks in upon me and made things easier to deal with.

I would like to express their deep appreciation to JFE 21 foundation for the financial support, greatly thanks Rochester University for providing the ZrO₂-coated CIPs for the experiment and the Kimura Corporation for preparing the Ni-P plated circular grooves.

I would like to express my heartfelt gratitude to my advisor of master's course, Prof. Weiyuan Yu of Lanzhou University of Technology.

I must express a lot thanks to Ms. Aki Asada for her continuing support during my stay in Japan.

I would like to express gratefulness for making my stay in Japan pleasant to a few more people: Dr. Weixing Xu, Dr. Huiru Guo, Dr. Jianguo Cao, Dr. Yaguo Li, Mr. Sisi Li, Mr. Qiang Wang, Mr Ming Feng, Mr. Zongliang Yao, Mr. Tailin Zhu, Pro. Dong Lu, Pro. Weiping Yang, Pro. Yuebo Ji, Dr. Jia Gu, Dr. Wenqing Song, Mr. Jingti Niu, Mr. Kosuke Sasaki, Mr. Nobuto Oura, Mr. Naoya Makita, Mr. Yuzurru Sidou, Mr. Masayoshi Kawasimi and Mr. Takuya Miura. Thanks for sharing your precious experiences with me and selfless assistance in my work and life.

I am also deeply indebted to the following excellent people: Dr. Xueli Wu, Dr. Paipai Pan, Dr. Xingguo Zhang, Dr. Limin Zang, Dr. Lijun Wang, Mr. Bin Wang, Mr. Liqiang Gu, Miss Baiyi Chen, Miss Jingyan Huang, Dr. Yanling Yu, Dr. Guan Gui, Dr. Jian Shi, Mrs. Yiyu Wang, Mr. Zijing Liu, Mr. Beiyi Liu, Mr. Chen Ye, Dr. Yanping Zhang, Mr. Longxiang Zhu, Mrs. Jiao Chen, Mr. Haodao Mo and Mrs. Ping Ao.

I was so fortunate to have my wife Wenjuan Zhang who is not only the love of my life, but also my best friend in my life. Thanks for your love and support.

Last my thanks would go to my beloved family for their loving considerations and great confidence in me all through these years. I also owe my sincere gratitude to my friends and my fellow classmates who gave me their help and time in listening to me and helping me work out my problems during the difficult course of the thesis.

Accomplishments

Papers

- [1] Youliang Wang, Yongbo Wu, Huiru Guo, Masakazu Fujimoto, Mitsuyoshi Nomura and Kunio Shimada, A New Magnetic Compound Fluid Slurry and its Performance in Magnetic Field-assisted Polishing of Oxygen-free Copper, *Journal of Applied Physics*, 117(2015) 17D712-1-4 (IF : 2.185).
- [2] Youliang Wang, Yongbo Wu, and Mitsuyoshi Nomura, Feasibility study on surface finishing of miniature V-grooves with magnetic compound fluid slurry, *Precision Engineering*, 45(2016) 67-78 (IF : 1.517)
- [3] Youliang Wang, Yongbo Wu and Mitsuyoshi Nomura, A novel magnetic field-assisted polishing method using magnetic compound slurry and its performance in mirror surface finishing of miniature V-grooves. *AIP Advances*, 6(2016)056602-1-6 (IF : 1.59)
- [4] Youliang Wang, Yongbo Wu, and Mitsuyoshi Nomura, Fundamental investigation on nano-precision surface finishing of electroless Ni-P-plated STAVAX steel using magnetic compound fluid slurry, *Precision Engineering*, (Resubmit after minor revision, IF : 1.517)
- [5] Youliang Wang, Yongbo Wu and Mitsuyoshi Nomura, Nano-precision Polishing of Oxygen-free copper using MCF (Magnetic Compound Fluid) slurry, *Advanced Materials Research*, 806(2015)455-460.
- [6] Yongbo Wu, Youliang Wang, Masakazu Fujimoto, Mitsuyoshi Nomura. Nano-precision Polishing of CVD SiC Using MCF (Magnetic Compound Fluid) slurry, *Journal of the Korean Society of Manufacturing Technology Engineers*, 23(2014) 547-554.

Academic Conference

- [1] Youliang Wang, Yongbo Wu, Huiru Guo, Masakazu Fujimoto, Mitsuyoshi Nomura and Kunio Shimada. A New Magnetic Compound Fluid Slurry and its Performance in Magnetic Field-assisted Polishing of Oxygen-free Copper. The 59th Annual Magnetism and Magnetic Materials (MMM) Conference. (2014年11月3日—7日, Honolulu, Hawaii, USA)
- [2] Youliang Wang, Yongbo Wu, and Mitsuyoshi Nomura, A novel magnetic field-assisted polishing method using magnetic compound slurry and its performance in mirror surface finishing of miniature V-grooves, MMM InterMag 2016. (2016年1月11日—15日, San Diego, USA)
- [3] Youliang Wang, Yongbo Wu, Mitsuyoshi Nomura. Nano-precision Polishing of Oxygen-free copper using MCF (Magnetic Compound Fluid) slurry. The 18th International Symposium on Advances in Abrasive Technology (ISAAT). (2015年10月4日—7日, Jeju Island, Korea)
- [4] Youliang Wang, Yongbo Wu, Mitsuyoshi Nomura. Magnetic field-assisted polishing of miniature V-grooves using MCF (Magnetic Compound Fluid) slurry. The 8th International Conference on Leading Edge Manufacturing in 21st Century (LEM21). (2015年10月18日—22日, Kyoto, Japan)
- [5] Youliang Wang, Yongbo Wu, Masakazu Fujimoto, Mitsuyoshi Nomura. Explorative investigation on inner surface finishing of capillary with MCF slurry. 2013年度精密工学会東北支部講演会. (2013年12月4日, 日本秋田)
- [6] 王 有良, 呉 勇波, 藤本 正和, 野村 光由. MCF スラリーを用いた CVD-Si セラミックスのナノ精度研磨. 日本実験力学 2014 年度講演会. (2014年8月28日—30日, 兵庫県立大学, 日本 兵庫)
- [7] Youliang Wang, Yongbo Wu, Masakazu Fujimoto, Mitsuyoshi Nomura. Ultra-precision polishing of polymer lens mold steel using MCF slurry. 1st

report, Fundamental polishing characteristics on free-oxygen copper for mold steel. 2014 年度砥粒加工学会. (2014 年 9 月 11 日—13 日, 岩手大学, 日本 岩手)

[8] Youliang Wang, Yongbo Wu, Masakazu Fujimoto, Mitsuyoshi Nomura. Ultra-precision polishing of polymer lens mold steel using MCF slurry. 2nd report, Form accuracy on polishing of micro-groove. 2014 年度砥粒加工学会. (2014 年 9 月 11 日—13 日, 岩手大学, 日本 岩手)

[9] 王 有良, 呉 勇波, 野村 光由, MCF スラリーを用いたミニチュア V 溝の鏡面仕上げの基礎研究, (2015 年 9 月 4-6 日, 東北大学, 日本 仙台)

Awards Travel Grants

1. 平成 27 年度精密工学会東北支部優秀研究奨励賞

2. 三豊科学技術振興協会国際交流助成

会議名: 13th Joint Magnetism and Magnetic Materials (MMM)-Intermag Conference

場 所: アメリカ・サンディエゴ

期 間: 2016 年 1 月 11 日 - 2016 年 1 月 15 日